

SYNTHESIS AND OPTOELECTRONIC APPLICATIONS OF BENZOTRIAZOLE  
AND DIBENZOSILOLE BASED ALTERNATING COPOLYMERS

A THESIS SUBMITTED TO  
THE GRADUATE SCHOOL OF NATURAL AND APPLIED SCIENCES  
OF  
MIDDLE EAST TECHNICAL UNIVERSITY

BY

OZAN ERLİK

IN PARTIAL FULFILLMENT OF THE REQUIREMENTS  
FOR  
THE DEGREE OF MASTER OF SCIENCE  
IN  
CHEMISTRY

OCTOBER 2014



Approval of the thesis:

**SYNTHESIS AND OPTOELECTRONIC APPLICATIONS OF  
BENZOTRIAZOLE AND DIBENZOSILOLE BASED ALTERNATING  
COPOLYMERS**

submitted by **OZAN ERLİK** in partial fulfillment of the requirements for the degree of  
**Master of Science in Chemistry Department, Middle East Technical University** by,

Prof. Dr. Gülbin Dural Ünver  
Dean, Graduate School of **Natural and Applied Sciences**

\_\_\_\_\_

Prof. Dr. İlker Özkan  
Head of Department, **Department of Chemistry**

\_\_\_\_\_

Assoc. Prof. Dr. Ali Çırpan  
Supervisor, **Department of Chemistry, METU**

\_\_\_\_\_

**Examining Committee Members:**

Prof. Dr. Levent Toppare  
Chemistry Dept., METU

\_\_\_\_\_

Assoc.Prof. Dr. Ali Çırpan  
Chemistry Dept., METU

\_\_\_\_\_

Assoc. Prof. Dr. Emren Esentürk  
Chemistry Dept., METU

\_\_\_\_\_

Assoc. Prof. Dr. Yasemin Arslan Udum  
Adv Tech., Gazi University

\_\_\_\_\_

Asisst. Prof. Dr. İrem Erel Göktepe  
Chem. Dept., METU

\_\_\_\_\_

**Date:** 27/10/2014

**I hereby declare that all information in this document has been obtained and presented in accordance with academic rules and ethical conduct. I also declare that, as required by these rules and conduct, I have fully cited and referenced all material and results that are not original to this work.**

Name, Last name: Ozan Erlik

Signature

## **ABSTRACT**

# **SYNTHESIS AND OPTOELECTRONIC APPLICATIONS OF BENZOTRIAZOLE AND DIBENZOSILOLE BASED ALTERNATING COPOLYMERS**

Erlik, Ozan

M.S., Department of Chemistry

Supervisor: Assoc. Prof. Dr. Ali Çırpan

October 2014, 109 pages

Dibenzosilole synonym of silafluorene based polymers have been extensively used as the donor moiety in D-A approach for several years for optoelectronic applications like electrochromic (EC) devices, organic light emitting diodes (OLEDs), organic field effect transistors (OFETs) and most widely organic photovoltaics (OPVs). Moreover, chalcogenophenes such as thiophene and selenophene are used as an energy bridge between the donor and acceptor units to adjust the electronic and optical properties of the conjugated polymers (CPs). In this study, benzotriazole moieties functionalized by different alkyl chains were used as the acceptor unit. Thiophene and selenophene groups were used as  $\pi$ -bridge molecules with their donor character. A silafluorene derivative was used as the donor molecule in the polymer backbone. In this manner, four different p-type conjugated polymers were synthesized via Suzuki coupling reaction. The electrochromic and photovoltaic studies of these polymers were performed. The thermal characterizations of these polymers were conducted using TGA (Thermal Gravimetric Analysis) and DSC (Differential Scanning Calorimetry) techniques. The redox behaviors of the polymers were investigated by CV (cyclic voltammetry) and optical properties were determined by UV-Vis spectrophotometer. In the device

fabrication, all components were integrated into ITO coated glass substrate in a moisture free glove box container. In this manner, power conversion efficiencies (PCE) of the polymer:PC<sub>71</sub>BM active layers were measured under standard AM 1.5 Global illumination (100mW/cm<sup>2</sup>). The highest PCE value was found as 2.57 % for **PBTBTSif** in the illumination of the photovoltaic studies.

**Keywords:** Benzotriazole, silafluorene, conjugated polymers, selenophene, organic solar cell, electrochemistry

## ÖZ

# BENZOTRIAZOL VE DİBENZOSİLOL TABANLI ALTERNATİF KOPOLİMERLERİN SENTEZİ VE OPTOELEKTRONİK UYGULAMALARI

Erlik, Ozan

Yüksek Lisans, Kimya Bölümü

Tez Yöneticisi: Doç. Dr. Ali Çırpan

Ekim 2014, 109 sayfa

Dibenzosilol, diğer bir deyişle, silafloren tabanlı polimerler optoelektronik uygulamalardan elektrokromik (EC) cihazlarda, organik ışık yayan diyotlarda (OLEDs), organik alan etkili transistörlerde (OFETs) ve daha çok organik fotovoltaiklerde (OPV) son yıllarda artan bir ilgiyle, D-A yaklaşımında donör olarak kullanılıyorlar. Ayrıca, konjüge polimerlerin (CP) elektronik ve optik özelliklerini ayarlamak adına, tiyofen ve selenofen gibi kalkojenofenler donör ve akseptör üniteleri arasında bir enerji köprüsü olarak kullanılmaktadırlar. Bu çalışmada, çeşitli alkil zincirleri ile fonksiyonlandırılmış benzotriazol üniteleri akseptör ünitesi olarak kullanıldı. Donör karaktere sahip tiyofen ve selenofen grupları  $\pi$ -köprüsü molekülleri olarak ayrı ayrı kullanıldılar. Bir silafloren türevi polimer omurgasında donör molekül olarak kullanıldı. Bu hususta dört farklı konjüge polimer Suzuki kenetleme reaksiyonu kullanılarak sentezlendi. Polimerlerin elektrokromik ve fotovoltaik çalışmaları yapıldı. Sentezlenen polimerlerin termal davranışları TGA (Termogravimetric Analiz) ve DSC (Diferansiyel Taramalı Kalorimetre) teknikleri kullanılarak gerçekleştirildi. Polimerlerin redoks davranışları dönüşümlü voltametri (CV) cihazı kullanılarak yapılırken optik özellikleri UV-Vis spektrofotometri yöntemiyle belirlendi.

Fotovoltaik cihaz yapımında kullanılan bütün malzemeler ITO kaplı cam yüzeye nemsiz ortam sağlayan eldivenli kabin içerisinde entegre edildi. Bu hususta birbirine harmanlanmış olan polimer PC<sub>71</sub>BM karışımının güç çevirim verimleri (PCE) bir standart olarak AM 1,5 G aydınlatma ile hesaplandı (100mW/cm<sup>2</sup>). Yapılan fotovoltaik çalışmalar ışığında en yüksek verim 2.57 % olarak **PBTBTSif** polimeri adına elde edildi

**Anahtar Kelimeler:** Benzotriazol, silafloren, konjüge polimerler, selenofen, organik güneş pili, elektrokimya

*To my precious family*

## ACKNOWLEDGEMENTS

I am grateful to my supervisor Assoc. Prof. Dr. Ali ırpan for his guidance, support, patience and endless care. I would like to thank Prof. Dr. Levent Toppare for his guidance and support.

I would like to thank TUBİTAK (113Z269) (Turkish Scientific and Technical Research Council) for the financial support.

I owe special thanks to Naime Akbařođlu Ünlü for her endless helps in every respect and also I want to thank Halil İbrahim Ünlü for his friendship.

Words are intimately meaningless to express my feelings, pleasure and gratefulness to their friendship, Seza Göker, Özde Ceren Hızal and Öykü Akçay. I owe them for their support.

I would like thank Şerife Özdemir Hacıođlu and Seda Çömez for their help in the electrochemical characterizations. I would like thank Gönül Hızalan for her help in the photovoltaic applications.

Many thanks to my childhood friends, Ömür Görgülü, Aliekber Yapar, Ethem Yapar, Turgay Topdal, Akın Bodrumlu, Onur Özden and Onurcan Ayhan for their priceless friendship.

Thanks go to all Cirpan and Toppare Research Group members for their cooperation.

Special thanks to Hande Ünay, Emre Ataođlu, Ahmet Özgür Saf, Şevki Can Cevher and Cansel Temiz for their friendship.

Endless thanks Nilay Aytaş for her patience, understanding, help and love. Finally, for their patience, support and favor, I would like thank my family.

## TABLE OF CONTENTS

ABSTRACT.....	v
ÖZ.....	vii
TABLE OF CONTENTS .....	xi
LIST OF TABLES.....	xv
LIST OF FIGURES .....	xvi
LIST OF SCHEMES .....	xx
LIST OF ABBREVIATIONS .....	xxi
CHAPTERS.....	1
MOTIVATION.....	1
INTRODUCTION .....	3
1.1. Introduction to Optoelectronic Systems .....	3
1.1.1. Electrochromism and Related Applications .....	3
1.1.2. Light Emitting Diodes .....	5
1.1.3. Field Effect Transistors .....	8
1.1.4. Photovoltaic Devices .....	9
1.1.4.1. Inorganic Solar Cells .....	10
1.1.4.2. Organic Solar Cells.....	10
1.1.4.3. Hybrid Solar Cells .....	11
1.2. Organic Solar Cells.....	12
1.2.1. Organic Semiconducting Materials .....	12
1.2.2. Band Theory .....	13
1.2.2.1. Band Gap Engineering.....	14
1.2.2.1.1. Bond Length Alternation .....	15
1.2.2.1.2. Aromaticity .....	16
1.2.2.1.3. Planarity .....	16
1.2.2.1.4. Substituent Effects .....	17
1.2.2.1.5. Intermolecular Influence.....	17
1.2.3. Donor Acceptor Approach.....	17

1.2.4. Doping Mechanism .....	18
1.2.5. Working Principles of an OPV .....	21
1.2.5.2. Exciton Diffusion and Generation of Free Charge Carriers.....	21
1.2.5.3. Charge Mobility and Collection at Electrodes .....	22
1.2.6. Device Architectures .....	23
1.2.6.1. Single Layer OPV .....	23
1.2.6.2. Bilayer OPV .....	24
1.2.6.3. Bulk Heterojunction (BHJ) OPV .....	25
1.2.6.4. Inverted Bulk Heterojunction OPV .....	26
1.2.7. Characterization of an OPV .....	27
1.2.8. Fundamental Parameter Affecting the OPV Efficiency .....	28
1.2.8.1. Short Circuit Current Density (Jsc).....	28
1.2.8.2. Open Circuit Voltage .....	29
1.2.8.3. Fill Factor .....	29
1.2.9. Palladium Mediated Cross Coupling Reactions.....	30
1.2.10.1. Benzotriazole Moiety .....	32
1.2.10.2. $\pi$ -Bridge Groups: Thiophene and Selenophene .....	32
1.2.10.3. Dibenzosilole based Polymers .....	33
1.2.11. Aim of the Study .....	34
EXPERIMENTAL .....	37
2.1. An Overview to Experimental Procedures and Techniques .....	37
2.2. Syntheses of the Monomers .....	38
2.2.1. Synthesis of 2-dodecylbenzotriazole (1).....	39
2.2.2. Synthesis of 4,7-dibromo-2-dodecyl-2H-benzo[d][1,2,3]triazole (2).....	39
2.2.3. Synthesis of 2-(2-octyldodecyl)-2H-benzo[d][1,2,3]triazole (3) .....	40
2.2.4. Synthesis of 4,7-dibromo-2-(2-octyldodecyl)-2H-benzo[d][1,2,3]triazole (4) .....	41
2.2.5. Synthesis of tributyl(thiophen-2-yl)stannane (5) .....	42
2.2.6. Synthesis of tributyl(selenophen-2-yl)stannane (6) .....	43
2.2.7. Synthesis of 2-dodecyl-4,7-di(thiophen-2-yl)-2H-benzo[d][1,2,3]triazole (7) .....	44

2.2.8. Synthesis of 2-dodecyl-4,7-di(selenophen-2-yl)-2H-benzo[d][1,2,3]triazole (8).....	45
2.2.9. Synthesis of 2-(2-octyldodecyl)-4,7-di(thiophen-2-yl)-2H-benzo[d][1,2,3]triazole (9).....	46
2.2.10. Synthesis of 2-(2-octyldodecyl)-4,7-di(selenophen-2-yl)-2H-benzo[d][1,2,3]triazole (10).....	47
2.2.11. Synthesis of 4,7-bis(5-bromothiophen-2-yl)-2-dodecyl-2H-benzo[d][1,2,3]triazole (11).....	48
2.2.12. Synthesis of 4,7-bis(5-bromoselenophen-2-yl)-2-dodecyl-2H-benzo[d][1,2,3]triazole (12).....	49
2.2.13. Synthesis of 4,7-bis(5-bromothiophen-2-yl)-2-(2-octyldodecyl)-2H-benzo[d][1,2,3]triazole (13).....	50
2.2.14. Synthesis of 4,7-bis(5-bromoselenophen-2-yl)-2-(2-octyldodecyl)-2H-benzo[d][1,2,3]triazole (14).....	51
2.3. Synthesis of Polymers .....	52
2.3.1. Synthesis of PTBTSif .....	52
2.3.2. Synthesis of PSBSSif.....	53
2.3.3. Synthesis of PBTBTSif .....	53
2.3.4. Synthesis of PBSBSSif .....	54
2.4. Electrochemical Studies .....	54
2.5. Spectroelectrochemical Studies .....	55
2.6. Kinetic Studies.....	55
2.7. Thermal Analyses .....	56
2.8. Solar Cell Applications.....	56
RESULTS AND DISCUSSION.....	59
3.1. Electrochemical Studies .....	59
3.2. Spectroelectrochemical Studies .....	64
3.3. Kinetic Studies.....	69
3.4. Thermal Analyses .....	72
3.5. Photovoltaic Studies .....	73
CONCLUSION .....	81
REFERENCES .....	83

APPENDIX A .....	89
NMR DATA.....	89
THERMAL ANALYSIS RESULTS .....	107

## LIST OF TABLES

### TABLES

Table 1. Summary of the electrochemical studies .....	62
Table 2. Summary of the spectroelectrochemical studies.....	69
Table 3. Summary of the Chronoamperometric Studies .....	72
Table 4. Summary of the photovoltaic studies .....	79

## LIST OF FIGURES

### FIGURES

Figure 1. Energy consumption trend from 1980 to 2030 .....	2
Figure 2. Literature examples of some organic electrochromic semiconductors.....	4
Figure 3. OLED structures .....	6
Figure 4. OLED structures .....	6
Figure 5. Working principle of an OLED .....	8
Figure 6. OFET device architecture .....	9
Figure 7. Band gap energy models for materials: a) metals; b) semiconductors; c) insulators .....	14
Figure 8. Band gap tuning model.....	15
Figure 9. Band gap tuning model.....	16
Figure 10. Hybridization of energy levels.....	18
Figure 11. Band model for trans-polyacetylene bearing to degenerate ground state	20
Figure 12. Proposed structures of polypyrrole.....	21
Figure 13. Förster and Dexter energy transfers.....	22
Figure 14. Working principle of an OPV 1) Excitation of donor upon absorption of light leading to exciton formation. 2) Exciton diffusion. 3) Charge separation 4) Migration of charges. 5) Collection of holes and electrons at anode and cathode electrons respectively .....	23
Figure 15. p-type Schottky device .....	24
Figure 16. Bilayer OPV structure.....	25
Figure 17. BHJ solar cell device structure. (The ordered structure is theoretical demanded arrangement of donor and acceptor molecules).....	26
Figure 18. Air Mass 1.5 Global standardization .....	28
Figure 19. Current-Voltage characteristics .....	30
Figure 20. An example of dibenzosilole based polymer.....	34
Figure 21. Synthesized Polymers.....	35
Figure 22. Synthesis of 2-dodecylbenzotriazole .....	39

Figure 23. Synthesis of 4,7-dibromo-2-dodecyl-2H-benzo[d][1,2,3]triazole .....	39
Figure 24. Synthesis of 2-(2-octyldodecyl)-2H-benzo[d][1,2,3]triazole.....	40
Figure 25. Synthesis of 4,7-dibromo-2-(2-octyldodecyl)-2H-benzo[d][1,2,3]triazole .....	41
Figure 26. Synthesis of tributyl(thiophen-2-yl)stannane .....	42
Figure 27. Synthesis of tributyl(selenophen-2-yl)stannane .....	43
Figure 28. Synthesis of 2-dodecyl-4,7-di(thiophen-2-yl)-2H-benzo[d][1,2,3]triazole .....	44
Figure 29. Synthesis of 2-dodecyl-4,7-di(selenophen-2-yl)-2H-benzo[d][1,2,3]triazole .....	45
Figure 30. Synthesis of 2-(2-octyldodecyl)-4,7-di(thiophen-2-yl)-2H-benzo[d][1,2,3]triazole .....	46
Figure 31. Synthesis of 2-(2-octyldodecyl)-4,7-di(selenophen-2-yl)-2H-benzo[d][1,2,3]triazole .....	47
Figure 32. Synthesis of 4,7-bis(5-bromothiophen-2-yl)-2-dodecyl-2H-benzo[d][1,2,3]triazole .....	48
Figure 33. Synthesis of 4,7-bis(5-bromoselenophen-2-yl)-2-dodecyl-2H-benzo[d][1,2,3]triazole .....	49
Figure 34. Synthesis of 4,7-bis(5-bromothiophen-2-yl)-2-(2-octyldodecyl)-2H-benzo[d][1,2,3]triazole .....	50
Figure 35. Synthesis of 4,7-bis(5-bromoselenophen-2-yl)-2-(2-octyldodecyl)-2H-benzo[d][1,2,3]triazole .....	51
Figure 36. Cyclic voltammograms of the polymers .....	60
Figure 37. Scan rate study of PTBTSif.....	63
Figure 38. Scan rate study of PSBSSif .....	63
Figure 39. Scan rate study of PBTBTSif .....	64
Figure 40. Scan rate study of PBSBSSif .....	64
Figure 41. Electronic absorption spectra of the PTBTSif in UV-Vis-NIR regions..	67
Figure 42. Electronic absorption spectra of the PSBSSif in UV-Vis-NIR regions..	67
Figure 43. Electronic absorption spectra of the PBTBTSif in UV-Vis-NIR regions	68
Figure 44. Electronic absorption spectra of the PBSBSSif in UV-Vis-NIR regions	68
Figure 45. Change in the percent transmittance for PTBTSif .....	70

Figure 46. Change in the percent transmittance for PSBSSif .....	70
Figure 47. Change in the percent transmittance for PBTBTSif .....	71
Figure 48. Change in the percent transmittance for PBSBSSif .....	71
Figure 49. Normalized film absorbance spectra for polymer and PCBM mixtures..	73
Figure 50. Relative thin film absorbance spectra of polymers.....	74
Figure 51. Current-Voltage characteristics of the PTBTSif.....	75
Figure 52. Current-Voltage characteristics of the PSBSSif .....	76
Figure 53. Current-Voltage characteristics of the PBTBTSif .....	76
Figure 54. Current-Voltage characteristics of the PBSBSSif .....	77
Figure 55. IPCE values of photovoltaic devices .....	78
Figure 56. Logarithmic J-V curve for the polymers .....	79
Figure 57. <sup>1</sup> H NMR result of 4,7-dibromo-2-dodecyl-2H-benzo[d][1,2,3]triazole (2) .....	89
Figure 58. <sup>1</sup> H NMR result of 4,7-dibromo-2-(2-octyldodecyl)-2H-benzo[d][1,2,3]triazole (4) .....	90
Figure 59. <sup>1</sup> H NMR result of tributyl(thiophen-2-yl)stannane (5).....	91
Figure 60. <sup>1</sup> H NMR of tributyl(selenophen-2-yl)stannane (6).....	92
Figure 61. <sup>1</sup> H NMR result of 2-dodecyl-4,7-di(thiophen-2-yl)-2H-benzo[d][1,2,3]triazole (7) .....	93
Figure 62. <sup>1</sup> H NMR result of 2-dodecyl-4,7-di(selenophen-2-yl)-2H-benzo[d][1,2,3]triazole (8) .....	94
Figure 63. <sup>1</sup> H NMR result of Synthesis of 2-(2-octyldodecyl)-4,7-di(thiophen-2-yl)-2H-benzo[d][1,2,3]triazole (9).....	95
Figure 64. <sup>1</sup> H NMR result of the 2-(2-octyldodecyl)-4,7-di(selenophen-2-yl)-2H-benzo[d][1,2,3]triazole (10) .....	96
Figure 65. <sup>1</sup> H NMR result of 4,7-bis(5-bromothiophen-2-yl)-2-dodecyl-2H-benzo[d][1,2,3]triazole (11) .....	97
Figure 66. <sup>13</sup> C NMR result of 4,7-bis(5-bromothiophen-2-yl)-2-dodecyl-2H-benzo[d][1,2,3]triazole (11) .....	98
Figure 67. <sup>1</sup> H NMR Result of 4,7-bis(5-bromoselenophen-2-yl)-2-dodecyl-2H-benzo[d][1,2,3]triazole (12) .....	99

Figure 68. <sup>1</sup> H NMR result of 4,7-bis(5-bromothiophen-2-yl)-2-(2-octyldodecyl)-2H-benzo[d][1,2,3]triazole (13).....	100
Figure 69. <sup>13</sup> C NMR result of 4,7-bis(5-bromothiophen-2-yl)-2-(2-octyldodecyl)-2H-benzo[d][1,2,3]triazole (13) .....	101
Figure 70. <sup>1</sup> H NMR result of 4,7-bis(5-bromoselenophen-2-yl)-2-(2-octyldodecyl)-2H-benzo[d][1,2,3]triazole (14) .....	102
Figure 71. <sup>1</sup> H NMR result of the PTBTSif .....	103
Figure 72. <sup>1</sup> H NMR result of PSBSSif .....	104
Figure 73. <sup>1</sup> H NMR result of PBTBTSif .....	105
Figure 74. <sup>1</sup> H NMR result of PBSBSSif.....	106
Figure 75. TGA result of PTBTSif .....	107
Figure 76. DSC result of PTBTSif .....	108
Figure 77. TGA result of PSBSSif .....	108
Figure 78. TGA result of PBTBTSif .....	109
Figure 79. DSC result of PBTBTSif.....	109

## LIST OF SCHEMES

### SCHEMES

Scheme 1. General reaction mechanism of a cross coupling reaction .....	31
Scheme 2. Synthetic route of monomers.....	38
Scheme 3. General synthesis mechanism of polymers .....	52

## LIST OF ABBREVIATIONS

EC	Electrochromic
CE	Coloration efficiency
LED	Light emitting diode
OLED	Organic light emitting diode
HOMO	Highest occupied molecular orbital
LUMO	Lowest unoccupied molecular orbital
OFET	Organic field effect transistor
PCE	Power conversion efficiency
CB	Conduction band
VB	Valence band
DA	Donor-Acceptor
OPV	Organic Photovoltaic
PET	Polyethylene terephthalate
ITO	Indium tin oxide
PSS	Polystyrenesulfonate
PEDOT	Polyethylene dioxythiophene
PCBM	[6,6]-Phenyl C 71 butyric acid methyl ester
BHJ	Bulk heterojunction
HIL	Hole injection layer
ETL	Electron transport layer
$\eta_e$	Power conversion efficiency
$J_{sc}$	Short circuit current density

$V_{oc}$	Open circuit voltage
FF	Fill factor
$P_{max}$	Maximum power
$P_{in}$	Power of the incident light
$R_{sh}$	Shunt resistor
$R_s$	Series resistor
AM 1.5G	Air mass 1.5 global
CV	Cyclic voltammetry
THF	Tetrahydrofuran
TBAPF <sub>6</sub>	Tetrabutylammonium hexafluorophosphate
ACN	Acetonitrile
NHE	Normal hydrogen electrode
$E_g^{op}$	Optic band gap
$E_g^{el}$	Electronic band gap
TGA	Thermal gravimetric analysis
DSC	Differential scanning calorimetry
UV	Ultraviolet
Vis	Visible
NIR	Near infrared
ICT	Intermolecular charge transfer
IPCE	Internal power conversion efficiency
EQE	External quantum efficiency

## **CHAPTER 1**

### **MOTIVATION**

The world population has been growing day by day. It seems that these new incomers have been adapted to this capitalist regime and hence sense of consumer society is fixed gradually in this manner. As a result of this, to meet the world energy need has become a controversial problem since natural sources have been consumed harshly by the humans. Moreover, energy demand shows parallelism in terms of level of development of the societies. Hereafter, International Energy Agency (IEA) predicts that developing economies will double their producing potential by 2020 to deal with their energy call. Furthermore, according to International Energy Outlook, increase in the energy consumption is foreseen as 23% in 2030 (Figure 1). In this manner, human beings have to find new energy sources other than the fossil fuels, nuclear energy and other insalubrious energy resources.<sup>1,2</sup> To address the renewable energy resources, although the hydroelectric power is the most widely used one, it is a limited source in terms of provision. Likely, wind power seems to be not meeting energy demand on the base of some estimates. For example, utilizable wind energy is 2-4 terawatt-years (TWyr) in total while it is foreseen that global energy consumption will increase from 13TWyr to 30 TWyr by 2050. On the other hand, solar energy serves a huge amount of power as 125,000 TW for the each impact to the earth surface. Thus, the rest of humanity is harvesting this solar power. One of the possible ways to utilize the solar energy is photovoltaic effect which converts the energy coming from sunlight into electrical power.<sup>[3]</sup>

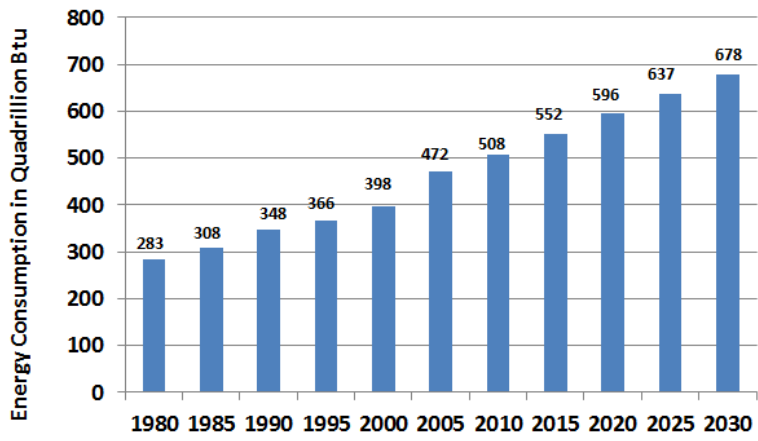


**Figure 1.** Energy consumption trend from 1980 to 2030

## INTRODUCTION

### 1.1. Introduction to Optoelectronic Systems

#### 1.1.1. Electrochromism and Related Applications

Electrochromism is the reversible alternation of the optical properties in the presence of an external electric field. In other words, if the color of materials shifts between two or more different colors via an electrochemical way, they are called as electrochromic (EC). Change in the color can occur not only between a transparent state and a colored state but also can happen between two colored states. When more than two redox states are available, EC devices show various colors and called as polyelectrochromics.<sup>4,5</sup> EC materials can be classified with respect to their optical properties. The first type of these materials goes back and forth between colored and transparent state. These materials are operable in absorption/transmission type appliances including smart windows and optical shutters. Examples are metal oxide films, viologens and organic polymers including poly(3,4-ethylenedioxy thiophene) (PEDOT). As to the second type of electrochromics including display technology, the goal would be attain two different colors without a bleached state. The most known example of this type of materials is polythiophene. The color of polythiophene is red in neutral state and blue in its oxidized state. The third and having most growing interest materials are conjugated macromolecules showing more than two different colors relying on their optical bands in a redox manner.<sup>6</sup> Furthermore, to obtain wide range color spectrum and produce flexible devices, organic ECs are designed and used at an increasing attention. Reynolds et. al. have reported several organic polymeric EC materials switching between different colors with a certain potential range showed in Figure 2.<sup>7</sup>

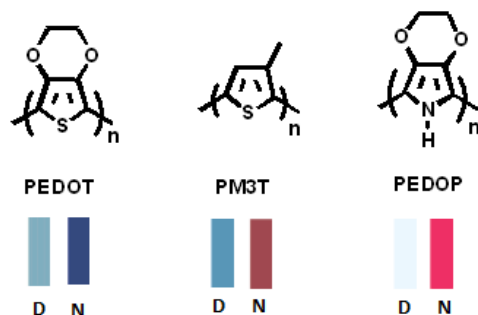


**Figure 2.** Literature examples of some organic electrochromic semiconductors

Several parameters affecting utility of an electrochromic device are available. These parameters are optical contrast, stability, switching time, coloration efficiency and optical memory.<sup>6,8,9,10</sup>

Firstly, optical contrast is an answer for the percent transmittance of an electrochromic device at various wavelengths on electromagnetic spectrum. Thus, the question is how much of the incoming light with a specific wave length is absorbed or reflected. In addition to this, by looking the cycles showing transmittance change, the optical stability of the materials at different potentials and bands on the spectrum can be observed.<sup>6</sup>

Secondly, stability is another factor affecting the electrochromic device efficiency. It is related with the degradation of the active matrix. This deterioration can be resulted from several reasons. One of them is an irreversible redox reaction. The other reason is the side products caused from electron loss or gain processes upon oxidation and reduction of the materials or contaminants. Another reason is caused by heat dissipation.<sup>6</sup>

Thirdly, switching time actually is known as the switching speed; the time for observing a change in the color of the materials during the oxidation and reduction processes. Switching time is affected by several factors including surface

characteristics of thin films, free charge conductivity of electrolyte and permission of ions to the surface of the thin films.

In the fourth place, coloration efficiency (CE) is an important parameter showing how well an electrochromic device works. It gives information on the power necessity. The transported charge per unit area ( $Q_d$ ) and change in optical density ( $\delta OD$ ) have to be known for the calculation of the CE value. Both CE and  $\delta OD$  are wavelength dependent functions.

$$\delta OD(\lambda) = \log[T_o(\lambda)/T_c(\lambda)]$$

$$\eta(\lambda) = \delta OD(\lambda)/Q_d$$

$\eta(\text{cm}^2/\text{C})$  is the efficiency of the CE and  $T_o$  and  $T_c$  are the transmittance values at the bleached and colored states respectively.<sup>6,8,9</sup>

Lastly, optical memory known as open-circuit stability is identified as the time to stay in the same absorption state with a certain color of the material with no external voltage. While solid state materials show high optical memory, materials in solution medium bleaches rapidly.<sup>10</sup>

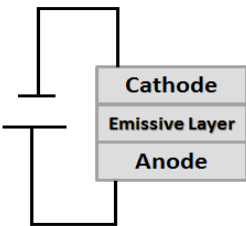
### **1.1.2. Light Emitting Diodes**

Lightening and display technology need too much power of electricity. In the matter of cope with this energy demand LEDs serve for a low cost technology. By comparison with the incandescent bulbs doing black body radiation and fluorescent tubes which release toxic gases, LEDs are eco-friendly light sources. Indeed, this technology has longer lifetime than other mentioned lighting sources.<sup>11</sup>

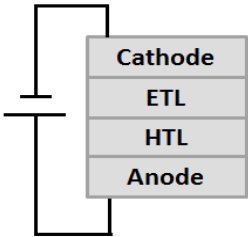
Diode is a circuit component which conducts the electrical current only in one direction. LEDs are semiconducting devices operating on the basis of p-n junction principle. The first known LED was made by H. J. Round in 1907 but first

commercial one was produced by Holonyak in 1962. This LED was based on the Ga/As/P (Galium, Arsenic and Phosphorous) inorganic semiconductors. Initially produced materials had been emitting only red light with long wavelength. By the improved technology, red and blue emitting diodes can be made also. Thus, by acquiring primary colors (RGB), white light emitting diodes can be produced and used for solid state lighting as well as obtaining wide range color spectrum.<sup>12</sup> Then, to overcome high cost production, organic counterparts have designed and produced as alternative to inorganic ones. Moreover by the invention of OLEDs (Organic Light Emitting Diodes) and PLEDs (Polymer Light Emitting Diodes) it is possible to manufacture flexible diodes. In OLEDs several device architectures are available as shown in Figure 3. An OLED can be designed in different ways as regards to differences in efficiency. The most efficient OLED structure is multilayer one due to the elimination of attenuation in exciton recombination and interruption in charge transport.<sup>13,14</sup>

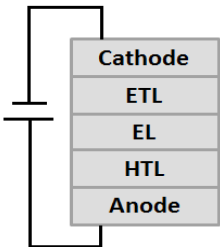
**A. Single Layer Device**



**B. Two-Layer Device**



**C. Three-Layer Device**



**D. Multilayer Device**

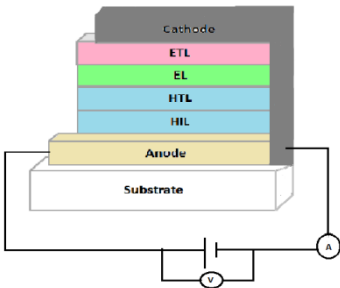


**Figure 3.** OLED structures

The working principle of an OLED is based on electroluminescence. Electroluminescence is the result of radiative recombination of electrons and holes in a semiconductor when subjected to an external electrical field. The emission of light can occur via fluorescence and/or phosphorescence. Moreover, the probability of existence of excitons on a triplet state is 75 % whereas probability on a singlet state is 25 %. Therefore, phosphorescence is desired for obtaining high quantum yields. These two processes illuminated in the ‘*Jablonski Diagram*’ was demonstrated in Figure 4.<sup>15,16</sup>

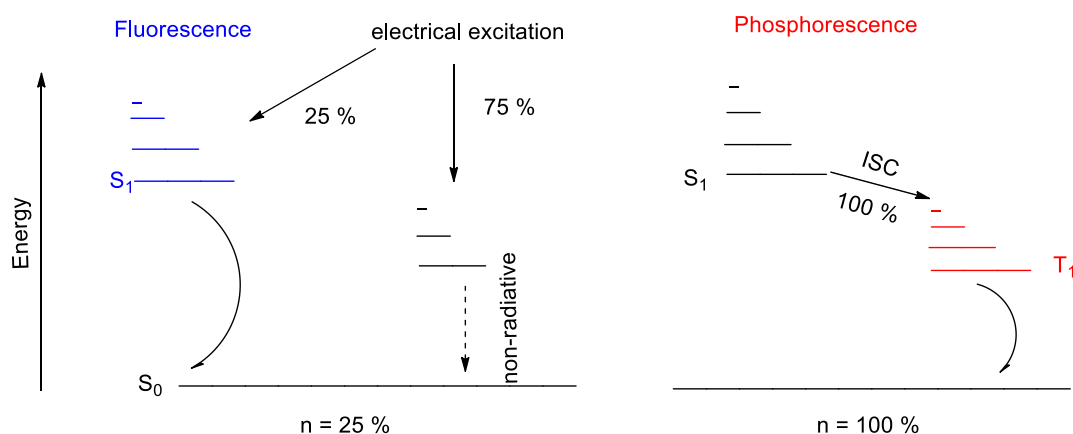


**Figure 4.** Representation of Fluorescent and Phosphorescent Processes. Internal quantum yield ( $n$ ) is very low for fluorescence with respect to phosphorescence

When an OLED is exposed to an electrical field, current circulate along the circuit. By the stimulation of electrodes on each side of the device, electrons from cathode with a low work function and holes from anode flow into active layer of the device. These two opposite charges re-combine at the interface of the emissive layer to form excitons and the light is emitted. The wavelength of emitted light depends on the band gap related with energetic position of the HOMO and LUMO energy levels of the semiconducting organic materials on the active layer. If more bright light is

demanded, the power of the current would be increased. The working principle of an OLED was illustrated in Figure 5.<sup>16</sup>

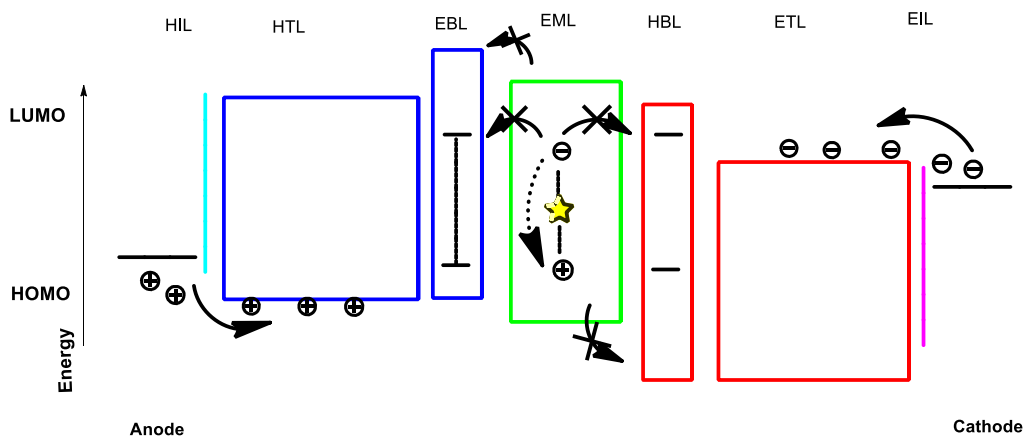


**Figure 5.** Working principle of an OLED

### 1.1.3. Field Effect Transistors

The originator and first patentee of field effect transistors is Lilienfeld.<sup>17</sup> Inorganic and organic transistors have manufactured until today. Inorganic ones are based on silicon and germanium whereas in organic field effect transistors semiconducting organic macromolecules are used. Today by the growing technology and improving knowledge about conjugated molecules, OFETs have become to run as amorphous silicon counterparts.<sup>17</sup>

The field effect transistors give a detailed idea about principles of the charge carrying properties of semiconducting materials. Although, field effect transistors can be classified into two main groups namely n-channel and p-channel in terms of their operating principle, ambipolar transistors are in demand recently. This means that both of the electrons and holes can be conducted.<sup>18</sup>

A field effect transistor includes several parts which are source, drain, dielectric material, semiconductor, gate and substrate. Gate is stimulated by a voltage and then by the effect of this voltage a p-channel arises between the insulator material and organic layer. In return, by applying a negative voltage between drain and source, positively charged particles go up to drain from source. The flowing rate of these holes is equipotent to current rate in the opposite direction. This current flowing continues until closing of the p-channel. By the saturation of the current on the drain hole mobility can be determined for a p-type OFET. The general representation of device architecture of an OFET was demonstrated in Figure 6.<sup>18,19</sup>

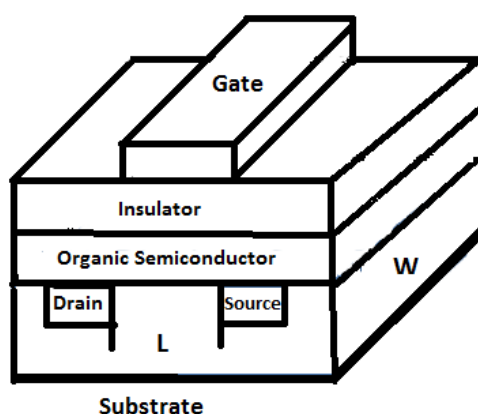


**Figure 6.** OFET device architecture

#### **1.1.4. Photovoltaic Devices**

Photovoltaics are devices converting the solar energy which is an inexhaustible energy source which can be converted to direct current electricity. The French scientist Alexandre Edmund Becquerel is the pioneer of the photovoltaics. In 1839, he found that an electrical current arises upon lightening an electrochemical cell. However, by the year of 1883 it has been realized that the solar energy can be converted to utilizable electrical energy.<sup>20,21</sup>

#### **1.1.4.1. Inorganic Solar Cells**

Silicon based solar cells which meet 90% of the worldwide solar energy production in today's world had been introduced in 1954 with 6% efficiency of a single crystal solar cell. Today, the highest efficiency with this type of solar cells has been reported as 27.6% by the single crystal materials and 20.4% by the polycrystalline devices. The key parameter in terms of efficiency is band gap. This value is 1.1 eV for silicon and this is the reason for preferring silicon based solar cells since the ideal band gap should be around 1.3 eV on the behalf of obtaining utmost quantum efficiency for single crystals. As an alternative to this single crystal silicon solar cells, inorganic thin film photovoltaic devices which are made of  $\text{Cu(InGa)Se}_2$  (CIGS) and CdTe type compounds are present to diminish the cost of the manufacturing. However, at the same time, via decreasing the thickness of the semiconducting layer, efficiency would decrease unfortunately. Above all else, by the development of technology, new multi-junction materials are designed and produced. Solar cell efficiency has reached to 43.5% by using concentrated multi-junction solar cells (GaInP/GaAs/GaInNAs). Because of the having high internal quantum efficiency, inorganic photovoltaic devices have high current density and high mobility of free charge carriers, these devices show good power conversion efficiency (PCE). However, these materials in the crystal form cannot be integrated onto flexible substrates. In addition to this, another problem arises from high production costs since it requires high temperatures for the integration of uncommon materials. Scientists seek for low-cost and high-efficiency hence, the researchers across the globe work on organic and hybrid solar cells recently.<sup>22, 23, 24</sup>

#### **1.1.4.2. Organic Solar Cells**

To cope with high prices for the production of optoelectronic devices, organic semiconductors including both macromolecules consisting of oligomers or polymers

and small molecules have been used in an increasing demand. These conjugated molecules have conductivity features owing to  $\pi$ -electron delocalization on their backbone. As a result of this  $\pi$ -electron delocalization electrons can be mobile through intermolecular or intramolecular bonds. The energy-gap of the organic conjugated molecules is within the 1.4-3.0 eV. The solar cell efficiency for organic semiconductors has been increased gradually. In this manner the cell efficiency which was below 10<sup>-5</sup>% in 1970s, is up to 10-12% recently.<sup>25</sup> In fact, by using tandem type organic solar cells this value can be enhanced to 15%.<sup>26</sup> Organic solar cells have been manufactured using solution processable conjugated polymers and thermally deposited small molecules. Solution processable small molecules have been widely applied for organic solar cells devices in recent years because they show strong absorption properties, and they can be easily purified and deposited onto flexible substrates at low cost.<sup>25,26,27</sup>

#### **1.1.4.3. Hybrid Solar Cells**

Since the inorganic solar cells are not cost effective and organic counterparts are not efficient as them, hybrid solar cells including both organic and inorganic semiconductors are key solutions for these problems. By the integration of the organic molecules on the inorganic surfaces, the flexible and solid devices can be produced in line with the requirements. In the heterojunction (HJ) device architecture, organic molecules are used for absorbers and inorganic ones are utilized as the acceptors of the active layer. In this system, inorganic materials are responsible for the electron transport process and organic layer provides the hole mobility. While organic layer brings in flexibility, low-cost production and light weight, inorganic part enables long term stability and enhanced electron mobility. Acceptor materials are fullerene derivatives in organic photovoltaic devices whereas in hybrid cells electron acceptors are nanocrystals. Acceptor materials can present as quantum dots as colloidal forms in organic layers and also they could be nanoparticles as mixed with polymers.<sup>28,29,30</sup>

## 1.2. Organic Solar Cells

### 1.2.1. Organic Semiconducting Materials

Organic semiconducting materials can be either small molecules or macromolecules including oligomers and polymers. The difference between the large molecules and the small ones results from the conjugation length and manufacturing process of them. Polymers are preferred instead of the small molecules because they are solution processable. Carbon is a tetravalent atom and its saturated molecules are bearing  $sp^3$  hybridization. However,  $sp^2p_z$  hybridization is valid for conjugated polymers. In this system, one s and two p orbitals participate in the hybridization and half-filled  $p_z$  orbitals are responsible for the formation of the  $\pi$ -bonds. An electron delocalization is present on the polymer backbone due to the alternating arrangement of double and single bonds. As a result of this  $\pi$ - electron delocalization, electron can move one bond to the other bond which enables these polymers to gain conductivity.<sup>31,32</sup>

The history of the conductive polymers dates back to 1960s. In those years, in two different continents, scientists had been studying on the conductive polymers. MacDiarmid and Heeger from USA were investigating on conductivity of polythiazyls  $(SN)_n$  as metallic inorganic polymers. Electrical conductivity of this type of polymers diminishes with increasing temperature. On the other hand, by cooling the polymer down to approximately  $-263\text{ }^\circ\text{C}$ , polymeric sulfur nitride becomes a superconductor.<sup>33,34</sup> At the same time with investigations on the inorganic polymer conductivities, in the far east Japanese chemist Hideki Shirakawa was found out incidentally an important mechanism about synthesizing polyacetylene thin films. He mistakenly used too much Ziegler-Natta catalyst for the polymerization of acetylene. Thus, he obtained polymeric thin films instead of a polymeric powder. Because of the insoluble character of this polymer, only an IR spectrum could be taken. Thus, it was clarified that the selectivity on the formation of trans and cis forms of the polyacetylene rely on the temperature. As a result of

these studies, via altering the temperature polymer in demand with respect to stereochemistry of polyacetylene could be obtained. The alternation in the stereochemistry would lead to differences in resistivity to electric current.<sup>35</sup> Later, these three scientists came together and they started to work on polyacetylenes. The polyacetylene films were exposed halogen vapors. Firstly, bromine vapor was used for doping of the films. Then, chlorine and iodine were used respectively. The best result as  $38 \text{ Scm}^{-1}$  was obtained by using iodine vapor. Thus, first organic polymer which shows conductivity as comparable with the metallic conductivity was synthesized. This work has ushered a new age on conductive polymers. Therefore, these three scientists were awarded with Nobel Prize in chemistry '*for the discovery and development of the conducting polymers*'<sup>35,36,37</sup>

### **1.2.2. Band Theory**

The conductivity of materials is directly related with their band gap value. Band gap of the materials is defined as the energy difference between HOMO (Highest Occupied Molecular Orbital) level and LUMO (Lowest Unoccupied Molecular Orbital) energy level. In other words, it is the energy gap between conduction band (CB) and valence band (VB) of the materials.<sup>39</sup>

Materials are classified as conductors, insulators, or semiconductors according to their electric conductivity. In a conductor, the valence band is partially filled, and since there are numerous empty levels, the electrons are free to move under the influence of an electric field; thus, in a metal the valence band is also the conduction band. On the other hand, insulator materials have large energy gap between HOMO and LUMO energy levels and in this type of materials, valence band is completely filled and conduction band is completely empty so they do not have electrical conductivity. In a semiconductor, the valence band and conduction band are separated from each other by a small energy gap. Valence band is completely empty and conduction band is completely filled in semiconducting materials. Electrons can

move to the conduction band from valence band by the enhancing the Fermi level.<sup>40</sup>  
 The band energy structures are shown in Figure 7.

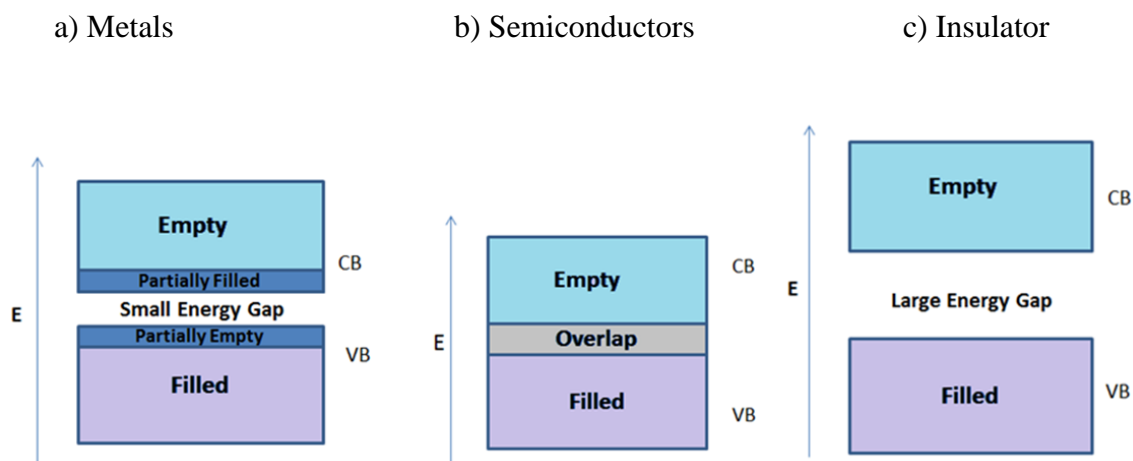


**Figure 7.** Band gap energy models for materials: a) metals; b) semiconductors; c) insulators

### 1.2.2.1. Band Gap Engineering

Electronic properties of semiconducting polymers can be altered by tuning the band gap of the materials. This process also called band gap engineering depend on several factors so that band gap of these delocalized systems can be explained as sum of the five main parameters namely, bond length alternation ( $E_{BLA}$ ), aromaticity ( $E_{Res}$ ), planarity ( $E_{\theta}$ ), substituents ( $E_{Sub}$ ), intermolecular interactions ( $E_{int}$ ) (Figure 8).<sup>42</sup>

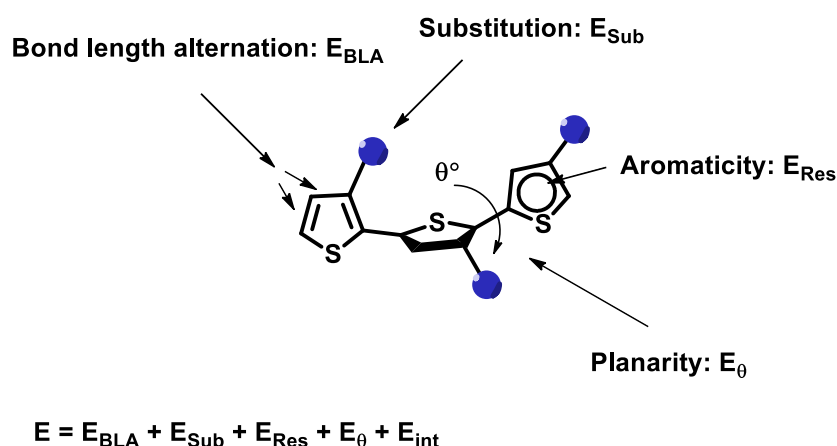


**Figure 8.** Band gap tuning model

#### 1.2.2.1.1. Bond Length Alternation

Conjugated heterocyclic polymers with non-degenerate ground states are present in two forms having different energies. One of them is aromatic form and the other one is quinoid form. In a molecule bearing aromatic form can be converted into quinoid form via  $\pi$ -electron delocalization. Aromatic form is energetically less stable than the quinoid form due to the increase in the stabilization energy. The relation between these two states is stereotyped in a mathematical expression called as bond length alternation (BLA). If a conjugated polymer is mainly subjected to aromatic form, the energy value of the BLA increases leading to a larger band gap. On the other hand, by increasing quinoid character on the backbone, BLA value decreases due to the increase in the double bond nature between the two adjacent rings. Decrease in the BLA value brings in lowering the band gap energy. For example, in polyphenylene, benzene rings are predominantly in the aromatic structure. However by the insertion of the double bonds between the rings quinoid character can be increased. This relation is shown in Figure 9.<sup>43</sup>

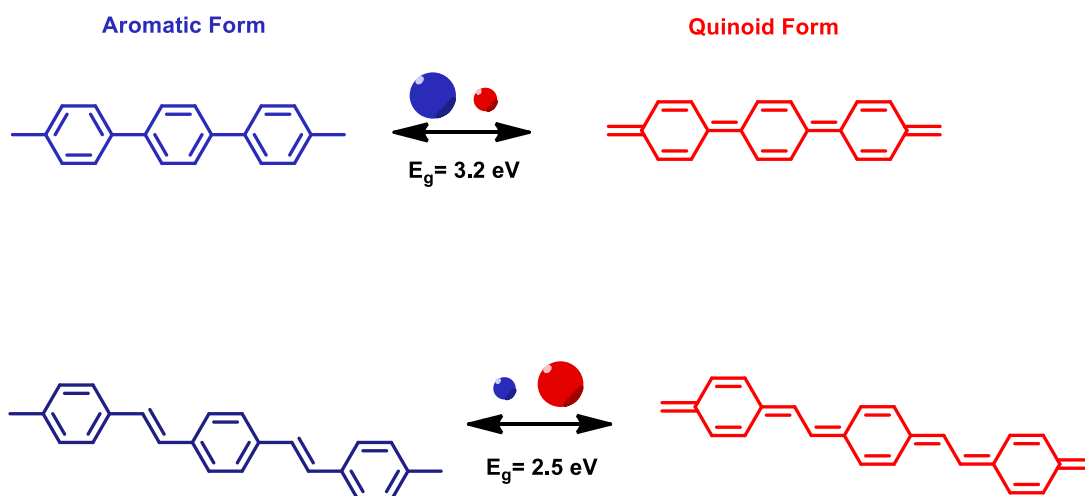


**Figure 9.** Band gap tuning model

#### 1.2.2.1.2. Aromaticity

As the aromaticity increases in the polymer chain, band gap of the molecules also increases since the aromaticity restrains the electrons on the ring due to the  $\pi$ -electron delocalization. Therefore electrons are not mobile enough and this leads to distortion on the conjugation length.<sup>44</sup>

#### 1.2.2.1.3. Planarity

If p orbitals are as perpendicular to each other, electron delocalization and so conjugation are interrupted. Therefore, planarity decreases the bond length alternation energy leading to lower energy difference between the HOMO and LUMO energy levels. Energy gap is inversely proportional to conjugation length. As the conjugation length increases, band gap of the materials decreases. However, this process is limited by a saturated effective conjugation after which the reduction on the band gap is negligible.<sup>43,44</sup>

#### **1.2.2.1.4. Substituent Effects**

Polymer substitution with different functional groups has been found to be one of the ways to achieving suitable band gap, as the electronic structure and correspondingly the optical property of the polymers can be adjusted. Electron withdrawing group contributes to both an increase in electron affinity and ionization potential. Electron donating groups reduces band gap by raising the HOMO energy level.<sup>45,46</sup>

#### **1.2.2.1.5. Intermolecular Influence**

Molecules in the solid state reveal lower band gap than that of the materials in the solution phase. Solid state brings about a more ordered crystalline structure leading to an increase in the intermolecular interactions and also enhancing the  $\pi$ - $\pi$  stacking causing red shift on the ground state spectrum and lower the band gap.<sup>46,47</sup>

#### **1.2.3. Donor Acceptor Approach**

Donor-Acceptor (D-A) approach was offered for the first time by Hovee and co-workers in 1963. This modality for conjugated molecules is widely used for tuning the HOMO and LUMO energy levels and thus the band gap of the materials. In this approach, there are two different moieties showing distinct electronic characteristics. While donor moiety is electron rich, the acceptor group has an electron deficient nature.<sup>48</sup> The main purpose of this method is lowering the band gap that is acquired by the hybridization of the HOMO and LUMO energy levels of the donor and acceptor molecules. Thus, new HOMO and LUMO levels arises for the conjugated polymer showed in Figure 10.<sup>49</sup>

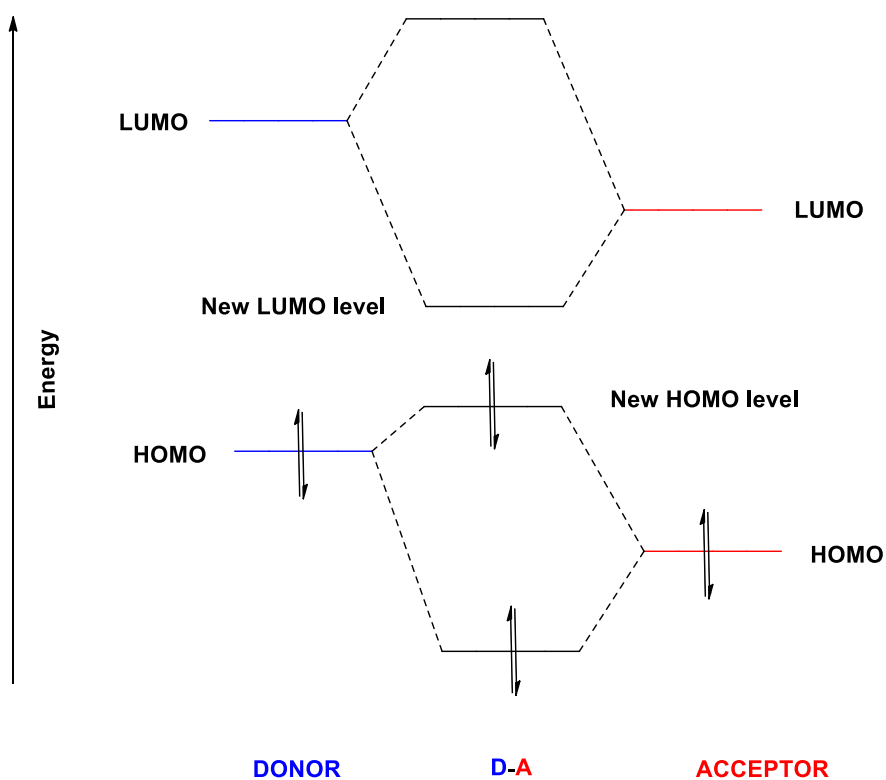
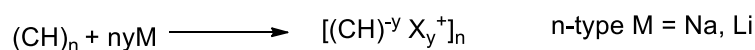
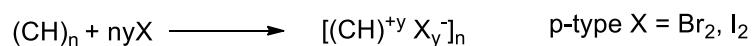


**Figure 10.** Hybridization of energy levels

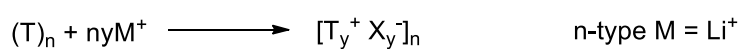
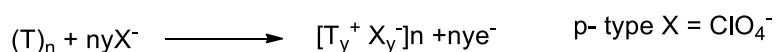
#### 1.2.4. Doping Mechanism

Conjugated polymers are not conductive in their ground state since electrons are not delocalized along the polymer chains. In order to obtain electrical conductivity free charge carriers are required. Therefore, to make the conjugated polymers gain electrical conductivity, the strategy called as ‘doping’ is applied. Doping process can be done by either n-doping or p-doping. If electrons are removed from the polymer this doping process is called as p-doping since positive charges come up. On the other hand, when electrons are injected to the polymer backbone, negatively charged anions arise as n-doping process. After all, these negatively or positively charged particles are neutralized by dopants. This mechanism is demonstrated in detail in following scheme.<sup>50</sup>

### Chemical doping of polyacetylene



### Electrochemical doping of polythiophene



In doping process, it is very important that the polymers sustain their original structure with no degradation on the polymer backbone. This reversibility specifies the polymer whether it can be used for electrochromic applications or not.<sup>51</sup>

By the redox reactions, electrons are either removed or added. As a result of this, while solitons form for having degenerate ground state molecules like polyacetylene, for the common heterocyclic conjugated polymers with non-degenerate ground states polarons and bipolarons arise.

Su and co-workers suggested a form on structural defects resulting from the formation of the free radicals on the backbone during the polymerization of polyacetylene. This proposed structure is called as soliton. Moreover, negatively and positively charged solitons form upon reduction and oxidation processes respectively (Figure 11).

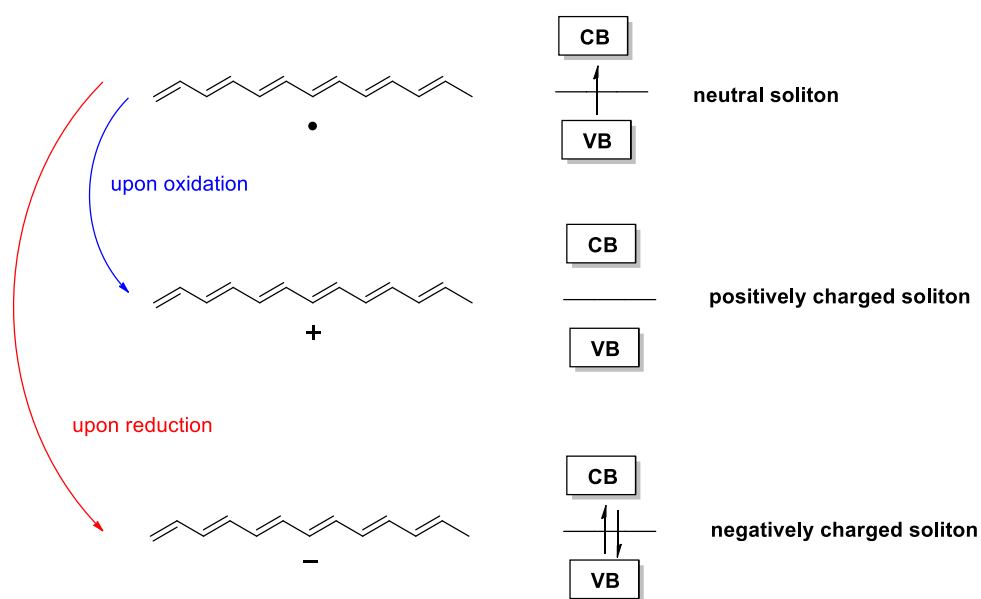


**Figure 11.** Band model for trans-polyacetylene bearing to degenerate ground state

Unlike the polyacetylene band structures, heterocyclic compounds have non-degenerate ground state energy. By the ionization of these polymers, radical ions called as polarons are formed as radical anions or radical cations. However, in theory a model with more stable forms called as bipolarons is available. This dication and dianion structures are the main components for the electrical conductivity. Polaron and bipolaron bands of polypyrrole (PPy) were showed as well as neutral state in Figure 12.<sup>51,52</sup>

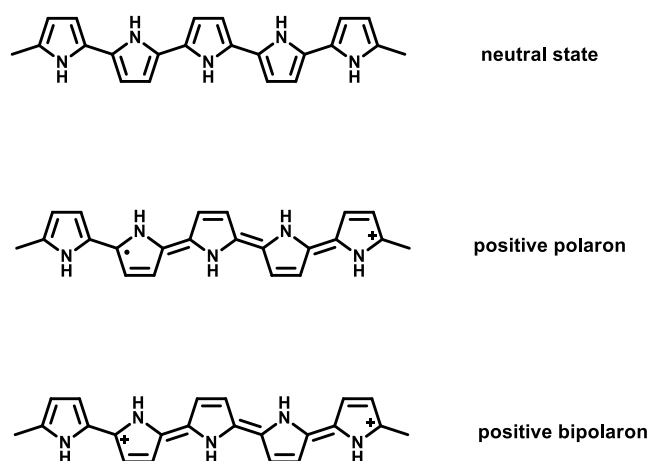


**Figure 12.** Proposed structures of polypyrrole

## 1.2.5. Working Principles of an OPV

### 1.2.5.1. Exciton Formation by Photogeneration Process

The efficiency of organic photovoltaic devices is directly related with the photon absorption process of the conjugated polymers in the active layer. When the sunlight is absorbed, electron-hole pairs called excitons are formed instead of formation of the free charge carriers. These excitons are Frenkel excitons and localized to the molecule, hence an extra amount of energy, termed as exciton binding energy is needed to produce free charge carriers. The exciton binding energy in commonly used organic materials (polymer, oligomers, small molecules) ranges from 0.3 to 1.4 eV.<sup>53,54,55</sup>

### 1.2.5.2. Exciton Diffusion and Generation of Free Charge Carriers

Excitons do not dissociate to free charge carrier at ambient temperature spontaneously due to their high binding energies and it needs an extra energy. An acceptor molecule like fullerene is required for obtaining a junction point to bring in electrostatic forces at the interface of donor and acceptor type polymers. Excitons have to find an interface just before fall back to the ground state since exciton

diffusion length is limited to a range of 5-20 nm which restricts the thickness of the active layer. As the thickness of the active layer increases, number of photons harvested will also increase however there will be also an increase in the loss of excitons due to the recombination resulted from the limited exciton diffusion length.<sup>53,54,55</sup>

The exciton diffusion is determined in two ways as regards to singlet or triplet states. Singlet state exciton diffuses via a mechanism called Förster resonant energy transfer (FRET) which is a long-range energy transfer including dipole-dipole coupling of transition states. On the other hand, Dexter energy transfer is an electron exchange mechanism and it is allowed for only singlet-singlet and triplet-triplet energy transfers. The latter is slower than the former process. These mechanisms were showed in Figure 13.<sup>55,56</sup>

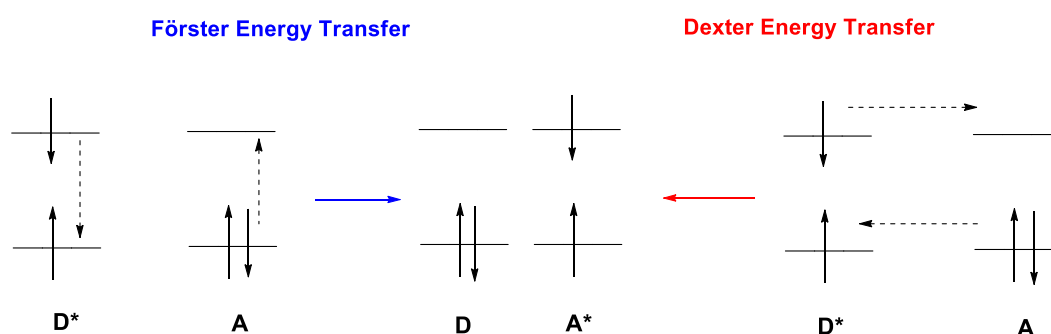


**Figure 13.** Förster and Dexter energy transfers

### 1.2.5.3. Charge Mobility and Collection at Electrodes

Free charges move to the opposite electrodes with different work functions to complete the circuit. This transport mechanism is related with the ability of charge carrier mobility. Inorganic materials have ordered crystalline structures leading to high charge carrier mobilities in the range of  $10^2$ - $10^3$   $\text{cm}^2/\text{Vs}$ . On the other hand,

organic materials have narrower bands and amorphous non-ordered surfaces resulting in low mobility. Moreover, formation of polarons is another factor reducing the charge mobility due to the requiring of hopping of charges.<sup>55</sup>

The general working principle from photogeneration to charge collection was showed in Figure 14.<sup>54</sup>

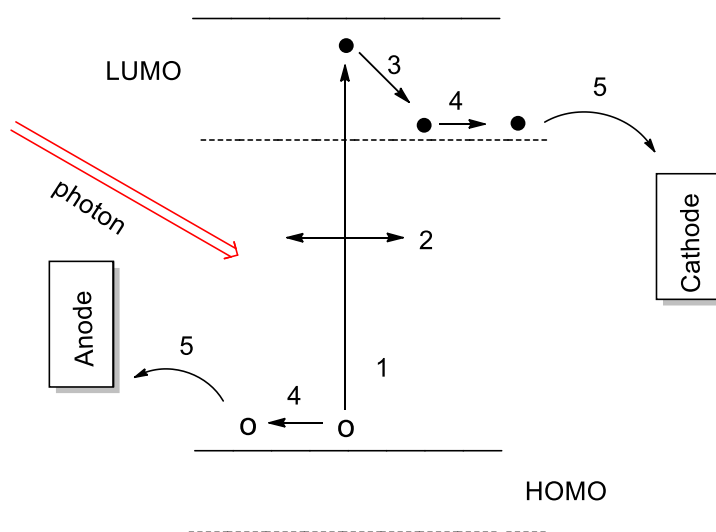


**Figure 14.** Working principle of an OPV 1) Excitation of donor upon absorption of light leading to exciton formation. 2) Exciton diffusion. 3) Charge separation 4) Migration of charges. 5) Collection of holes and electrons at anode and cathode electrons respectively

## 1.2.6. Device Architectures

### 1.2.6.1. Single Layer OPV

The original organic photovoltaics were constructed by using single layer organic molecules located between the metal electrodes having distinct work functions. Schottky model is used for the explanation of operating principle of the single layer

organic solar cells. In this model, a Schottky barrier arises between an organic layer bearing an electron donor character and an electrode close to the vacuum level energetically. As the exciton diffusion length is restricted at about 10 nm, the charges dissociate only in these distances from the p-type semiconducting material to the electrode contribute to the electrical conductivity. In addition to this, the only force for dissociation of excitons into free charges arises from the electrostatic forces between the electrodes. As this force is not sufficient for the dissociation, efficiency of this type of solar cells is very low. A Schottky type OPV was showed in Figure 15.<sup>57</sup>

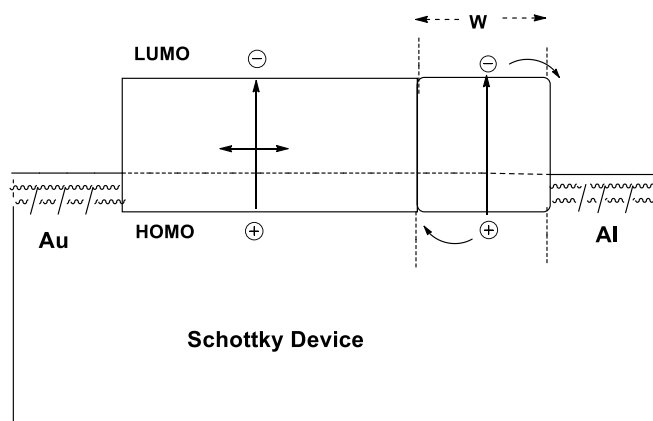


**Figure 15.** p-type Schottky device

### 1.2.6.2. Bilayer OPV

In this type solar cell structure, separately p-type and n-type two organic layers are superposed on each other. There is a junction point at the interface of the p-type donor molecule and n-type acceptor molecule and excitons can be dissociated at this donor-acceptor interface. However, because of the low exciton diffusion length, most of the generated excitons cannot reach to the interface and recombination takes place leading to low efficiency. Therefore, thickness of the active layer for the effective photon absorption cannot be increased. Figure 16 demonstrates bilayer architecture. In this structure, substrate is either a rigid glass or flexible polymer

such as PET. ITO is used for the transparent anode electrode. PEDOT:PSS is hole injection layer and it is used also for smoothing the ITO surface. Polymer is donor material and PCBM is the acceptor molecule derived from Buckminsterfullerene. Lastly, aluminum is utilized as the cathode.<sup>58</sup>

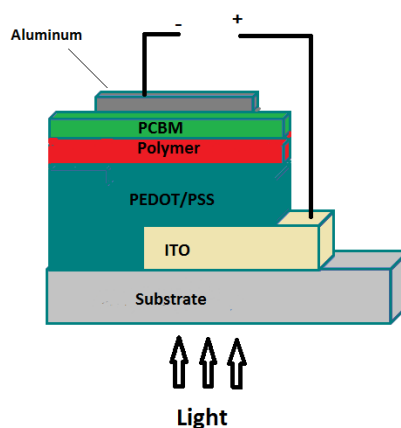


**Figure 16.** Bilayer OPV structure

### 1.2.6.3. Bulk Heterojunction (BHJ) OPV

The bulk heterojunction concept has come as a solution to problems resulting from low exciton diffusion distances. In this system, donor polymer and acceptor PCBM is in active layer blend and so surface of the interface between the donor and acceptor molecules increases leading to a decrease in the recombination of excitons. As a principle, when the light is absorbed, the electron hole pairs called exciton forms. Excitons migrate in a small distance and find an interface. At this junction point, electrons and holes stay together as a boundary are separated from each other. As the free charges, electrons go to the cathode (aluminum) through the electron injection layer (LiF) and positively charged holes are collected on anode; indium tin oxide (ITO). Thus, the circuit is completed and current is formed. Bulk heterojunction solar cells are classified in two structures with respect to their active layer order (Figure 17).<sup>58,59</sup>

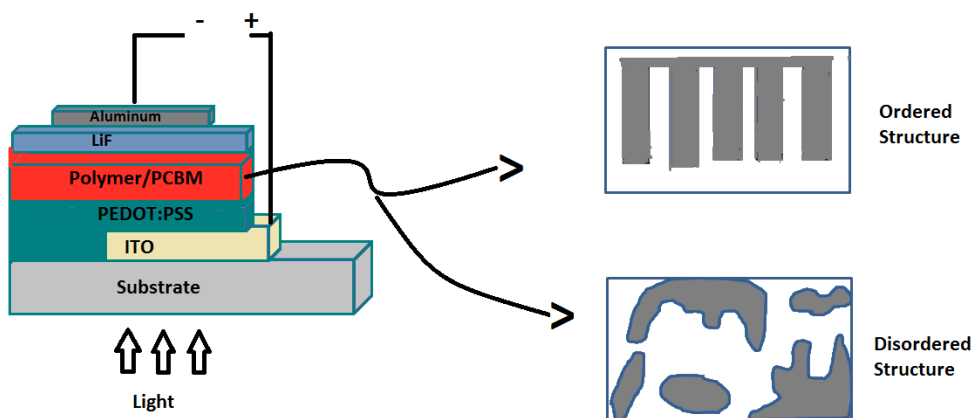


**Figure 17.** BHJ solar cell device structure. (The ordered structure is theoretical demanded arrangement of donor and acceptor molecules)

#### 1.2.6.4. Inverted Bulk Heterojunction OPV

The original BHJ system is in the form of Anode/HIL/Polymer blend/EIL/Cathode. Most commonly, PEDOT:PSS is used for HIL (hole injection layer), and Ca or LiF are used for the EIL (electron injection layer). The problem with this regular heterojunction structure results from acidic PEDOT:PSS and metals with low work function. PEDOT:PSS degrades the surface of the anode leading to instability for the device. In addition to this, materials like LiF can be oxidized easily due to low work function resulting in enhancing the series resistance and so decrease the device efficiency. To overcome these problems, inverted bulk heterojunction solar cells have been designed. In this type of devices, dual character of the indium tin oxide is taken advantage where work function value is between the band gap values of mostly used organic molecules. It means that ITO can be used not only for hole collector but also can be used for the electron taker. In this approach, ITO can be modified by integrating alkali metals with low work function onto the ITO surface leading to reducing work function of ITO. On the other hand cathode is replaced by the high work function metal oxides coated with silver or gold.<sup>60</sup>

### 1.2.7. Characterization of an OPV

The efficiency of an organic solar cell relies on the current and voltage values of the circuit. In the cell efficiency determination, dark current value is measured as well as quantification of the current under light. The photovoltaic power conversion efficiency (PCE) is identified according to the given formula;

$$\eta_e = \frac{P_{\max}}{P_{\text{in}}} \quad \text{FF} = \frac{J_{\max} * V_{\max}}{I_{\text{sc}} * V_{\text{oc}}} \quad P_{\max} = V_{\text{oc}} * J_{\text{sc}} * \text{FF}$$

$\eta_e$  is the PCE value,  $V_{\text{oc}}$  is open circuit voltage,  $I_{\text{sc}}$  is short circuit current,  $P_{\text{in}}$  is the incident light and FF is the fill factor. The all measurements are standardized to AM (Air Mass) 1.5 Global.<sup>58</sup>

#### Air Mass

During the passage of the sunlight through the atmosphere, solar power is reduced by scattering, reflection and absorption due to the gas clouds, dusts and water vapor. This attenuation resulting from the atmosphere is called as air mass (AM) and sunlight hits into the earth surface with  $48.2^\circ$  with respect to the zenith angle (Figure 18).<sup>61</sup>

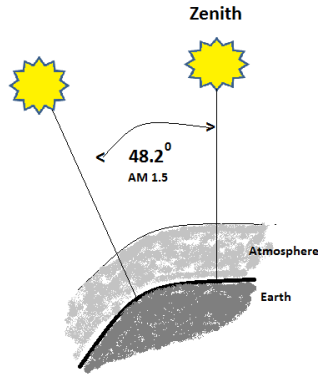


**Figure 18.** Air Mass 1.5 Global standardization

## 1.2.8. Fundamental Parameter Affecting the OPV Efficiency

### 1.2.8.1. Short Circuit Current Density ( $J_{sc}$ )

Short circuit current density ( $J_{sc}$ ) is the generated current in the circuit when no external potential is present. The  $J_{sc}$  is directly related with external quantum efficiency (EQE) which is the ratio of the number of photons incident on a solar cell to the number of generated charge carriers. Then,  $J_{sc}$  is directly depending on the EQE parameters. ( $EQE = \eta_{abs} * \eta_{diff} * \eta_{diss} * \eta_{tr} * \eta_{cc}$ )<sup>62,63</sup>

$\eta_{abs}$  is a parameter related with the light absorption efficiency. Absorption of incoming light depends on the energy difference between the HOMO and LUMO levels and molar extinction coefficients of the materials as well as emissive layer density.<sup>64,65</sup>

$\eta_{diff}$  is defined as capability related with diffusion of the electron-hole pairs to the donor-acceptor interface. The surface characteristics and orderliness on the active layer are main parameters affecting the diffusion performance.<sup>66,67</sup>

$\eta_{\text{diss}}$  is illustrated with dissociation efficiency of excitons. The donor-acceptor interface brings about a junction point creating a force to break the boundary between the hole and electron. This force should exceed exciton binding energy which is about 0.3 eV.<sup>63,67</sup>

$\eta_{\text{tr}}$  is the charge transfer efficiency and it is known that the migration of charges in the active layer is explained via *hopping* process influenced by defects on the active layer and recombination of the excitons.<sup>63,68</sup>

$\eta_{\text{cc}}$  is the efficiency related with the ability of electrodes to charge collection. This parameter depends on the electronic characteristics of the used electrodes. For example, the work function of cathode electrode should be larger than electron affinity of the acceptor molecule and ionization potential energy of the donor material should exceed the work function value of the anode electrode.<sup>63</sup>

### 1.2.8.2. Open Circuit Voltage

$V_{\text{oc}}$  is defined as the measured potential between two electrodes when the current value is zero. There are some empirical approximations to explain this phenomenon with tangible data. Brabec and co-workers suggested a strategy in 2001 to identify the  $V_{\text{oc}}$  value of the materials in which it is the energy difference between HOMO of the donor and LUMO of the acceptor molecules. By the Scharber's studies on this issue, a formula identifying the experimental  $V_{\text{oc}}$  value was obtained in 2006.<sup>69,70</sup>

$$V_{\text{oc}} = (1/q) [E(\text{HOMO})_{\text{donor}} - E(\text{LUMO})_{\text{acceptor}}] - 0.3 \text{ V}$$

### 1.2.8.3. Fill Factor

Fill factor is the main parameter determining the power conversion efficiency. It is the relation between the recombination and transportation of the charge carriers. As the recombination increases fill factor decreases. The FF is defined as the ratio of

the maximum power from the solar cell to the product of  $V_{oc}$  and  $J_{sc}$ . Graphically, the FF is a measure of the "squareness" of the solar cell and is also the area of the largest rectangle which will fit in the IV curve. The FF is illustrated in Figure 19. Fill factor depend on the diode quality so that it deviates from the theoretical ideal value because of the physical parameters. This reduction from the ideal value is explained by fluctuations on the series resistance ( $R_s$ ) and shunt resistance ( $R_{sh}$ ). Series resistance should be zero for an ideal diode and if its value increases there would be a reduction on the fill factor. On the other hand, to get the ideal fill factor value, shunt resistance should be infinite. As the shunt resistance reduces, alternative current paths arises that cause reduction in the current through the cell.<sup>63</sup>

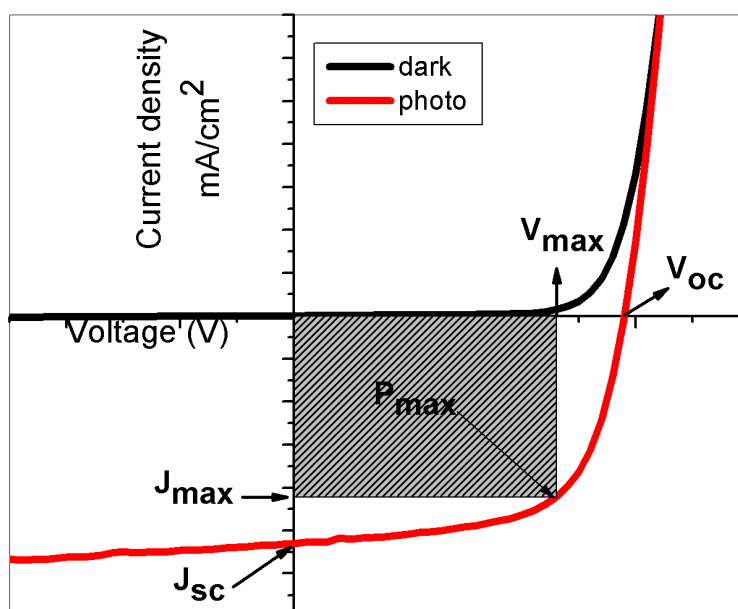
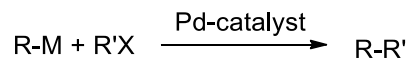


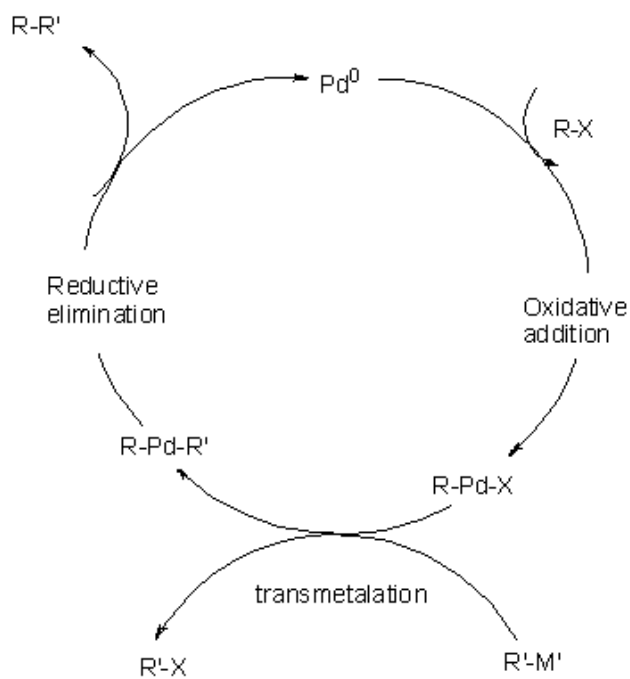
**Figure 19.** Current-Voltage characteristics

### 1.2.9. Palladium Mediated Cross Coupling Reactions

Cross coupling reactions provide wide range synthesis opportunity by using organometallic compounds. These reactions are summarized by the given equation;



The production of conjugated polymers occurs through the formation of the new carbon-carbon sigma bonds. In the cross coupling reactions, firstly, an oxidative addition reaction of a transition metal (palladium) occurs into the R-X bond. Then, a transmetalation reaction takes place between the organohalide compound and organometallic reagent. Lastly, organo addition reaction arises. (Scheme 1) <sup>43,72</sup>



**Scheme 1.** General reaction mechanism of a cross coupling reaction

## 1.2.10. Moieties in Donor-Acceptor Approach: Toward the High Efficiency

### 1.2.10.1. Benzotriazole Moiety

Since benzotriazole unit bears diimine moiety, it is a moderate electron deficient unit with respect to the mostly used electron acceptor units such as benzothiadiazole and quinoxaline. However, nitrogen atom has trivalent character and so benzotriazole can be functionalized through this atom. By the alkyl chain attachment on the moiety, solubility problem can be overcome and also electron donating character of the alkyl chains can be modified.<sup>73,74</sup> Since the first benzotriazole synthesis by Tanimoto and Yamamoto<sup>75</sup>, this unit has been used for the optoelectronic applications. Recently, using a benzotriazole derivative as an acceptor group, You and co-workers have obtained the power conversion efficiency exceeding 7% in their cell design in 2011.<sup>76</sup>

### 1.2.10.2. $\pi$ -Bridge Groups: Thiophene and Selenophene

Sulfur and selenium are among the group 16 atoms which are called as chalcogens. The electron donor  $\pi$ -bridge cyclic molecules have been widely used for the alternating electronic and optical properties of the materials in the donor-acceptor approach. The most widely used heterocyclic conjugated molecule as a  $\pi$ -bridge unit is thiophene but selenophene also has been used for past few years.

Because the aromaticity of selenophene is less than that of the thiophene, quinoid structure is more stable for selenophene with respect to the sulfur containing counterpart.<sup>77,78</sup> Owing to its high quinoid character, bond length alternation value is low leading to lower band gap. Moreover, because of the more polarizable structure of it, intermolecular interaction between selenium moieties is high leading to enhanced charge transportation property. However, selenophene is more rigid than the thiophene unit. Therefore, solubility of thiophene is higher than that of the

selenophene. Furthermore, due to the elevated HOMO energy level of selenophene,  $V_{oc}$  value of it is less than that of the thiophene. However, by the decrease in the band energy, the amount of absorbed light and so internal quantum efficiency for selenophene is high with respect to the thiophene unit.<sup>79,80,81</sup>

### 1.2.10.3. Dibenzosilole based Polymers

Silole unit has been used extensively for a few years as the donor group. Alkyl units attached to the silicon atom provide enhanced hyper conjugation and it stabilizes the partially negative carbon atom. Due to the good overlapping between the  $\sigma^*$  orbital of the exocyclic silicon-carbon bonds and  $\pi^*$  orbital of the butadiene moiety, low lying LUMO can be obtained leading to reduced band gap. Moreover, silicon atom makes the butadiene HOMO level more stable resulting enhanced ambient stability.<sup>82,83</sup>

In 2007, Leclerc et al. published an article on silafluorene based polymers. In their study, a silafluorene derivative was used as the electron donor group, thiophene unit was the  $\pi$ -bridge material and benzothiadiazole group was chosen as the acceptor moiety. The power conversion efficiency was 1.6% with  $V_{oc}$  as 0.97 V and 1.9 eV band gap.<sup>84</sup>

In 2011, Bo and co-workers have reported a high efficient organic solar cell with PCE 6 % based on the silafluorene unit. The only difference in the polymer structure than that of the Leclerc's study is that they have introduced alkoxy groups into the acceptor moiety. The polymer backbone was showed in Figure 20.<sup>85</sup>

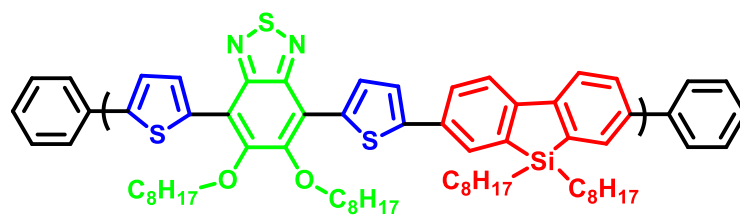


**Figure 20.** An example of dibenzosilole based polymer

### 1.2.11. Aim of the Study

Donor-acceptor approach is most widely used method to obtain low band gap polymers and high power conversion efficiency for organic solar cell applications as mentioned in previous sections. For that purpose, derivatives of benzotriazole were chosen as acceptor moieties, thiophene and selenophene units was used for the  $\pi$ -bridge donor groups, and lastly, a silafluorene derivative was used as the donor unit in this approach. In this manner, four different polymers namely, **PTBTSif**, **PSBSSif**, **PBTBTSif** and **PBSBSSif** were synthesized by Suzuki coupling. Then, optoelectronic properties of the polymers were performed. Synthesized polymers were demonstrated in Figure 21. The reason for choosing these units for getting high efficient solar cells was explained in detail in the previous section.

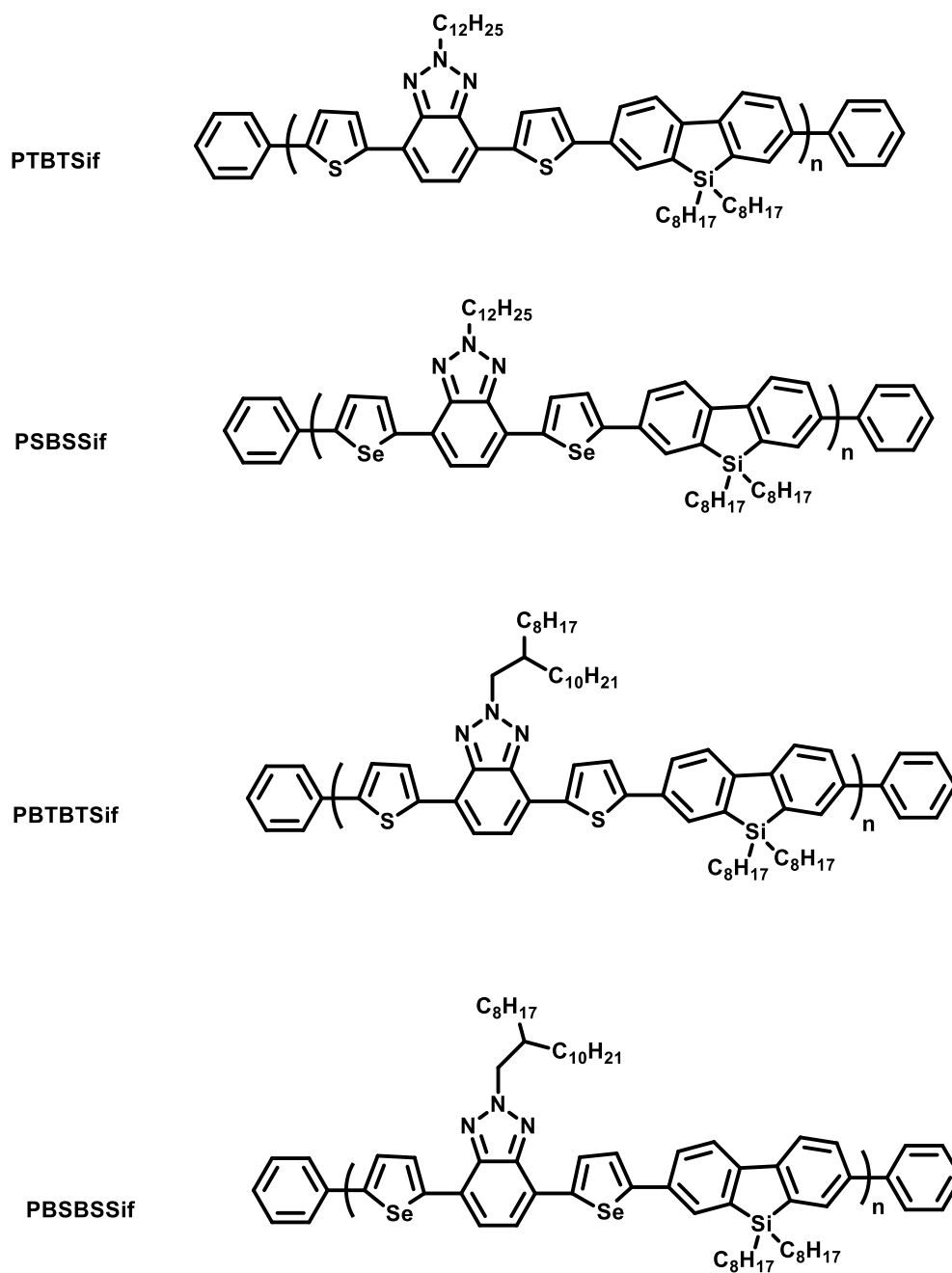


**Figure 21.** Synthesized Polymers



## CHAPTER 2

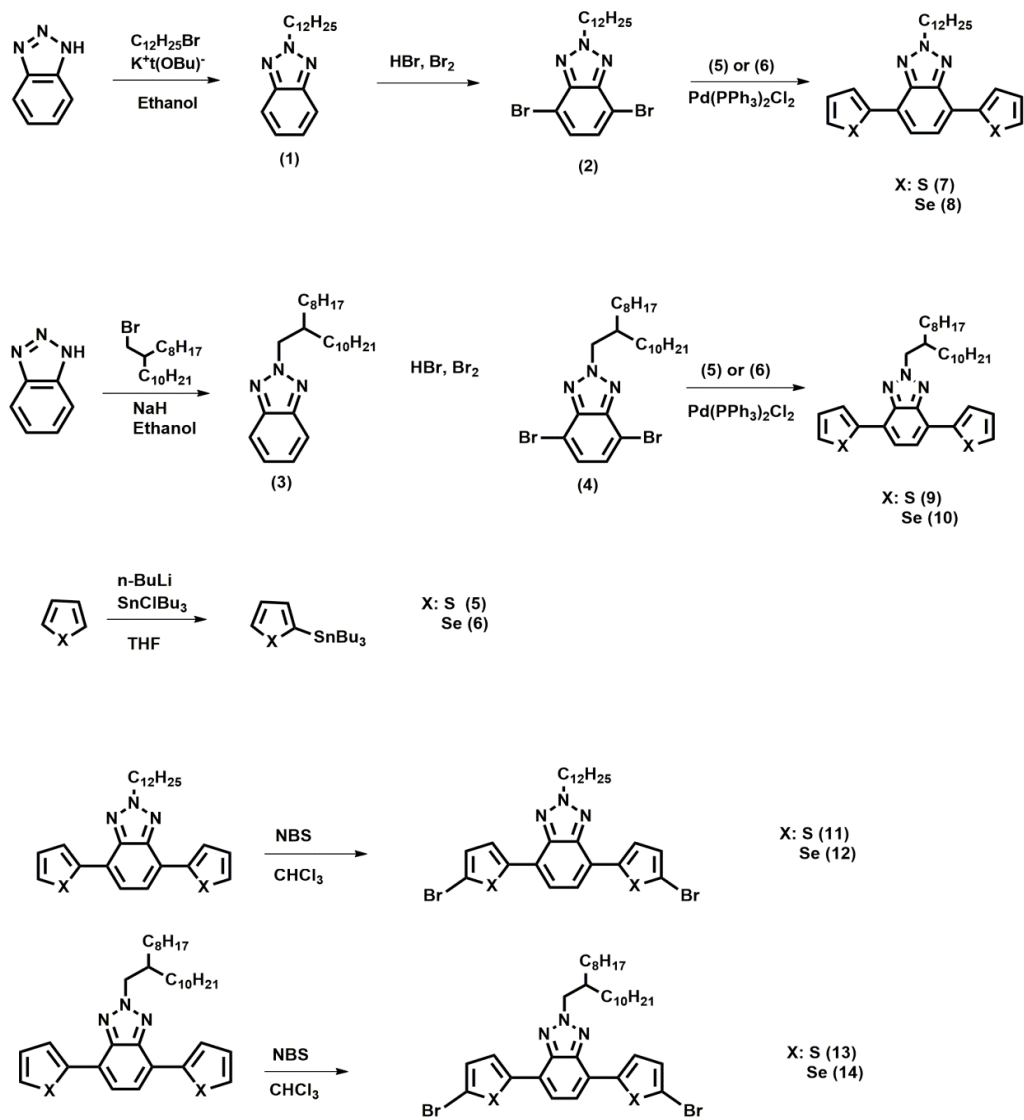
### EXPERIMENTAL

#### 2.1. An Overview to Experimental Procedures and Techniques

All of the chemicals utilized in synthesis of the polymers were purchased from Sigma-Aldrich and used without any further purification. THF (tetrahydrofuran) and toluene were used as freshly dried solvents by using metallic sodium and benzophenone while other solvents were used as received without any drying operation.  $^1\text{H}$  and  $^{13}\text{C}$  spectra of the polymers and monomers were recorded on a Bruker Spectrospin Avance DPX-400 Spectrometer and the chemical shifts were reported in the ppm with respect to tetramethylsilane (TMS) as the internal reference. Electrochemical studies were performed by Voltalab 50 potentiostat with three-electrode system in a cell where working electrode (WE) was ITO (indium tin oxide), platinum was used as counter electrode (CE) and silver wire calibrated to  $\text{Fc}/\text{Fc}^+$  redox couple was utilized as the reference electrode (RE). Electronic band gap energy values were calculated by determining the HOMO (highest occupied molecular orbital) and LUMO (lowest unoccupied molecular orbital) levels. In the identification of these values, the potential energy difference of normal hydrogen electrode (NHE) against vacuum was used. Spectroelectrochemical studies of the polymers were investigated by Varian Carry 500 UV-Vis spectrophotometer. For purification of the materials with column chromatography Merck Silica Gel 60 was used for the stationary phase with several organic solvents as mobile phase. Thermal analyses were carried out by using Perkin Elmer Pyris 1 to investigate the thermal properties of the polymers, such as decomposition temperature ( $T_d$ ), glass transition temperature ( $T_g$ ) and melting point ( $T_m$ ). Solar cell fabrication was carried

out under inert atmosphere in a glove-box system. Current-voltage characteristics of the polymers were performed by using Keithley SMU 236.

## 2.2. Syntheses of the Monomers



**Scheme 2.** Synthetic route of monomers

### 2.2.1. Synthesis of 2-dodecylbenzotriazole (1)

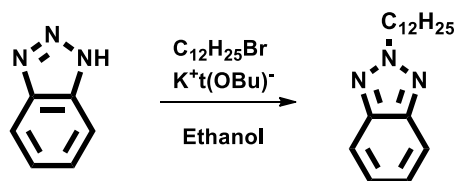


**Figure 22.** Synthesis of 2-dodecylbenzotriazole

1H-benzo[d][1,2,3]triazole (4.00 g, 33.6 mmol),  $K^+t(OBu)^-$  (4.00 g, 35.3 mmol) and 1-bromododecane (10.5 g, 40.3 mmol) were put in a two necked round bottom flask and this solid mixture was dissolved in ethanol (40 mL). The reaction mixture was refluxed overnight (approximately 18 hours) at ambient atmosphere. After the TLC analysis for the completion of the reaction, ethanol was evaporated and then, the residue was partitioned between chloroform and brine. The organic phase was separated and dried with magnesium sulfate. Solvent was removed under reduced pressure. Column chromatography (2:1 Hex: $CHCl_3$ ) was used to give the compound **1** as a colorless oil (3.00 g, 31%).

### 2.2.2. Synthesis of 4,7-dibromo-2-dodecyl-2H-benzo[d][1,2,3]triazole (2)

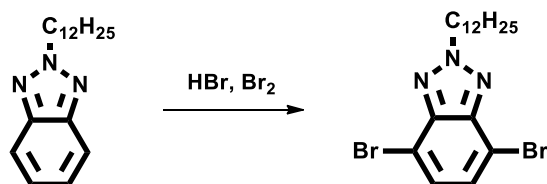


**Figure 23.** Synthesis of 4,7-dibromo-2-dodecyl-2H-benzo[d][1,2,3]triazole

2-Dodecylbenzotriazole (3.00 g, 10.4 mmol) was put in a two necked round bottom flask. Then it was dissolved in hydrobromic acid (48%, 30 mL) and refluxed at 110

°C for 1 hour. After that, bromine (4.20 g, 26.1 mmol) in hydrobromic acid (48%, 20 mL) was added drop wise to the reaction mixture. The reaction mixture was refluxed at 130 °C and stirred overnight. The reaction mixture was cooled down to room temperature and poured into saturated Na<sub>2</sub>CO<sub>3</sub> solution to eliminate excess bromine. Later on, the residue was partitioned between chloroform and distilled water. This organic solution was dried by MgSO<sub>4</sub> and filtered. Subsequently, chloroform was evaporated under reduced pressure and dark brown oil was obtained. To purify this compound, silica packed flash column chromatography (50:1, Hex:EtOAc) was used to give titled compound as a white solid (4.07 g, yield 88%). <sup>1</sup>H NMR (400 MHz, CDCl<sub>3</sub>) δ 7.38 (s, 2H), 4.73 – 4.68 (m, 2H), 2.07 (dd, *J* = 14.6, 7.4 Hz, 2H), 1.28 (s, 3H), 1.18 (s, 15H), 0.81 (t, *J* = 6.8 Hz, 3H).

### 2.2.3. Synthesis of 2-(2-octyldodecyl)-2H-benzo[d][1,2,3]triazole (3)

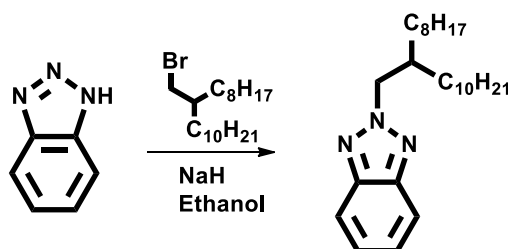


**Figure 24.** Synthesis of 2-(2-octyldodecyl)-2H-benzo[d][1,2,3]triazole

1H-benzo[d][1,2,3]triazole (4.00 g, 33.6 mmol) was dissolved in dry DMF (15 mL) and the reaction mixture was cooled below 0 °C. Then NaH (967 mg, 40.3 mmol) was added to the reaction medium at this temperature. After stirring for one hour the temperature was raised to 60 °C and 9-(bromomethyl)nonadecane (14 g, 40.3 mmol) was added to reaction mixture. This reaction was stirred at this temperature overnight. After the evaporation of DMF under vacuum, the residue was washed with water and extracted by chloroform. This organic solution was dried by MgSO<sub>4</sub>

and filtered. Subsequently, organic solvent was evaporated under reduced pressure. Silica packed flash column chromatography (3:1, Hex:DCM) was used to give compound **3** as pale-yellow oil. (3.76 g, yield 28%)

#### 2.2.4. Synthesis of 4,7-dibromo-2-(2-octyldodecyl)-2H-benzo[d][1,2,3]triazole (**4**)

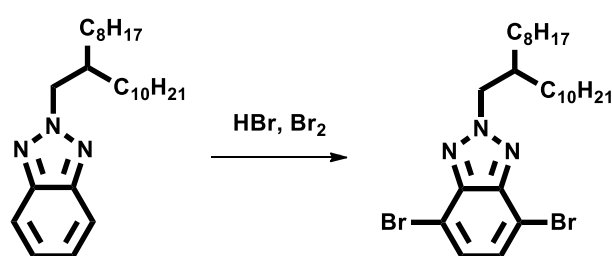


**Figure 25.** Synthesis of 4,7-dibromo-2-(2-octyldodecyl)-2H-benzo[d][1,2,3]triazole

2-(2-Octyldodecyl)-2H-benzo[d][1,2,3]triazole (3.76 g, 9.40 mmol) was dissolved in hydrobromic acid (48%, 30 mL) in a two-necked round bottom flask. This solution was stirred and refluxed at 110 °C for one hour and then bromine (3.75 g, 23.5 mmol) in hydrobromic acid (48%, 20 mL) was added drop wise to the reaction mixture. The mixture was refluxed at 130 °C overnight. Then, the residue was partitioned between chloroform and distilled water. Organic layer was dried over MgSO<sub>4</sub> and filtered. The solvent was evaporated under vacuum. Column chromatography (1:1, Hex:CHCl<sub>3</sub>) was used to give compound **4** as a yellow oil. (2.52 g, yield 48%)

### 2.2.5. Synthesis of tributyl(thiophen-2-yl)stannane (5)

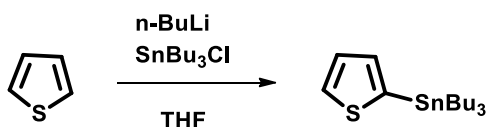


**Figure 26.** Synthesis of tributyl(thiophen-2-yl)stannane

Thiophene (2.00 g, 23.8 mmole) was dissolved in the dry THF (10 mL) in a two neck round bottom flask under argon atmosphere. The temperature was cooled down to  $-78\text{ }^\circ\text{C}$  and *n*-butyl lithium (2.5 M in hexane, 10 mL, 26 mmol) was added drop wise to the reaction within one hour at this temperature. Subsequently, the reaction mixture was stirred for one hour at  $0\text{ }^\circ\text{C}$  and for another one hour at room temperature. Then, the temperature was cooled down to  $-78\text{ }^\circ\text{C}$  again and tributyltin chloride (8.5 g, 26 mmol) was drop wise added to the reaction mixture within half an hour. This solution was stirred overnight at room temperature under argon. After the quenching of the reaction with water, THF was evaporated under vacuum and the residue was partitioned between distilled water and chloroform. Organic layer was extracted and dried with  $\text{MgSO}_4$ . Chloroform was evaporated under reduced pressure. Then silica packed column was standardized by basic triethyl amine and chromatography (9:1, Hex: $\text{Et}_3\text{N}$ ) was used to give the titled compound as a pale yellow oil. (8.80 g, yield 95%).  $^1\text{H}$  NMR (400 MHz,  $\text{CDCl}_3$ ),  $\delta$ (ppm): 7.55 (d, 1H), 7.18 (dd, 1H), 7.10 (d, 1H), 1.50 (t, 6H), 1.26 (dd, 6H), 1.03 (m, 6H), 0.82 (t, 9H)

### 2.2.6. Synthesis of tributyl(selenophen-2-yl)stannane (6)

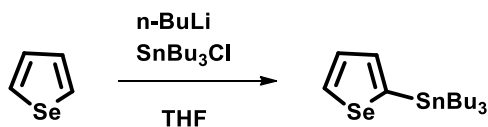


**Figure 27.** Synthesis of tributyl(selenophen-2-yl)stannane

Selenophene (1.00 g, 7.63 mmol) was dissolved in the dry THF (10 mL) in a two neck round bottom flask under argon atmosphere. The temperature was cooled down to  $-78\text{ }^\circ\text{C}$  and *n*-butyl lithium (2.5 M in hexane, 3.40 mL, 8.40 mmol) was added dropwise to the reaction within one hour at this temperature. Subsequently, the reaction mixture was stirred for one hour at  $0\text{ }^\circ\text{C}$  and for one hour at room temperature. Then, the temperature was cooled down to  $-78\text{ }^\circ\text{C}$  again and tributyltin chloride (2.73 g, 8.40 mmol) was drop wise added to the reaction mixture within half an hour. This solution was stirred overnight at room temperature under argon. After the quenching of the reaction, THF was evaporated under vacuum and the residue was partitioned between distilled water and chloroform. Organic layer was extracted and dried with  $\text{MgSO}_4$ . Chloroform was evaporated under reduced pressure. Then silica packed column was standardized by basic triethyl amine and chromatography (9:1, Hex: $\text{Et}_3\text{N}$ ) was used to give the titled compound as a pale yellow oil. (yield 75 %).  $^1\text{H}$  NMR (400 MHz,  $\text{CDCl}_3$ )  $\delta$  8.28 – 8.23 (m, 1H), 7.41 (dt,  $J = 5.0, 3.3$  Hz, 2H), 1.54 – 1.45 (m, 7H), 1.32 – 1.21 (m, 8H), 1.05 – 1.00 (m, 6H), 0.82 (t,  $J = 7.3$  Hz, 12H).

### 2.2.7. Synthesis of 2-dodecyl-4,7-di(thiophen-2-yl)-2H-benzo[d][1,2,3]triazole (7)

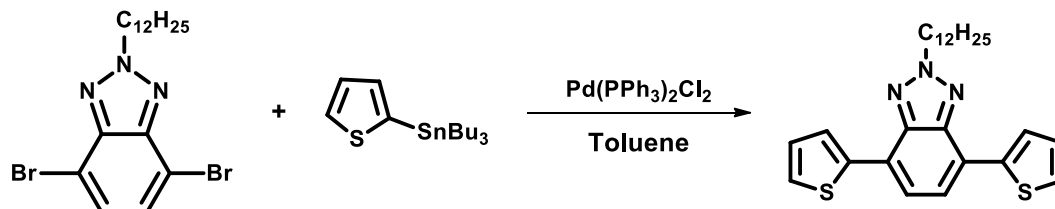


**Figure 28.** Synthesis of 2-dodecyl-4,7-di(thiophen-2-yl)-2H-benzo[d][1,2,3]triazole

4,7-dibromo-2-dodecyl-2H-benzo[d][1,2,3]triazole (500 mg, 1.12 mmole) and tributyl(thiophen-2-yl)stannane (1.10 g, 3.36 mmol) were placed in a two neck round bottom flask. Argon was passed through the flask rigorously for half an hour at room temperature. Then dry toluene (10 mL) was added to the reaction mixture and the mixture was stirred for 30 minutes under argon atmosphere at room temperature. Then bis(triphenylphosphine)palladium (II) (7.5 mol% 59 mg), dichloride was added to the reaction mixture and was refluxed overnight at around 100 °C. The reaction was quenched with water and the mixture was extracted with chloroform. The combined organic phases were washed with water and dried with MgSO<sub>4</sub> and filtered. Solvent was evaporated under reduced pressure and column chromatography (4:1, Hex: CHCl<sub>3</sub>) was used to give compound **7** as green viscous oil. (445 mg, yield 88 %). <sup>1</sup>H NMR (400 MHz, CDCl<sub>3</sub>), δ(ppm): 8.10 (dd, J= 1.1 Hz, 2H), 7.64 (s, 2H), 7.38 (dd, J= 1.1 Hz, 2H), 7.19 (q, 2H), 4.82 (t, J= 7.3 Hz, 2H), 2.20 (m, 2H), 0.87 (t, J= 6.8 Hz, 3H)

### 2.2.8. Synthesis of 2-dodecyl-4,7-di(selenophen-2-yl)-2H-benzo[d][1,2,3]triazole (8)

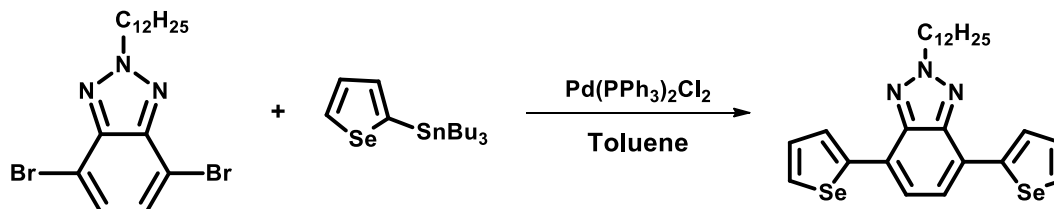


**Figure 29.** Synthesis of 2-dodecyl-4,7-di(selenophen-2-yl)-2H-benzo[d][1,2,3]triazole

4,7-Dibromo-2-dodecyl-2H-benzo[d][1,2,3]triazole (500 mg, 1.12 mmole) and tributyl(selenophen-2-yl)stannane (1.43 g, 3.40 mmole) were placed in a two neck round bottom flask. Argon was passed through the flask intensely for half an hour at room temperature. Then dry toluene (10 mL) was added to the reaction mixture and the mixture was stirred for 30 minutes under argon atmosphere at room temperature. Then bis(triphenylphosphine)palladium (II) (7.5 mol% 59 mg), dichloride was added to the reaction mixture and was refluxed overnight at around 100 °C. The reaction was quenched with water and the mixture was extracted with chloroform. The combined organic phases were washed with water and dried with MgSO<sub>4</sub> and filtered. Solvent was evaporated under reduced pressure and column chromatography (20:1, Hex: EtOAc) was used to give compound **8** as brownish viscous oil. (480 mg, yield 79 %). <sup>1</sup>H NMR (400 MHz, CDCl<sub>3</sub>), δ(ppm): 8.20 (d, J = 3.8 Hz, 2H), 8.08 (d, J = 4.8 Hz, 2H), 7.61 (s, 2H), 7.43 (dd, J = 5.6, 3.9 Hz, 2H), 4.82 (t, J = 7.2 Hz, 2H), 2.25-2.16 (m, 2H), 1.41 (s, 4H), 1.30-1.23 (m, 14 H), 0.87 (t, J = 6.8 Hz, 3H)

### 2.2.9. Synthesis of 2-(2-octyldodecyl)-4,7-di(thiophen-2-yl)-2H-benzo[d][1,2,3]triazole (9)

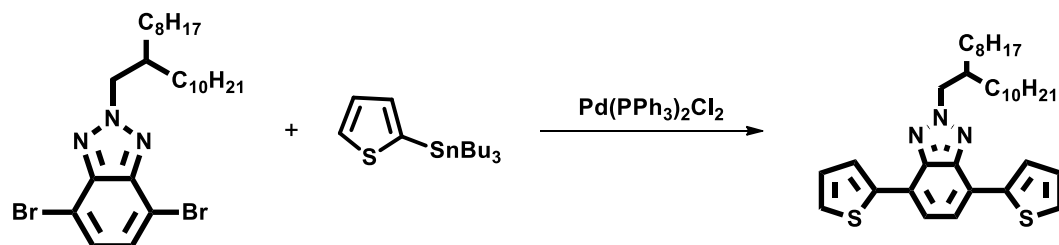


**Figure 30.** Synthesis of 2-(2-octyldodecyl)-4,7-di(thiophen-2-yl)-2H-benzo[d][1,2,3]triazole

4,7-Dibromo-2-(2-octyldodecyl)-2H-benzo[d][1,2,3]triazole (500 mg, 0.90 mmole) and tributyl(thiophen-2-yl)stannane (1.00 g, 2.70 mmole) were placed in a two neck round bottom flask. Argon was passed through the flask intensely for half an hour at room temperature. Then dry toluene (10 mL) was added to the reaction mixture and the mixture was stirred for 30 minutes under argon atmosphere at room temperature. Then bis(triphenylphosphine)palladium (II) (7.5 mol% 47 mg), dichloride was added to the reaction mixture and was refluxed overnight at around 100 °C. The reaction was quenched with water and the mixture was extracted with chloroform. The combined organic phases were washed with water and dried with MgSO<sub>4</sub> and filtered. Solvent was evaporated under reduced pressure and column chromatography (4:1, Hex: CHCl<sub>3</sub>) was used to give compound **9** as yellow solid. (381 mg, yield 75 %). <sup>1</sup>H NMR (400 MHz, CDCl<sub>3</sub>), δ(ppm): 8.03 (dd, J = 3.6, 1.0 Hz, 2H), 7.56 (s, 2H), 7.30 (dd, J = 5.1, 1.0 Hz, 2H), 7.11 (dd, J = 5.1, 3.7 Hz, 2H), 4.68 (d, J = 6.6, 2H), 2.29-2.20 (m, 1H), 1.30 (dd, J = 12.4, 6.8 Hz, 7H), 1.17 (d, J = 9.13 Hz, 24H), 0.79 (dd, J = 7.0, 4.5 Hz, 6H)

### 2.2.10. Synthesis of 2-(2-octyldodecyl)-4,7-di(selenophen-2-yl)-2H-benzo[d][1,2,3]triazole (10)

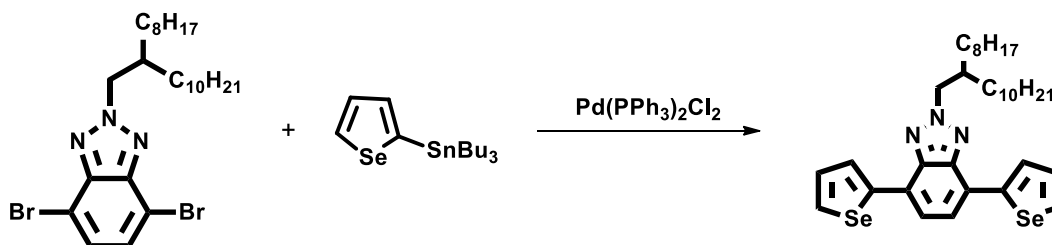


**Figure 31.** Synthesis of 2-(2-octyldodecyl)-4,7-di(selenophen-2-yl)-2H-benzo[d][1,2,3]triazole

4,7-Dibromo-2-(2-octyldodecyl)-2H-benzo[d][1,2,3]triazole (500 mg, 0.90 mmole) and tributyl(selenophen-2-yl)stannane (1.13 g, 2.70 mmole) were placed in a two neck round bottom flask. Argon was passed through the flask intensely for half an hour at room temperature. Then dry toluene (10 mL) was added to the reaction mixture and the mixture was stirred for 30 minutes under argon atmosphere at room temperature. Then bis(triphenylphosphine)palladium (II) (7.5 mol% 59 mg), dichloride was added to the reaction mixture and was refluxed overnight at around 100 °C. The reaction was quenched with water and the mixture was extracted with chloroform. The combined organic phases were washed with water and dried with MgSO<sub>4</sub> and filtered. Solvent was evaporated under reduced pressure and column chromatography (25:1, Hex: EtOAc) was used to give compound **10** as yellowish solid. (444 mg, yield 71 %). <sup>1</sup>H NMR (400 MHz, CDCl<sub>3</sub>), δ(ppm): 8.19 (d, J = 3.8 Hz, 2H), 8.08 (d, J = 5.6 Hz, 2H), 7.61 (s, 2H), 7.42 (dd, J = 5.6, 3.9 Hz, 2H), 4.75 (d, J = 6.4 Hz, 2H), 2.30 (d, J = 2.3 Hz, 1H), 1.44-1.36 (m, 6H), 1.25 (d, J = 9.1 Hz, 26H), 0.87 (td, J = 6.8, 4.0 Hz, 6H)

### 2.2.11. Synthesis of 4,7-bis(5-bromothiophen-2-yl)-2-dodecyl-2H-benzo[d][1,2,3]triazole (**11**)

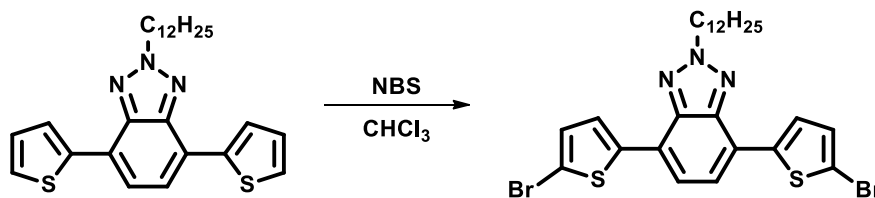


**Figure 32.** Synthesis of 4,7-bis(5-bromothiophen-2-yl)-2-dodecyl-2H-benzo[d][1,2,3]triazole

2-Dodecyl-4,7-di(thiophen-2-yl)-2H-benzo[d][1,2,3]triazole (445 mg, 1.00 mmol) was dissolved in chloroform (40 mL) and N-bromosuccinimide, NBS, (445 mg, 2.5 mmol) was added to the reaction mixture slowly at room temperature under dark. After completion of the addition, reaction was stirred overnight. The mixture was partitioned between chloroform and distilled water. Organic layer was separated, dried (MgSO<sub>4</sub>) and the solvent was evaporated under reduced pressure. The residue was purified by using silica packed column chromatography (15:1, Hex:DCM) to give **11** as green solid. (485 mg, 80 %). <sup>1</sup>H NMR (400 MHz, CDCl<sub>3</sub>), δ(ppm): 7.78 (d, J = 3.9 Hz, 2H), 7.50 (s, 2H), 7.12 (d, J = 4.1 Hz, 2H), 4.79 (t, J = 7.2 Hz, 2H), 2.17 (m, 2H), 1.43-1.38 (m, 4H), 1.28-1.23 (m, 4H), 0.87 (t, J = 6.8 Hz, 6H) <sup>13</sup>C NMR (400 MHz, CDCl<sub>3</sub>) δ 139.90, 139.41, 129.04, 125.11, 121.19, 120.38, 111.33, 75.47, 75.16, 74.84, 55.10, 30.06, 28.18, 27.76, 27.69, 27.58, 27.48, 27.15, 24.72, 20.83, 12.25, -0.84.

### 2.2.12. Synthesis of 4,7-bis(5-bromoselenophen-2-yl)-2-dodecyl-2H-benzo[d][1,2,3]triazole (**12**)

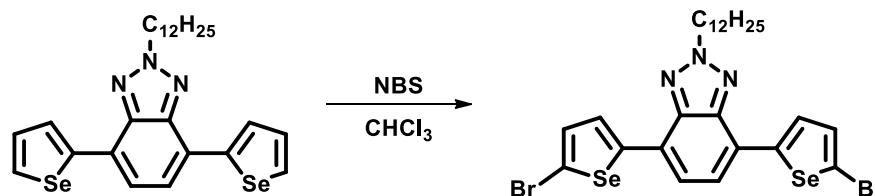


**Figure 33.** Synthesis of 4,7-bis(5-bromoselenophen-2-yl)-2-dodecyl-2H-benzo[d][1,2,3]triazole

2-Dodecyl-4,7-di(selenophen-2-yl)-2H-benzo[d][1,2,3]triazole (480 mg, 0.88 mmole) was dissolved in chloroform (40 mL) and N-bromosuccinimide, NBS, (392 mg, 2.2 mmole) was added to the reaction mixture portionwise at room temperature under dark. After completion of the addition, reaction was stirred overnight. The mixture was partitioned between chloroform and distilled water. Organic layer was separated, dried (MgSO<sub>4</sub>) and the solvent was evaporated under reduced pressure. The residue was purified by using silica packed column chromatography (3:1, Hex:DCM) to give **12** as yellow solid (452 mg, 73 %). <sup>1</sup>H NMR (400 MHz, CDCl<sub>3</sub>), δ(ppm): 7.80 (d, J = 4.2 Hz, 2H), 7.53 (s, 2H), 7.33 (d, J = 4.2 Hz, 2H), 4.79 (t, J = 7.1 Hz, 2H), 2.18 (dd, J = 8.3, 5.6 Hz, 2H), 1.40 (m, 4H), 1.25 (m, 14H), 0.87 (t, J = 6.8 Hz, 3H)

### 2.2.13. Synthesis of 4,7-bis(5-bromothiophen-2-yl)-2-(2-octyldodecyl)-2H-benzo[d][1,2,3]triazole (**13**)

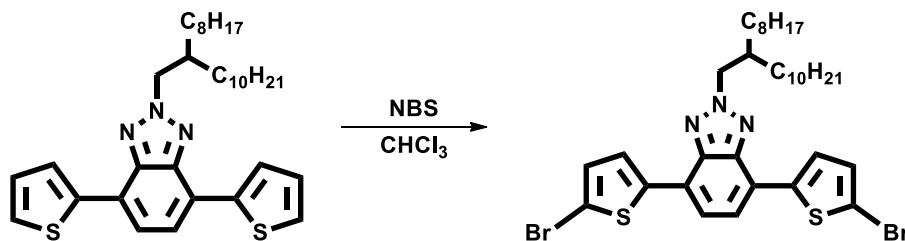


**Figure 34.** Synthesis of 4,7-bis(5-bromothiophen-2-yl)-2-(2-octyldodecyl)-2H-benzo[d][1,2,3]triazole

2-(2-Octyldodecyl)-4,7-di(thiophen-2-yl)-2H-benzo[d][1,2,3]triazole (485 mg, 0.86 mmol) was dissolved in CHCl<sub>3</sub> (40 mL) and NBS (254 mg, 2.15 mmol) was added to the reaction mixture slowly at room temperature under dark. After completion of the addition, reaction was stirred overnight. The mixture was partitioned between chloroform and distilled water. Organic layer was separated, dried (MgSO<sub>4</sub>) and the solvent was evaporated under reduced pressure. The residue was purified by using silica packed column chromatography (5:1, Hex:CHCl<sub>3</sub>) to give **13** as green solid (471 mg, yield 76 %). <sup>1</sup>H NMR (400 MHz, CDCl<sub>3</sub>), δ(ppm): 7.71 (d, J = 4.0 Hz, 2H), 7.45 (s, 2H), 7.05 (d, J = 4.0 Hz, 2H), 4.66 (d, J = 6.6 Hz, 2H), 2.21 (d, J = 5.9 Hz, 1H), 1.36-1.27 (m, 6H), 1.17 (d, J = 8.2 Hz, 26H), 0.83-0.77 (m, 6H) <sup>13</sup>C NMR (400 MHz, CDCl<sub>3</sub>) δ 141.59, 141.29, 130.88, 126.86, 122.97, 122.16, 113.14, 39.20, 31.94, 31.91, 31.46, 29.91, 29.68, 29.61, 29.37, 29.34, 26.27, 22.71, 14.15.

#### 2.2.14. Synthesis of 4,7-bis(5-bromoselenophen-2-yl)-2-(2-octyldodecyl)-2H-benzo[d][1,2,3]triazole (**14**)

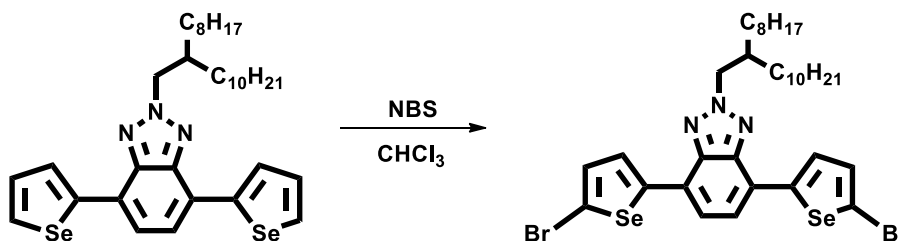
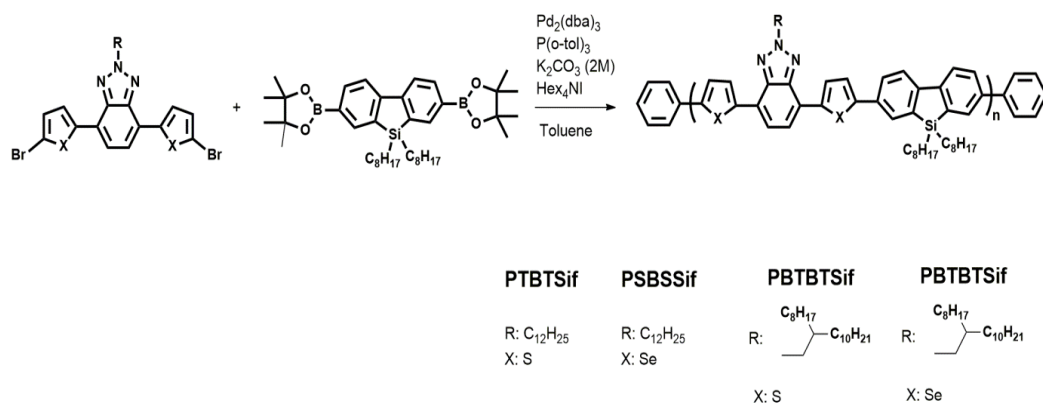


**Figure 35.** Synthesis of 4,7-bis(5-bromoselenophen-2-yl)-2-(2-octyldodecyl)-2H-benzo[d][1,2,3]triazole

2-(2-Octyldodecyl)-4,7-di(selenophen-2-yl)-2H-benzo[d][1,2,3]triazole (444 mg, 0.68 mmol) was dissolved in CHCl<sub>3</sub> (40 mL) and NBS (300 mg, 1.69 mmol) was added to the reaction mixture slowly at room temperature under dark. After completion of the addition, reaction was stirred overnight. The mixture was partitioned between chloroform and distilled water. Organic layer was separated, dried (MgSO<sub>4</sub>) and the solvent was evaporated under reduced pressure. The residue was purified by using silica packed column chromatography (50:1, Hex:EtOAc) to give **14** as pale brown solid (383mg, yield 69 %) <sup>1</sup>H NMR (400 MHz, CDCl<sub>3</sub>), δ(ppm): 7.71 (d, J = 4.2 Hz, 2H), 7.47 (s, 2H), 7.26 (d, J = 4.2 Hz, 2H), 4.66 (d, J = 6.3 Hz, 2H), 2.23-2.16 (m, 1H), 1.30 (dd, 19.9, 9.2 Hz, 6H), 1.22-1.16 (m, 26H), 0.80 (td, J = 6.8, 2.9 Hz, 6H)

## 2.3. Synthesis of Polymers



**Scheme 3.** General synthesis mechanism of polymers

### 2.3.1. Synthesis of PTBTSif

In a 50 mL two-neck round bottom flask K<sub>2</sub>CO<sub>3</sub> solution (2M, 0.5 mL) was added and the system was purged with argon for 30 minutes. Then, freshly dried toluene (5mL) was added to the mixture and argon purging was continued. 4,7-Bis(5-bromothiophen-2-yl)-2-dodecyl-2H-benzo[d][1,2,3]triazole (100 mg, 0.164 mmol), 9,9-Dioctyl-9H-9-silafluorene-2,7-bis(boronic acid pinacol ester) (108 mg, 0.164 mmol) and a catalytic amount of tetrahexyl ammonium iodide was then added to the reaction followed by argon purging for an additional 30 minutes. After that, Tris(dibenzylideneacetone)dipalladium(0) (5.0 mol%, 7.5 mg) and tris(*o*-tolyl)phosphine (10 mol%, 5.00 mg) was added to the reaction mixture. The temperature was raised to 105 °C from room temperature. The polymerization reaction was sustained at this temperature under argon atmosphere for 40 hours. Bromobenzene (103 mg, 0.656 mmol) and extra catalyst (3.50 mg) were then added and the mixture was stirred for four hours then phenyl boronic acid, (160 mg, 1.312 mmole) was added and the mixture was stirred at 105 °C overnight. The reaction

mixture was cooled to room temperature and precipitated in methanol. The mixture was filtered and precipitate was purified by Soxhlett apparatus. Firstly, the precipitate was washed with acetone for 5 hours and then with hexane for 10 hours to remove oligomers and small molecules. The polymer was collected by chloroform and the solvent was evaporated. The residue was precipitated into methanol and pure polymer was obtained by vacuum filtration (80 mg, yield 40 %).

### 2.3.2. Synthesis of PSBSSif

The same procedure with synthesis of **PTBTSif** was applied to synthesize the PSBSSif. In this manner, 4,7-bis(5-bromoselenophen-2-yl)-2-dodecyl-2H-benzo[d][1,2,3]triazole (110 mg, 0.156 mmol), 9,9-dioctyl-9*H*-9-silafluorene-2,7-bis(boronic acid pinacol ester) (101 mg, 0.156 mmol), tris(dibenzylideneacetone)dipalladium(0) as a catalyst (5.0 mol%, 9.0 mg) and tris(*o*-tolyl)phosphine as the co-catalyst (10 mol%, 4.8 mg) were taken in determined amounts. Bromobenzene and phenyl boronic acid were taken as 98.0 mg and 152 mg respectively. Material in large quantity which was not collected with chloroform and chlorobenzene was collected from filter directly. However polymeric materials collected with chloroform was quantified and made ready for further applications. Yield of this poly-condensation reaction was very low due to the solubility problem. The amount of the soluble polymer was 20 mg.

### 2.3.3. Synthesis of PBTBTSif

The same procedure with synthesis of **PTBTSif** was applied to synthesize the PSBSSif. In this manner, 4,7-bis(5-bromothiophen-2-yl)-2-(2-octyldodecyl)-2H-benzo[d][1,2,3]triazole (90.0 mg, 0.125 mmole), 9,9-dioctyl-9*H*-9-silafluorene-2,7-bis(boronic acid pinacol ester) (82.0 mg, 0.125 mmol), tris(dibenzylideneacetone)dipalladium(0) as a catalyst (5 mol%, 5.7 mg) and tris(*o*-

tolyl)phosphine as the co-catalyst (11 mol%, 4.3 mg) were taken in the determined amounts. Bromobenzene (0.375 mmol) and phenyl boronic (0.750 mmol) acid were taken as 60 mg and 91 mg respectively. The amount of the polymer was 60 mg (yield 35 %)

#### 2.3.4. Synthesis of PBSBSSif

The same procedure with synthesis of **PTBTSif** was applied to synthesize the PBSBSSif. 4,7-bis(5-bromoselenophen-2-yl)-2-(2-octyldodecyl)-2H-benzo[d][1,2,3]triazole (100 mg, 0.122 mmole), 9,9-dioctyl-9H-9-silafluorene-2,7-bis(boronic acid pinacol ester) (81.0 mg, 0.122 mmol), tris(dibenzylideneacetone)dipalladium(0) as the catalyst (5.0 mol%, 5.6 mg) and tris(*o*-tolyl)phosphine as the co-catalyst (11 mol%, 4.0 mg) were taken in the determined amounts. Bromobenzene (0.366 mmole) and phenyl boronic (0.732 mmol) acid were taken as 57 mg and 89 mg respectively. The amount of the polymer was 60 mg (yield 35 %). The final polymer amount was 20 mg.

#### 2.4. Electrochemical Studies

These studies were conducted to determine the electrochemical properties of the semi-conducting polymers. For this purpose, potentiostat was used with three-electrode system. In potentiometric approach, counter electrode (CE) was used to control the potential against the working electrode (WE). The difference in the potential between the WE and reference electrode (RE) was determined.

By using the cyclic voltammetry technique, the redox behaviors of the polymers were investigated. This oxidation and reduction tendencies of the polymers were determined by monitoring the redox reactions between the conducting polymers and anion of the electrolyte solution at a constant rate. As a result of this, attained voltammogram gives a graph of current versus potential. Furthermore, by

determination of the oxidation and reduction onsets on the cyclic voltammogram, HOMO and LUMO values were measured as well as electronic band gap energy ( $E_g^{el}$ ). In addition to this, by changing the potentials, color changes in the polymers were identified for further applications. To perform this study, polymer was dissolved in chloroform and resulting colored solution was sprayed onto ITO (WE) coated glass substrate. Then it was submerged in the  $NBu_4^+PF_6^-/ACN$  (tetrabutylammonium hexafluorophosphate/acetonitrile) electrolyte-solvent couple which is in a quartz cuvette. Platinum and silver wire submerged in that cuvette were used as CE and RE respectively.

## 2.5. Spectroelectrochemical Studies

This analysis method was performed by a three electrode system same as was the case for electrochemical studies. By using this technique, absorption spectrum of the polymers were identified at different potentials. Hence, during these analyses, not only neutral states of the polymers but also their polaron and bipolaron bands were examined. Moreover, this study gives information about the optical band gap ( $E_g^{op}$ ) which determined by the  $\lambda_{onset}$  of neutral state of the polymer.

## 2.6. Kinetic Studies

The electrochromic device (EC) and its application areas were discussed in introduction part and the importance of optical transmittance and switching time for an EC material was emphasized. Optical transmittance or optical contrast of the polymers in neutral state and doped states namely polaron and bipolaron are determined by the square wave potential as a function of time. Switching time of the polymers was measured from these data.

## 2.7. Thermal Analyses

The degradation temperatures of the polymers are investigated by using TGA (Thermal Gravimetric Analysis). In this technique, weight loss of the polymers with respect to increased temperature was analyzed. 5 % weight was determined as the point where significant decomposition started to occur. To perform these analyses Perkin Elmer Pyris 1 TGA was utilized.

For determination of the relation between the crystalline and amorphous forms of the polymers DSC (Differential Scanning Calorimetry) was utilized. In this method, glass transition temperature ( $T_g$ ) and melting points ( $T_m$ ) of the polymers are identified. For this purpose Perkin Elmer Differential Scanning Calorimetry was used.

## 2.8. Solar Cell Applications

The BHJ type organic solar cells were fabricated with the structure of ITO/PEDOT:PSS/Polymer:PC<sub>71</sub>BM/Ca/Al. The active layer was prepared with different polymer:PC<sub>71</sub>BM ratios. ITO was etched and then ITO coated glass substrate was washed using detergent and water and then with acetone and isopropyl alcohol sequentially in an ultrasonic bath for 15 minutes. The solvent on the surface of the ITO was evaporated by the temperature treatment performed on a hot plate at 50 °C for 15 min. Subsequently, the last cleaning procedure was performed in Harrick Plasma Cleaner. After the cleaning of the ITO surface filtered PEDOT:PSS (0.45 μm PVDF membrane) was integrated on ITO surface by spin coating with 5000 rpm for one minute. The substrate was dried for 10 min at 150 °C on a hot plate. The mixture of polymer:PC<sub>71</sub>BM was filtered with 0.2 μm syringe filter. This filtered active layer was coated on PEDOT:PSS layer at different rpm by G3P-8 spin coater under nitrogen atmosphere in a glove-box system. After that, calcium and aluminum were coated on the active layer surface with thermal deposition technique. All current density-voltage (J-V) characteristics of the

devices were measured using a Keithley 2400 sourcemeter under AM 1.5G-filtered irradiation (100 mW cm<sup>-2</sup>) from a 1 kW Atlas Material Testing Solutions solar test 1200 solar simulator. The light intensity was measured with a Newport Optical Powermeter 1916-C radiant power meter.

The FF (fill factor) of the devices is affected mainly by charge mobility and surface morphology of the active layer. The hole mobility of the thin films was calculated by space charge limited current method (SCLC) technique. The modified J-V curves were plotted by the Child's formula,

$$J_{\text{SCL}} = \frac{9}{8} \epsilon_0 \epsilon_r \mu \frac{V^2}{L^3}$$

Here,  $\mu$  is the carrier mobility,  $V$  is applied voltage,  $L$  is thickness of polymer,  $\epsilon_r$  is the relative permittivity and  $\epsilon_0$  is permittivity of free space.



## CHAPTER 3

### RESULTS AND DISCUSSION

#### 3.1. Electrochemical Studies

Suitability of the polymers for optoelectronic applications can be tested by performing electrochemical studies which gives information about the HOMO and LUMO energy levels of the materials as well as their band gap energies. Cyclic voltammetry analyses were conducted for determining these values. Thus, redox behaviors of the materials under investigation were explored. For these studies, polymers dissolved in chloroform (5mg/mL) were coated onto ITO surface by spray coating technique. In the meantime, for the CV studies, three-electrode system was established in the quartz cell including an electrolyte solution which consisted of TBAPF<sub>6</sub> (tetrabutylammonium hexafluorophosphate) and acetonitrile (ACN). In three-electrode system, polymer coated ITO was used as the working electrode, platinum (Pt) was chosen as the counter electrode and silver wire calibrated to Fc/Fc<sup>+</sup> redox couple (300 mV) was utilized as the pseudo reference electrode. Oxidation and reduction potentials of the polymers were investigated at the 100 mVs<sup>-1</sup> as the scan rate.

Cyclic voltammograms show that all polymers possess p-doping and n-doping characters. In the p-type doping/dedoping processes for **PTBTSif**, polymer showed a reversible redox couple at 1.16 V and 0.95 V. The n-type doping/dedoping redox couple was observed at -1.72 V and -1.50 V. In the case of **PSBSSif**, polymer was oxidized at 1.03 V and it was reduced at 0.78 V reversibly with p-type doping/dedoping processes. The reversible n-type doping/dedoping peaks were observed at -1.78 V and -1.54 V respectively. The p-type reversible oxidation and

reduction couples of **PBTBTSif** and **PBSBSSif** were reported as 0.94/0.73 V and 0.99/0.62 V respectively. In addition to this, in the n-type doping/dedoping process, these polymers were reduced and oxidized at -1.88/-1.68 and -1.78/-1.57. The cyclic voltammograms of these four polymers were depicted in Figure 36.

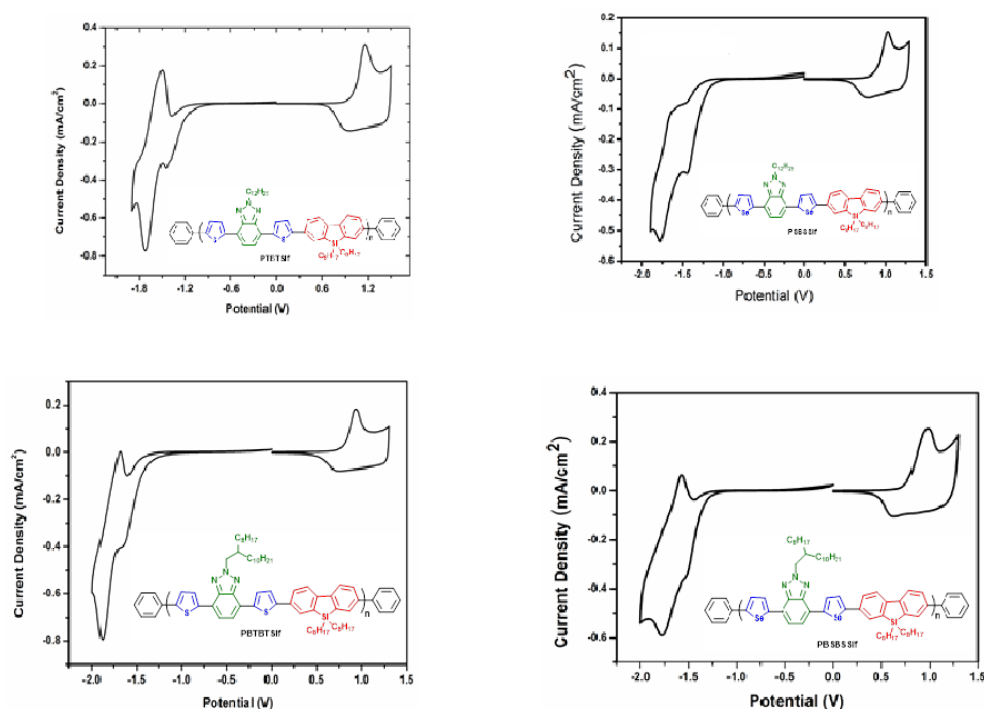


**Figure 36.** Cyclic voltammograms of the polymers

Since the polymers were both p- and n-dopable, their HOMO and LUMO energies could be calculated from CV data. HOMO energy level was calculated by the formula,  $\text{HOMO} = -(4.75 + E_{\text{ox,onset}} - 0.3)$  eV and LUMO energy level was calculated via similar formula,  $\text{LUMO} = -(4.75 + E_{\text{red,onset}} - 0.3)$ . According to calculated HOMO and LUMO energy levels, selenophene based polymers showed high lying HOMO level as expected because of their lower stability to ambient atmosphere with respect to the thiophene based polymers. In addition to this, it was also shown that selenophene is more electron-rich in comparison with thiophene and due to having this character this unit gives higher reactivity in electrophilic

substitution reactions. Although high lying HOMO cause decrease in open circuit voltage ( $V_{oc}$ ) value, this reduces the band gap energy that leads to increase in the amount of harvested photons. HOMO energy levels of the polymers were measured as -5.48 eV, -5.31 eV, -5.24 eV and -5.18 eV for **PTBTSif**, **PSBSSif**, **PBTBTSif** and **PBSBSSif** respectively and LUMO energy levels of the polymers were found as -3.30, -3.27, -3.02 and -3.12 in the same order. LUMO energy level is important not only for achieving low band gap molecules but also for effective intermolecular charge transfer process between donor polymer and acceptor molecule ( $PC_{71}BM$ ). The difference between the LUMO energy levels of donor and acceptor (-3.91 eV LUMO energy level) should be in the range of 0.3-0.5 eV. As a result of this, the most effective intermolecular charge transfer is expected for the **PTBTSif**. Electronic band gap ( $E_g^{el}$ ) values of the polymers were calculated by the formula;  $E_g^{el} = E_{HOMO} - E_{LUMO}$  and these values were found to be 2.18 eV for **PTBTSif**, 2.04 eV for **PSBSSif**, 2.22 eV for **PBTBTSif** and 2.06 eV for **PBSBSSif**.  $\pi$ -bridge effect on the band gap of the polymers was evident. The electronic band gap energy difference between the thiophene based **PTBTSif** and selenophene based **PSBSSif** was recorded as 0.14 eV and difference between the **PBTBTSif** bearing thiophene  $\pi$ -bridge and **PBSBSSif** bearing selenophene  $\pi$ -bridge donor groups was reported as 0.16 eV. As a consequence, polymers having thiophene  $\pi$ -bridge on their backbones have low lying HOMO level with larger band gaps. The electrochemical studies were summarized in Table 1.

**Table 1.** Summary of the electrochemical studies

	$E_{p-doping}$ (V)	$E_{p-dedoping}$ (V)	$E_{n-doping}$ (V)	$E_{n-dedoping}$ (V)	$E_{ox,onset}$	$E_{red,onset}$	HOMO (eV)	LUMO (eV)	$E_g^{el}$
<b>PTBTSif</b>	1.16	0.95	-1.72	-1.50	1.03	-1.15	-5.48	-3.30	2.18
<b>PSBSSif</b>	1.03	0.78	-1.78	-1.54	0.86	-1.18	-5.31	-3.27	2.04
<b>PBTBTSif</b>	0.94	0.73	-1.88	-1.68	0.79	-1.43	-5.24	-3.02	2.22
<b>PBSBSSif</b>	0.99	0.62	-1.78	-1.57	0.73	-1.33	-5.18	-3.12	2.06

The current density values were determined in the given potential range at different scan rates. According to the modified Randles-Sevcik equation;

$$i_p = (n^2F^2\Gamma v)/(4RT)$$

If current changes linearly proportional to the scan rate, it can be said that the mass transfer of anion of the electrolyte solution to polymer surface is non-diffusion controlled. It means that, supporting electrolyte anion construct an anion layer on the oxidized polymer and the mass transfer occurs between these layers reversibly. The cyclic voltammograms plotted by different scan rates were shown in the Figures 37-40.

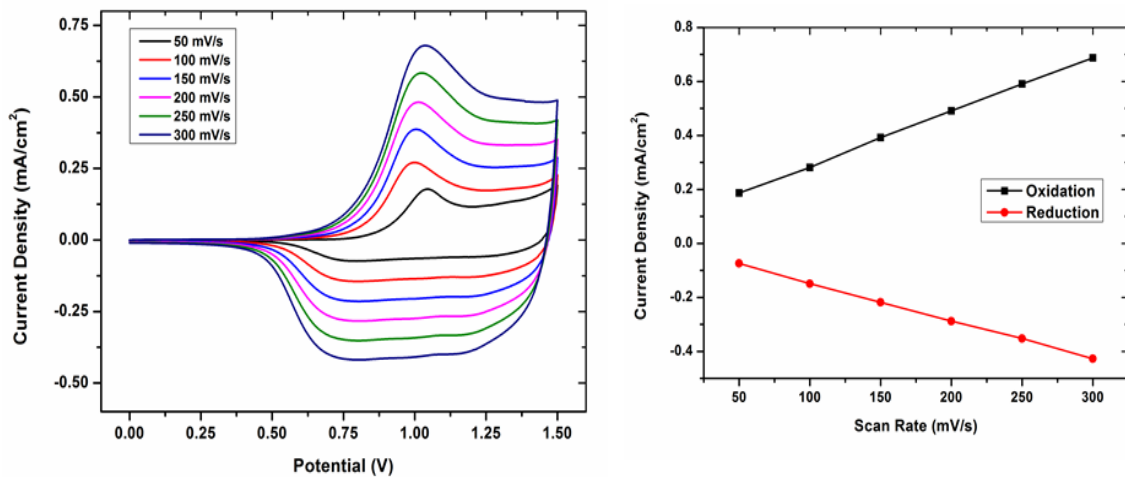


**Figure 37.** Scan rate study of PTBTSif

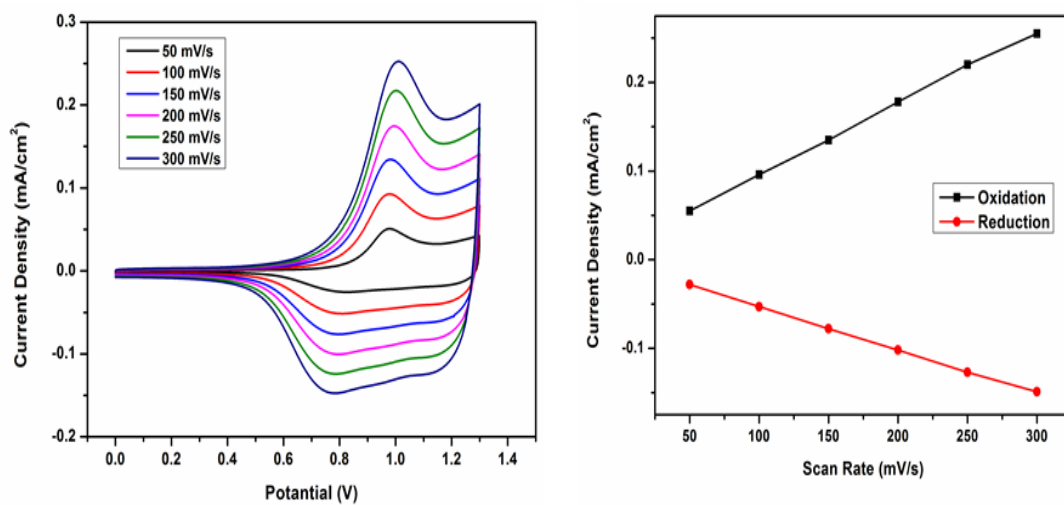


**Figure 38.** Scan rate study of PSBSSif

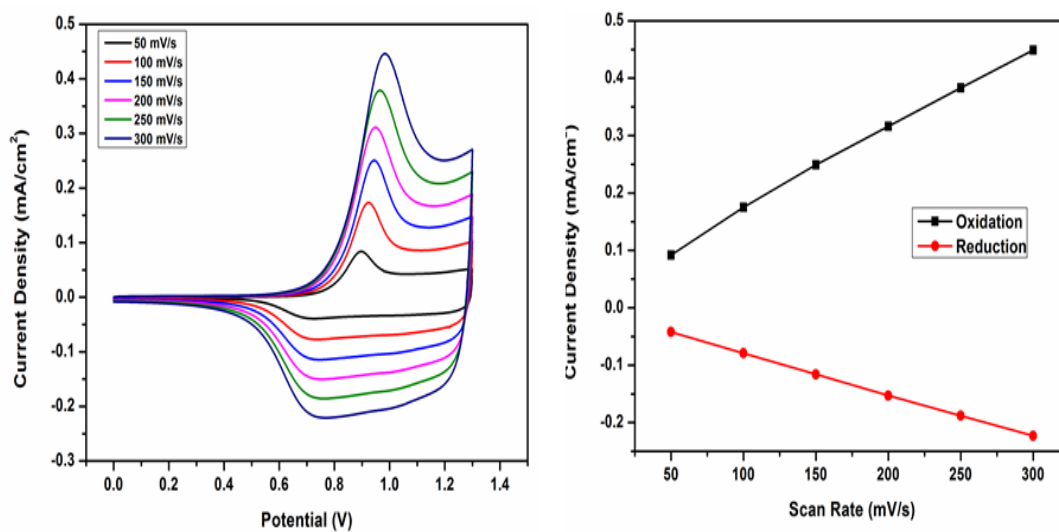


**Figure 39.** Scan rate study of PBTBTSif

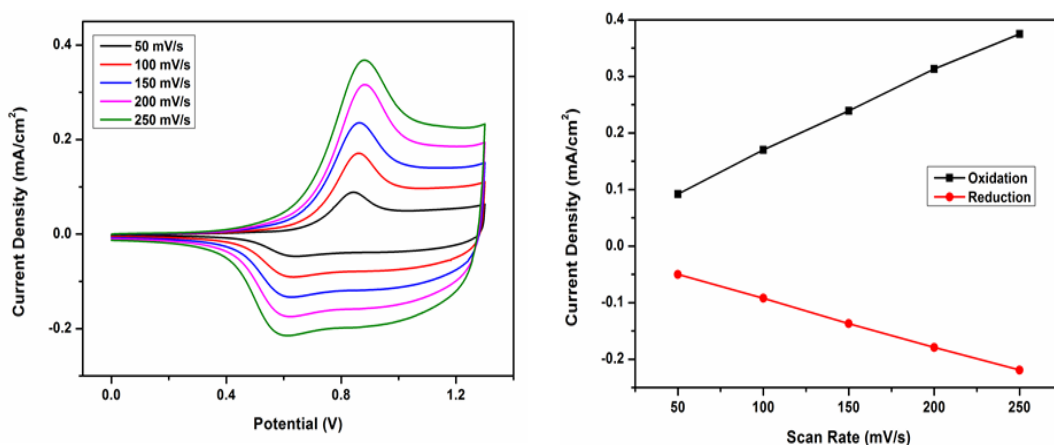


**Figure 40.** Scan rate study of PBSBSSif

### 3.2. Spectroelectrochemical Studies

Polymers were investigated in the p-doped spectra to obtain quantitative information on their light absorption behaviors as a function of wavelength. For that purpose, polymer solutions were coated onto ITO integrated glass surface and absorption spectra of the polymers in the UV-Vis-NIR region was taken in a quartz

cell filled with tetrabutylammonium hexafluorophosphate in acetonitrile as the electrolyte solution,

The first absorption peak that observed in the visible region correspond to  $\pi$ - $\pi^*$  transition between the HOMO and LUMO energy levels of the polymer. **PTBTSif**, **PSBSSif**, **PBTBTSif** and **PBSBSSif** showed maximum absorption peaks at 510 nm, 502 nm, 515 nm and 542 nm respectively. In comparison with **PTBTSif**, its branched alkyl chained counterpart, **PBTBTSif** showed red shift absorption with 5 nm. Similarly, **PBSBSSif** bearing branched alkyl chains showed red shift absorption with respect to the **PSBSSif** with 40 nm. The reason of this red shift is that  $\pi$ - $\pi$  stacking among the chains in the polymer backbone enhances due to the increase in the intermolecular interactions. Normally, it is expected that the intermolecular interactions weaken by the increase in the length of the alkyl chains. However, these red shifts in the mentioned studies were resulted from the decrease in the reorganization energy leading to smaller geometry relaxations. Moreover, onset values of the wavelengths of the polymers were recorded as 634 nm, 721 nm, 697 nm and 766 nm in the same order for mentioned polymers. The optical band gap values were measured from these onset values by the formula;  $E_g^{op} = 1241/\lambda_{onset}$ . These values were recorded as 1.96 eV, 1.72 eV, 1.78 eV and 1.62 eV for **PTBTSif**, **PSBSSif**, **PBTBTSif** and **PBSBSSif** respectively.  $\pi$ -bridge effect was seen clearly from band gap energies. Band gap of the selenophene based **PSBSSif** is lower than that of the thiophene based **PTBTSif** with 0.24 eV and similar result was depicted from the difference in band gap values of **PBTBTSif** and **PBSBSSif** which is lower in energy by 0.16 eV. The reason of this effect is coming from the high lying HOMO energy levels of the selenophene bearing  $\pi$ -bridges. In consequence of electrochemical and spectroelectrochemical studies, it was seen that optical band gap values of the polymers were lower than their electronic band gaps energies resulted from electron binding energy.

Upon oxidation of the polymers with an external voltage, new bands called as polaron (radical cation) and bipolaron (dication) bands form on the spectra. The polaron bands formed in the visible region and bipolaron bands appeared in the NIR

(near infrared) region. As the oxidation potential increases absorbance intensity in neutral state decreases while polaron or bipolaron band intensity enhance. All polymers except **PBSBSSif** showed two maxima at around 700 nm and 1200 nm for **PTBTSif**, 705 nm and 1203 nm for **PSBSSif**, 729 nm and 1350 nm for **PBTBTSif** and 1200 nm for **PBSBSSif**. The colors of the polymers in each state were determined by the International Commission on Illumination (CIE) system based on three variables, Luminance (L), hue (a), saturation (b). In this system, L indicates whether the color is dark or light, a scale is in the red-green range and b variable is in the yellow-blue color range. **PTBTSif** was orange (L: 86.504, a: 4.861, b: 34.937) in its neutral state and upon oxidation the color shifted to yellow (L: 89.205, a: 1.098, b: 37.029) and in the tail of the polaron band it was shifted to yellowish green (L: 81.401, a: -7.970, b: 2.804). **PSBSSif** was pink in its neutral state and its color shifted to light blue under positive voltage. **PBTBTSif** was appeared as reddish in its neutral state (L: 80.460, a: -3.659, b: 1.970) and by applying the positive voltage on it the colors shifted to the light blue (L: 79.443, a: -9.034, b: -0.800). **PBSBSSif** was light purple in its neutral state (L: 70.176, a: -2.327, b: -1.644) and color become light blue (L: 85.149, a: -8.842, b: 1.768) due to the formation of the new bands. The reason of decrease in the polaron band intensity is that polarons were converted into dications namely bipolarons with increasing potential. The electronic absorption spectra of the polymers were demonstrated in Figures 41-44 and also spectroelectrochemical studies were summarized in Table 2.

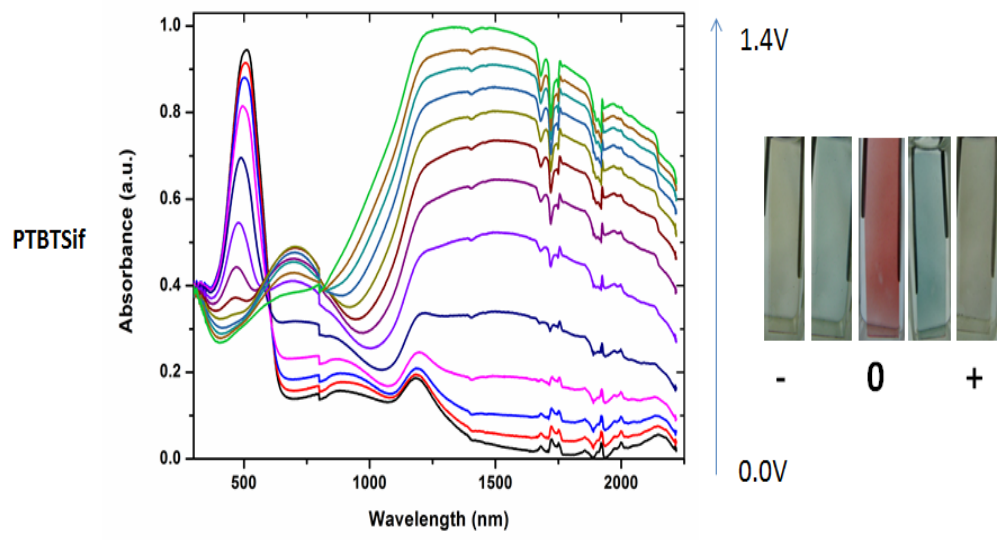


**Figure 41.** Electronic absorption spectra of the PTBTSif in UV-Vis-NIR regions

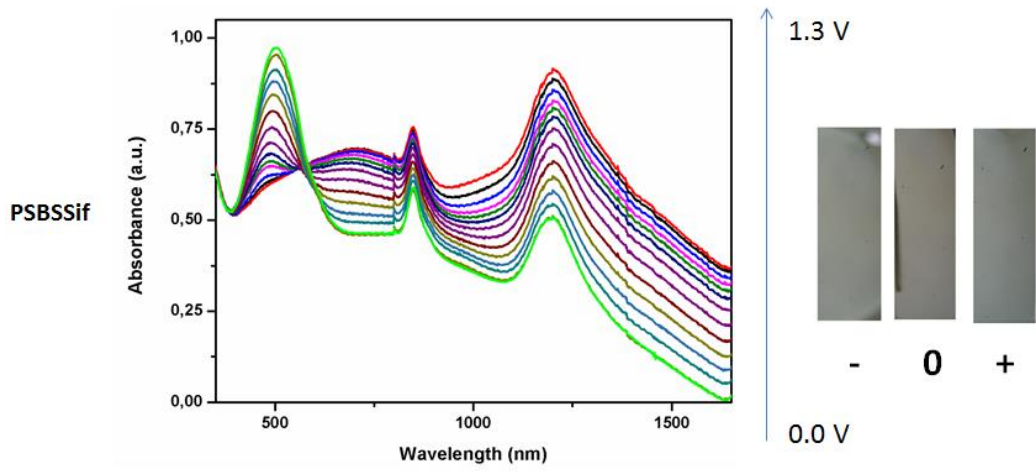


**Figure 42.** Electronic absorption spectra of the PSBSSif in UV-Vis-NIR regions

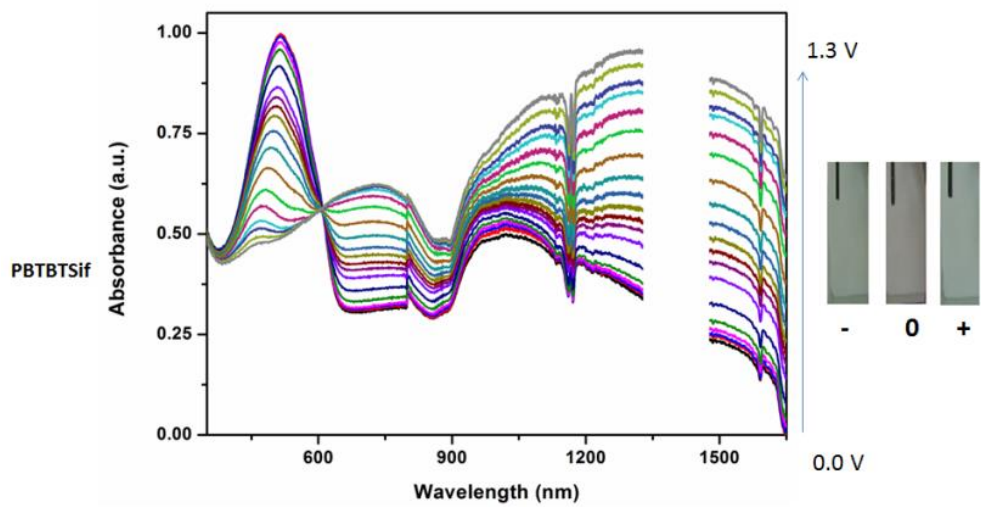


**Figure 43.** Electronic absorption spectra of the PBTBTSif in UV-Vis-NIR regions

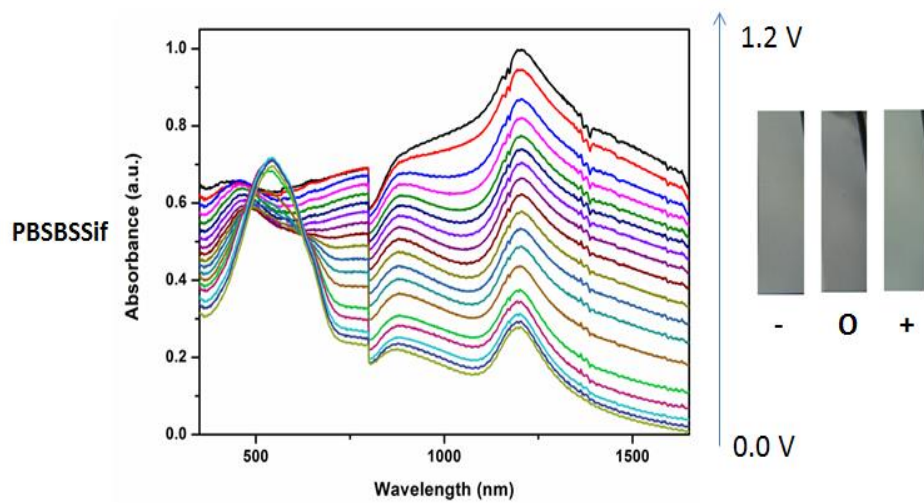


**Figure 44.** Electronic absorption spectra of the PBSBSSif in UV-Vis-NIR regions

**Table 2.** Summary of the spectroelectrochemical studies

	$\lambda_{\max}$ (nm)	$\lambda_{\text{onset}}$ (nm)	$E_g^{\text{op}}$ (eV)
<b>PTBTSif</b>	510	634	1.96
<b>PSBSSif</b>	502	721	1.72
<b>PBTBTSif</b>	515	697	1.78
<b>PBSBSSif</b>	544	766	1.62

### 3.3. Kinetic Studies

Percent transmittance change and switching times of the polymers were investigated by alternating oxidation and reduction processes with 5 seconds time intervals for each cycle. Optical contrast and switching time values were summarized in Table 3 and shown in Figures 45-48. Optical contrast values of **PTBTSif** were calculated as 24 % (510 nm), 10 % (700 nm) and 35 % (1220 nm). Its selenophene based counterpart **PSBSSif** showed unstable cycles in visible region and optical contrast value of this polymer was 12 % (1200 nm). The reason of this instability in visible region for the latter polymer resulted from the fact that selenophene is less stable to ambient atmosphere compare to thiophene. **PBTBTSif** exhibited 16 % (520 nm) and 24 % (1350 nm) percent transmittances and optical contrast value for **PBSBSSif** was measured as 23 % at 1200 nm. Optical contrast values enhances toward the NIR region since molecules achieve more quinoid character in this region and so stability of the polymers increases.

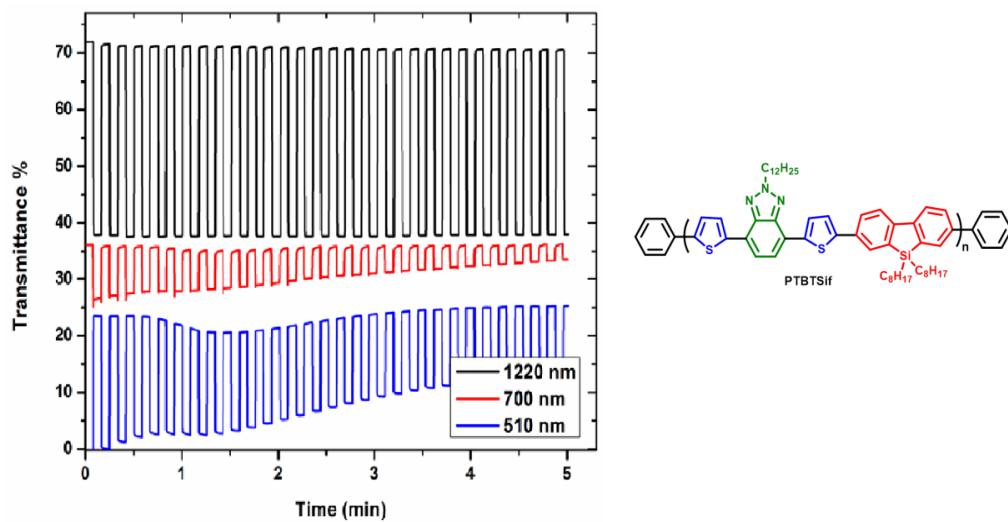


**Figure 45.** Change in the percent transmittance for PTBTSif

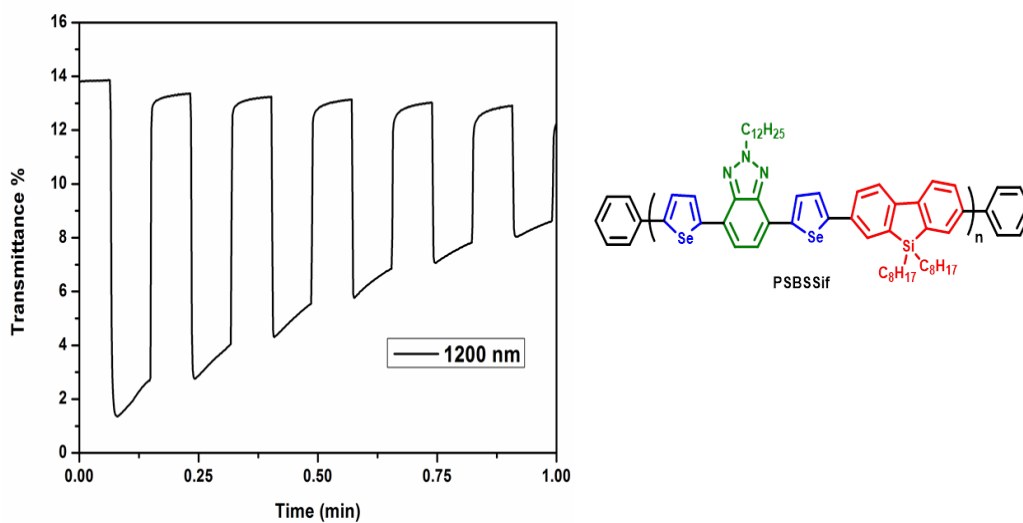


**Figure 46.** Change in the percent transmittance for PSBSSif

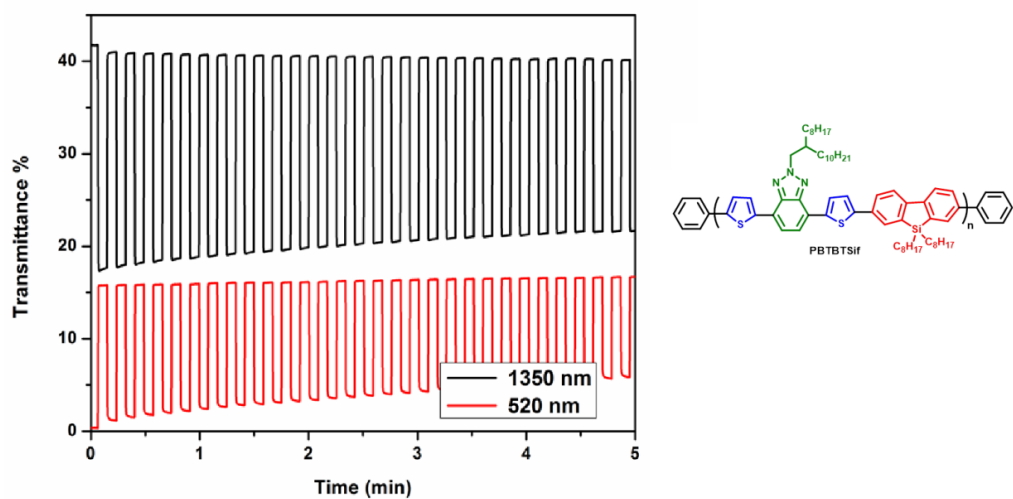


**Figure 47.** Change in the percent transmittance for PBTBTSif

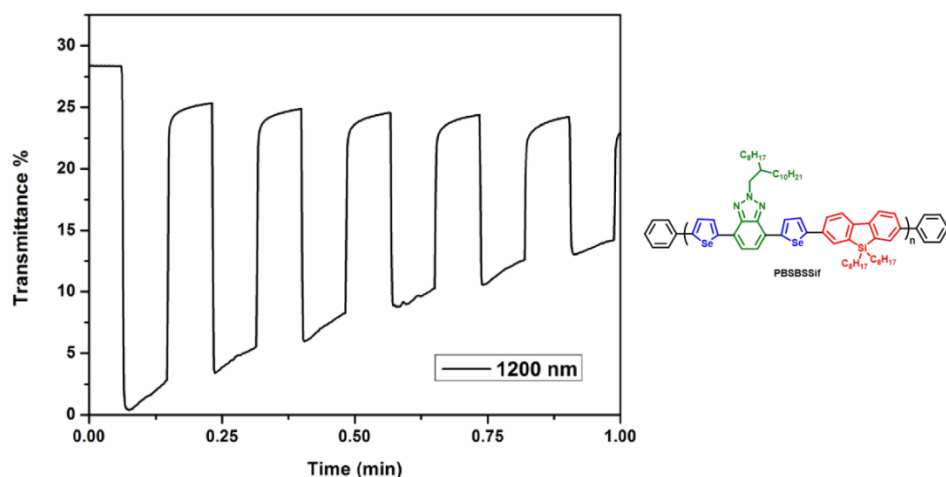


**Figure 48.** Change in the percent transmittance for PBSBSSif

**PTBTSif** exhibited remarkable switching times as 0.4 s (510 nm), 0.5 s (700 nm) and 0.4 s (1220 nm). This value for **PSBSSif** was 0.6 s at 1200 nm. **PBTBT** and **PBSBS** showed higher switching times with respect to the first two polymers bearing straight alkyl chains and switching times were recorded as 0.7 s (520 nm) and 0.7 s (1350 nm) for **PBTBTSif** and 1.0 s at 1200 nm for **PBSBSSif**. As the alkyl chain length of the polymers increase, switching times also increase

concordantly. This may be due to branched and long alkyl chains on the polymer make difficult doping/de-doping mechanism occurring on the polymer backbone.

**Table 3.** Summary of the Chronoamperometric Studies

	<b>Optical Contrast (<math>\Delta T</math> %)</b>	<b>Switching Time (s)</b>
<b>PTBTSif</b>	24 % (510 nm)	0.4
	10 % (700 nm)	0.5
	35 % (1220 nm)	0.4
<b>PSBSSif</b>	12 % (1200 nm)	0.6
<b>PBTBTSif</b>	16 % (520 nm)	0.7
	24 % (1350 nm)	0.7
<b>PBSBSSif</b>	23 % (1200 nm)	1.0

### 3.4. Thermal Analyses

Thermogravimetry analyses of the polymers were performed under N<sub>2</sub> atmosphere using TGA and DSC. According to the TGA graphs, the first mass loss with 5 % of **PTBTSif** was seen at around 430 °C and subsequently, the huge mass loss with 43 % until 800 °C which resulted from breaking of the covalent bonds on the polymer backbone. **PSBSSif** is stable until 420 °C and at this temperature first 5 % mass loss and from that point 63 % weight loss was seen until 800 °C. **PBTBTSif** exhibited 5 % mass loss at 430 °C and it lost 55 % its weight toward the 800 °C. **PTBTSif** and

**PBTBTSif** did not show glass-transition temperatures ( $T_g$ ), which may deduced from the rigid structure of the polymers. TGA and DSC results were showed in Appendix B.

### 3.5. Photovoltaic Studies

Synthesized polymers were designed as the donor materials in the active layer for a bulk heterojunction solar cell. Moieties bearing different alkyl chains were used to enhance the solubility of the polymers. Normalized thin film light absorbance spectrums were investigated for mixture of the polymer and PCBM in 1:2 ratio showed in Figure 49 and for pristine polymers they are demonstrated in Figure 50.

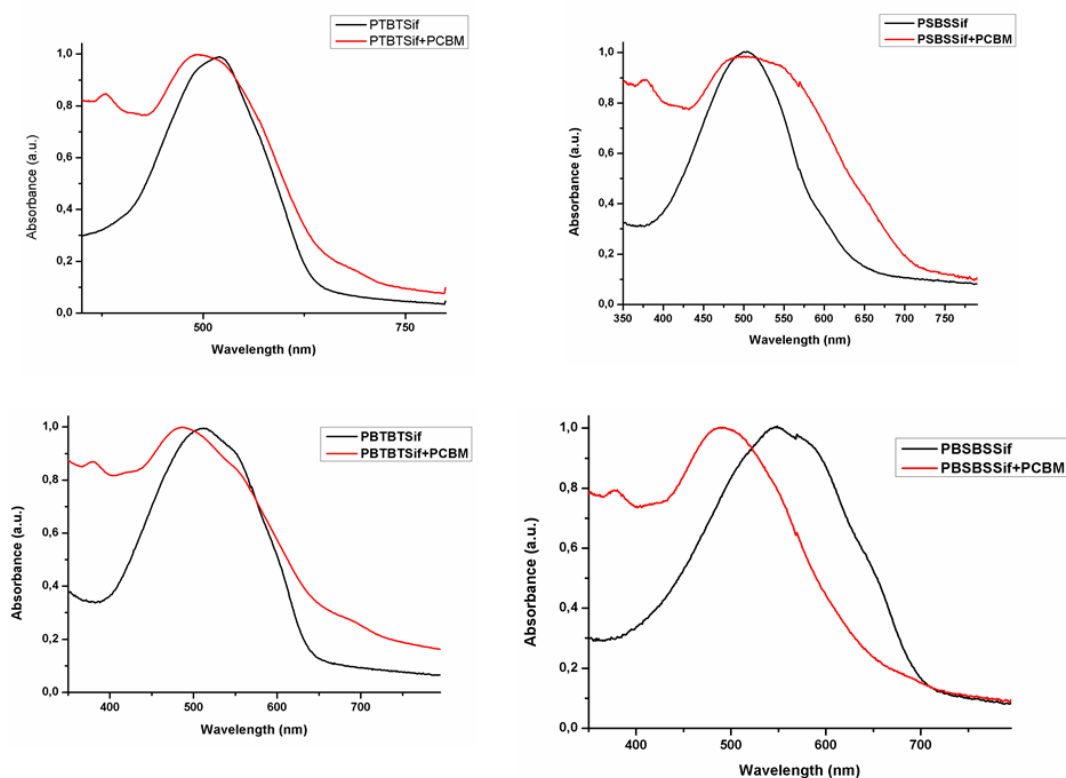


**Figure 49.** Normalized film absorbance spectra for polymer and PCBM mixtures

Unsurprisingly, all polymers except **PBSBSif** showed more broad absorptions in mixture forms because of the enhanced light absorption capacity. The mixtures of polymers and PCBM showed an additional peak absorbance on the left side of the spectrum resulting from intermolecular charge transfer (ICT) between the donor polymer and acceptor PCBM. Furthermore, **PBSBSif** exhibited broadest absorption in the visible region among the other polymers.

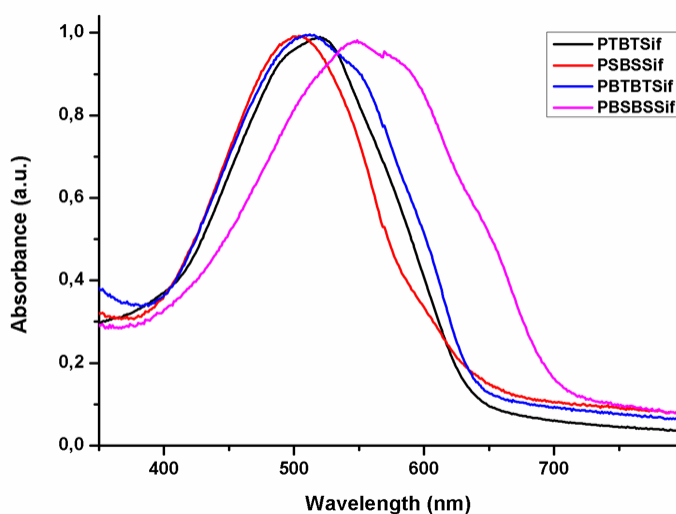


**Figure 50.** Relative thin film absorbance spectra of polymers

In photovoltaic studies, current density-voltage characteristics shown in Figures 51-54 were investigated and power conversion efficiencies of the polymers were measured at different conditions. In the light of these measurements, highest PCE was reported for **PBTBTsif** as 2.57 %. The highest efficiency values of other polymers were found as 1.78 % for **PTBTsif**, 1.85 % for **PSBSif** and 1.81 % for **BSBSif**. Among the polymers **PTBTsif** showed deepest HOMO level however, **PBTBTsif** has highest open circuit voltage value with 0.90 V because of the formation of charge transfer states between the donor polymer and acceptor fullerene. These polaron pairs can be seen by looking IPCE curves. A shoulder appeared at around 700 nm for **PTBTsif**. In addition to this, fill factor value was

very low for **PBTBTSif** with respect to the other polymers despite the fact that **PBTBTSif** has the highest current density and voltage characteristics. This resulted due to charge transport properties of the cells. It means that mobility of the electron and holes can be quite different from each other and this can lead to accumulation of positively charge carriers on one electrode resulting low fill factor. Polymers showed high current density values in 1:2 polymer/PCBM ratios due to the enhancing morphology. Solar cell characteristics were summarized in Table 4.

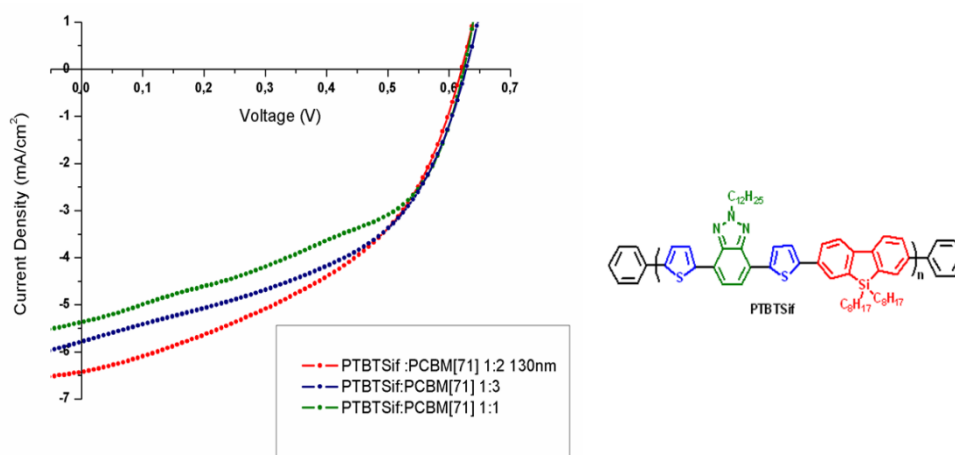


**Figure 51.** Current-Voltage characteristics of the PTBTSif

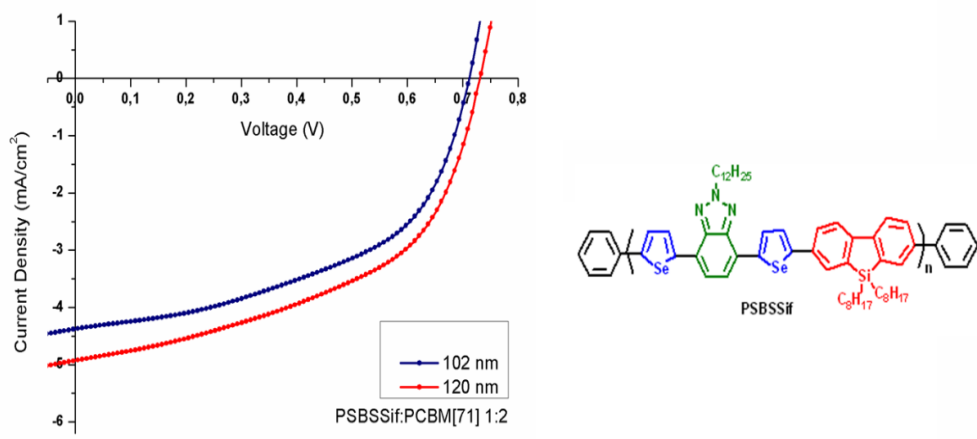


**Figure 52.** Current-Voltage characteristics of the PSBSSif

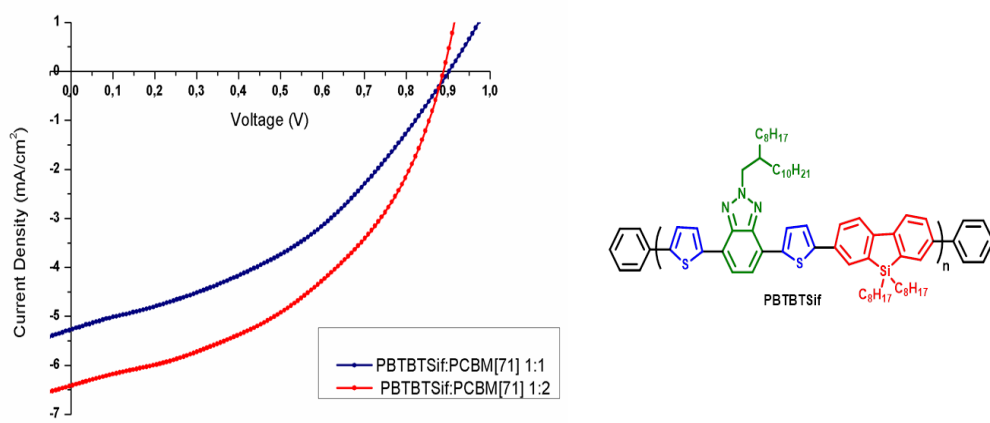


**Figure 53.** Current-Voltage characteristics of the PBTBTSif

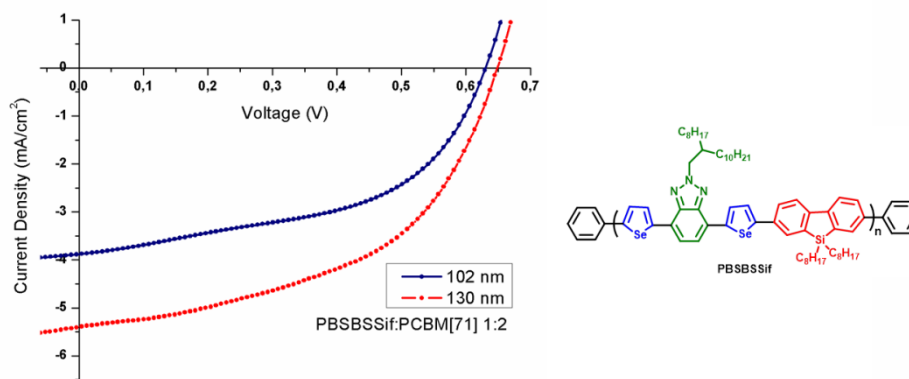


**Figure 54.** Current-Voltage characteristics of the PBSBSSif

The incident photon to current efficiency of cells prepared by 1:2 Polymer:PC<sub>71</sub>BM ratio is shown in Figure 55. It was investigated in the range of 250-1000 nm by using monochromatic light. The IPCE indicates the ratio of number of charges collected by electrodes to the number of incident photons. The maximum IPCE for **PTBTSif** was measured as 34 % at 375 nm. **PSBSSif** showed a maximum at 468 nm with 23 %. The lowest maximum IPCE value among the four polymers was measured for **PBTBTSif** as 19 % at 472 nm. The maximum EQE in a cell composed of **PBSBSSif** was measured as 22 % at 470 nm.

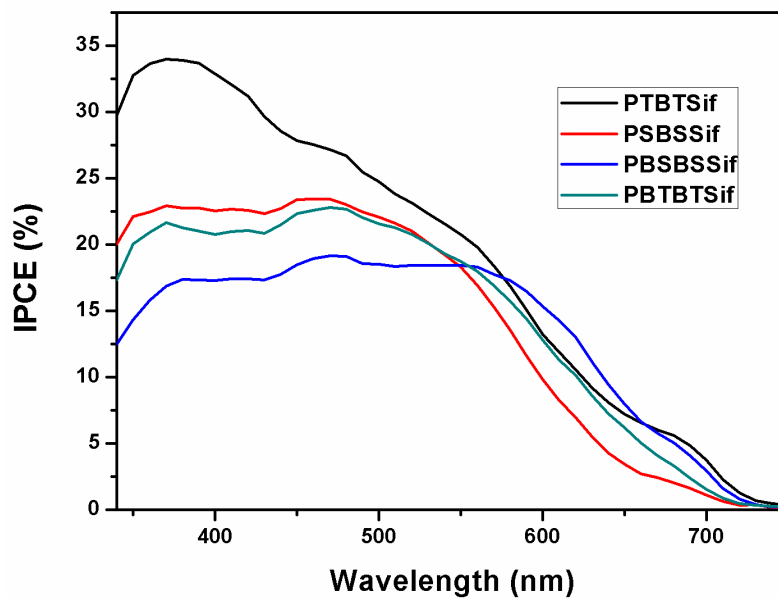


**Figure 55.** IPCE values of photovoltaic devices

Figure 56 demonstrates current density ( $J$ ) - voltage ( $V$ ) characteristics in the form of  $\log J$ - $\log V$  for the ITO/PEDOT:PSS/copolymer:PCBM/Ca/Al devices and hole mobility of the thin films were shown in Table 4. Although hole mobility of the **PSBSSif** was higher than that of the **PBSBSSif**, FF (fill factor) values was almost equal for these polymers. This is because the surface morphology of the **PBSBSSif** is better than that of the **PSBSSif** as an evidence for decrease in the re-organization energy in this polymer leading to highly ordered structure.

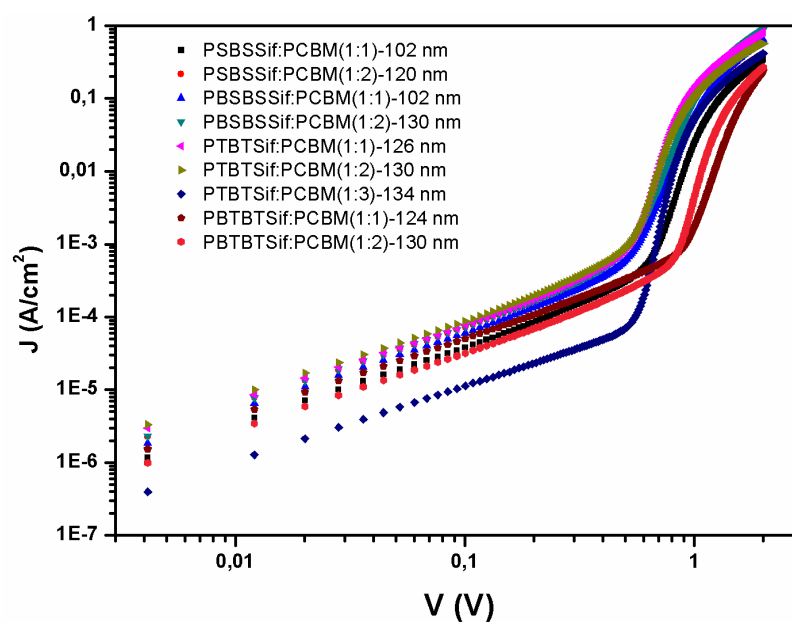


**Figure 56.** Logarithmic  $J$ - $V$  curve for the polymers

**Table 4.** Summary of the photovoltaic studies

Polymer	Polymer : PCBM ratio	Thickness <sup>s</sup> (nm)	$V_{oc}$ (V)	$J_{sc}$ (mA/cm <sup>2</sup> )	$V_{max}$ (V)	$J_{max}$ (mA/cm <sup>2</sup> )	$\mu$ (cm <sup>2</sup> V <sup>-2</sup> s <sup>-1</sup> )	FF (%)	$\eta$ (%)
PTBTSif	1:1	130	0.63	4.81	0.48	3.32	$1.81 \times 10^{-3}$	53	1.60
	1:2	130	0.63	6.44	0.42	4.27	$2.74 \times 10^{-3}$	42	1.78
	1:3	130	0.63	5.80	0.45	3.87	$1.56 \times 10^{-3}$	48	1.75
PSBSif	1:2	102	0.71	4.38	0.49	3.18	$5.33 \times 10^{-4}$	50	1.55
	1:2	120	0.73	4.97	0.53	3.54	$1.07 \times 10^{-3}$	51	1.85
PBTBTSif	1:1	130	0.90	5.28	0.56	3.43	$1.69 \times 10^{-3}$	40	1.92
	1:2	130	0.89	6.43	0.57	4.51	$2.44 \times 10^{-3}$	45	2.57
PBSBSif	1:2	102	0.63	3.88	0.47	2.70	$4.53 \times 10^{-4}$	52	1.26
	1:2	130	0.65	5.41	0.44	4.12	$9.26 \times 10^{-4}$	52	1.81



## CHAPTER 4

### CONCLUSION

Conjugated semiconducting polymers were synthesized by donor-acceptor-donor (DAD) approach for optoelectronic applications. In this manner, monomers were synthesized chemically by Stille coupling reactions and polymers were synthesized chemically by Suzuki poly-condensation reactions. Polymers were investigated in several aspects as electrochemically and optical. In addition to these investigations, photovoltaic studies were conducted for all polymers.

In all these studies alkyl chain effect and  $\pi$ -bridge donor moiety effects were explored separately. Polymers containing selenophene units in their backbone showed lower band gap values with respect to polymers bearing thiophene  $\pi$ -bridge units due to the increase in the energetic position of the HOMO energy level. Furthermore, it was seen that optical band gaps of the polymers were lower than that of the electronic band gaps because of the count for electron binding energy. Another inference is that selenophene based polymers are oxidized easily and they have lower stabilities in visible region with respect to the thiophene based ones. In addition to this, polymers with branched alkyl chains showed red shift character in comparison with polymers with straight alkyl chains due to the decrease in re-organization energy leading to increase in the crystalline nature. Kinetic studies exhibited that most stable polymers is **PTBTSif** and it showed good switching times in the range of 0.4-0.5 seconds.

The bulk heterojunction solar cells were fabricated using four different polymers as the donor materials. The highest PCE was reported as 2.57 % for **PBTBTSif** with high  $V_{oc}$  value (0.89 V), moderate  $J_{sc}$  value (6.43 mA/cm<sup>2</sup>) and low fill factor with

45 %. Other polymers also exhibited good PCE values as 1.78 % for **PTBTSif**, 1.85 % for **PSBSSif** and 1.81 % for **PBSBSSif**. Moreover, IPCE were obtained as 34 % for **PTBTSif** at 375 nm, 23 % for **PSBSSif** at 468 nm, 19 % for **PBTBTSif** at 472 nm and 22 % for **PBSBSSif** at 470 nm. It is expected that solar cell efficiency for these polymers will be increased by ongoing studies.

## REFERENCES

- [1] V. Devabhaktuni, *Renewable and Sustainable Energy Reviews*, 19, 2013, 555-569
- [2] US Department of Energy, *International Energy Outlook 2013*, Technical report DOE/EIA-0484 (2013): <http://www.eia.gov/forecasts/eio/> [last accessed on September 2014]
- [3] A. Slaoui and R.T. Collins, *MRS Bulletin*, 32, March 2007, 211-218
- [4] W. Liptay, *Angew. Chem. Internat. Edit.*, 8(3), 1969, 178-188
- [5] R. J. Mortimer, *Chemical Society Reviews*, 26, 1997, 147-156
- [6] A. A. Argun, P. H. Aubert, B. C. Thompson, I. Schwendeman, C.L. Gaupp, J. Hwang, N.J. Pinto, D. B. Tanner, A. G. MacDiarmid, J. R. Reynolds, *Chem. Mater.*, 16, 2004, 4401-4412
- [7] B. C. Thompson, P. Schottland, K. Zong, J. R. Reynolds, *Chem. Mater.*, 12, 2000, 1563-1571
- [8] D. D. Yao, R. A. Rani, A. P. O'Mullane, K. Kalantar-zadeh, J. Z. Ou, *J. Phys. Chem.*, 118, 2014, 10867-10873
- [9] R. E. Hummel, K. H. Guenther, *Handbook of Optical Properties*, Volume I, 1995, p.110
- [10] U. Bulut, A. Cirpan, *Synthetic Metals*, 148, 2005, 65-69
- [11] E. F. Schubert, T. Gessmann, J. K. Kim, *Encyclopedia of Chemical Technology*, 2005, p.1
- [12] N. Yeh, J-P. Chung, *Renewable and Sustainable Energy Reviews*, 13, 2009, 2175-2180
- [13] N. T. Kalyani, S. J. Dhoble, *Renewable and Sustainable Energy Reviews*, 16, 2012, 2696-2723
- [14] A. P. Kulkarni, C. J. Tonzola, A. Babel, S. A. Jenekhe, *Chem. Mater.*, 16, 2004, 4556-4573
- [15] U. Mitschke, P. Baurle, *J. Mater. Chem.*, 10, 2000, 1471-1507
- [16] S. Reineke, *Rev. Mod. Phys.*, 85, 2013, 1245-1293

- [17] G. Horowitz, *Adv. Mater.*, 10 (5), 1998, 365-377
- [18] M. J. Malachowski and J. Zmija, *Opto-Electronics Review*, 18(2), 2010, 126-136
- [19] J. Zaumseil and H. Sirringhaus, *Chem. Rev.*, 107, 2007, 1296-1323
- [20] C. E. Fritts, *Proc. Am. Assoc. Adv. Sci.*, 33, 1983, 97
- [21] S. R. Wenham, M. A. Green, *Prog. Photovolt: Res. Appl.*, 4, 1996, 3-33
- [22] A. F. Fahrenbruch and R. H. Bube, 'Fundamentals of Solar Cells', Academic Press, New York, p. 1-23, 1983
- [23] S. E. Habas, A. S. Platt, F. A. M. van Hest, D. S. Ginley, *Chem. Rev.*, 110, 2010, 6571-6594
- [24] M. A. Green, K. Emery, Y. Hishikawa, W. Warta, E. D. Dunlop, *Prog. Photovolt: Res. Appl.*, 20, 2012, 12-20
- [25] G. Horowitz, *Adv. Mater.*, 2, 1998, 129
- [26] N. Li, D. Baran, K. Forberich, F. Machui, T. Ameri, M. Turbiez, M. Carrasco-Orozco, M. Drees, A. Facchetti, F. C. Krebs and C. J. Brabec, *Energy Environ. Sci.*, 6, 2013, 3407-3413
- [27] D. Wöhrle and D. Meissner, *Adv. Mater.* 3 (3), 1991, 129-138
- [28] S. Gunes and N. S. Sariciftci, *Inorganica Chimica Acta*, 361, 2008, 581-588
- [29] M. Wright and A. Uddin, *Solar Energy Materials & Solar Cells*, 107, 2012, 87-111
- [30] T. Xu and Q. Qiao, *Energy Environ. Sci.*, 4, 2011, 2700-2720
- [31] H. Spanggaard and F. C. Krebs, *Solar Energy Materials & Solar Cells*, 83, 2004, 125-146
- [32] H. P. Su, J. R. Schrieffer, S. Kivelson and A. J. Heeger, *Reviews of Modern Physics*, 60 (3), 1998, 781-851
- [33] A. G. MacDiarmid, *Angew. Chem. Int. Ed.*, 40, 2001, 2581-2590
- [34] A. J. Heeger, *Angew. Chem. Int. Ed.*, 40, 2001, 2591-2611
- [35] H. Shirakawa, *Angew. Chem. Int. Ed.*, 40, 2001, 2574-2580
- [36] C. K. Chiang, C. R. Fincher, Y. W. Park, A. J. Heeger, H. Shirakawa, E. J. Luis, S. C. Gau, A. G. MacDiarmid, *Physical Review Letters*, 39 (17), 1977, 1098-1101
- [37] A. Facchetti, *Chem. Mater.* 23, 2011, 733-758

- [39] J. M. Nunzi, C.R. Physique, 3, 2002, 523-542
- [40] I. Schwendeman, PhD Thesis, University of Florida, 2002
- [41] J. Rocali, Macromol. Rapid Commun., 28, 2007, 1761-1775
- [42] Y. J. Cheng, S. H. Yang, C. S. Hsu, Chem. Rev., 109 (11), 2009, 5868-5923
- [43] C. Winder and N. S. Sariciftci, J. Mater. Chem., 14, 2004, 1077-1086
- [44] R. J. Waltman, J. Bargon and A. F. Diaz, J. Phys. Chem., 87 (8), 1983, 1459-1463
- [45] J. Roncali, R. Garreau, A. Yassar, P. Marque, F. Garnier and M. Lemaire, J. Phys. Chem., 91 (27), 1987, 6706-6714
- [46] R. D. McCullough, R. D. Lowe, M. Jayaraman and D. L. Anderson, J. Org. Chem., 85, 1993, 904
- [47] H. Zhou, L. Yang and W. You, Macromolecules, 45, 2012, 607-632
- [48] A. Ajayaghosh, Chem. Soc.Rev., 32, 2003, 181-191
- [49] D. Kumar and R. C. Sharma, Eur. Polym. J., 34, 1998, 1053-1060
- [50] W. A. Gazotti, A. F. Nogueira, E. M. Giroto, L. Micaroni, M. Martini, S. Neves and M. A. De-Paoli, 'Handbook of Advanced Electronic and Photonic Materials and Devices, Volume 10, 2001, p. 55
- [51] J. L. Bredas, J. C. Scott, K. Yakushi and G. B. Street, Phys. Rev. B, 30, 1984, 1023-1025
- [52] C. Deibel, T. Strobel and V. Dyakonov, Adv. Mater., 22, 2010, 4097-4111
- [53] P. W. M. Blom, V. D. Mihailetschi, L. J. A. Koster and D. E Markov, Adv. Mater., 19, 2007, 1551-1566
- [54] J. L. Bredas, J. E. Norton, J. Cornil and V. Coropceanu, Accounts of Chemical Research, 42 (11), 2009, 1691-1699
- [55] A. Moliton and J. M. Nunzi, Polym. Int., 55, 2006, 583-600
- [56] H. Hoppe and N. S. Sariciftci, J. Mater. Res., 19 (7), 2004, 1924-1945
- [57] S. Gunes, H. Neugebauer and N. S. Sariciftci, Chem. Rev., 107, 2007, 1324-1338
- [58] K. M. Coakley and M. D. McGehee, Chem. Mater., 16, 2004, 4533-4542
- [59] L. M. Chen, Z. Hong, G. Li and Y. Yang, Adv. Mat., 21, 2009, 1434-1449
- [60] I. Kim, PhD Thesis, Arizona State University, 2010
- [61] A. J. Heeger, 25<sup>th</sup> Anniversary Article, Adv. Mater., 2013

- [62] X. Yang and A. Uddin, *Renewable and Sustainable Energy Reviews*, 30, 2014, 324-336
- [63] E. Bundgaard and F. C. Krebs, *Solar Energy Materials and Solar Cells*, 91, 2007, 954-985
- [64] E. Bundgaard, S. E. Shaheen, F. C. Krebs and D. S. Ginley, *Solar Energy Materials and Solar Cells*, 91, 2007, 1631-1637
- [65] S. H. Park, A. Roy, S. Beaupre, S. Cho, N. Coates, J. S. Moon, D. Moses, M. Leclerc, K. Lee and A. J. Heeger
- [66] G. Dennler, M. C. Scharber and C. J. Brabec, *Adv. Mater.*, 21, 2009, 1323-1338
- [67] V. D. Mihailetschi, H. Xie, B. de Boer, L. J. A. Koster and P. W. M. Blom, *Adv. Funct. Mater.*, 16, 2006, 699-708
- [68] C. J. Brabec, A. Cravino, D. Meissner, N. S. Sariciftci, T. Fromherz, M. T. Rispens, L. Sanchez and J. C. Hummelen, *Adv. Funct. Mater.*, 11 (5), 2001, 374-380
- [69] M. C. Scharber, D. Mühlbacher, M. Koppe, P. Denk, C. Waldauf, A. J. Heeger and C. J. Brabec, *Adv. Mater.*, 18, 2006, 789-794
- [70] N. Miyauro and A. Suzuki, *Chem. Rev.*, 95, 1995, 2457-2483
- [71] P. Espinet and A. M. Echavarren, *Angew. Chem. Int. Ed.*, 43, 2004, 4704-4734
- [72] J. L. Banal, J. Subbiah, H. Graham, J. K. Lee, K. P. Ghiggino and W. W. H. Wong, *Polym. Chem.*, 4, 2013, 1077-1083
- [73] W. W. H. Wong, J. Subbiah, S. R. Puniredd, W. Pisula, D. J. Jones and A. B. Holmes, *Polym. Chem.*, 5, 2014, 1258-1263
- [74] A. Tanimoto and T. Yamamoto, *Adv. Synth. Catal.*, 346, 2004, 1818-1823
- [75] S. C. Price, A. C. Stuart, L. Yang, H. Zhou and W. You, *J. Am. Chem. Soc.*, 133, 2011, 4625-4631
- [76] R. R. Gupta, T. M. Krygowski and M. K. Cyranski, *Aromaticity in Heterocyclic Compounds*, p.292, 2009
- [77] M. R. Detty, *Chemistry of Heterocyclic Compounds*, 1994, p.112
- [78] L. Ye, S. Zhang, L. Huo, M. Zhang and J. Hou, *Acc. Chem. Res.* 47, 2014, 1595-1603

- [79] X. Wang, Y. Sun, S. Chen, X. Guo, M. Zang, X. Li, Y. Li and H. Wang, *Macromolecules*, 42, 2012, 1208-1216
- [80] L. Dou, W. H. Cheng, J. Gao, C. C. Chen, J. You and Y. Yang, *Adv. Mater.*, 25, 2013, 825-831
- [81] C. Duan, W. Cai, F. Huang, J. Zhang, M. Wang, T. Yang, C. Zhong, X. Gong and Y. Cao, *Macromolecules*, 43, 2010, 5262-5268
- [82] G. Lu, H. Usta, C. Risko, L. Wang, A. Facchetti, M. A. Ratner and T. J. Marks, *J. Am. Chem. Soc.*, 130, 2008, 7670-7685
- [83] P. L. T. Boudreault, A. Michaud and M. Leclerc, *Macromol. Rapid Commun.*, 28, 2007, 2176-2179
- [84] J. Song, C. Du, C. Li and Z. Bo, *Journal of Polymer Science Part A: Polymer Chemistry*, 49, 2011, 4267-4274



## APPENDIX A

### NMR DATA

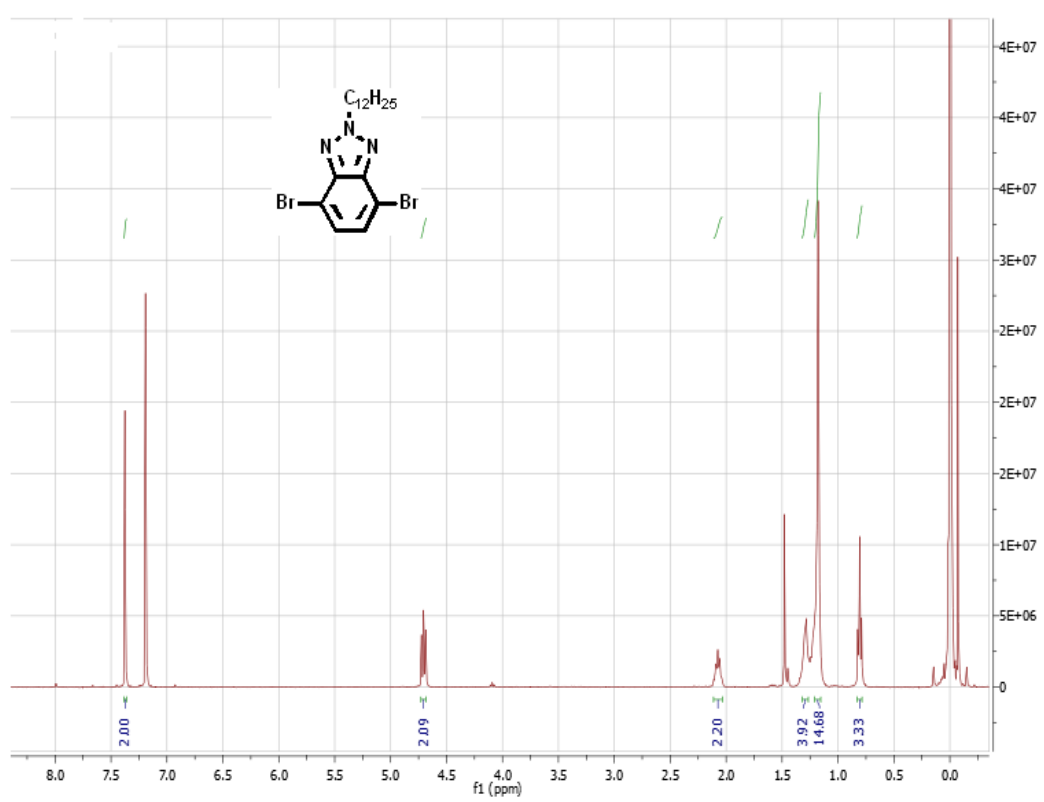


**Figure 57.**  $^1\text{H}$  NMR result of 4,7-dibromo-2-dodecyl-2H-benzo[d][1,2,3]triazole (2)

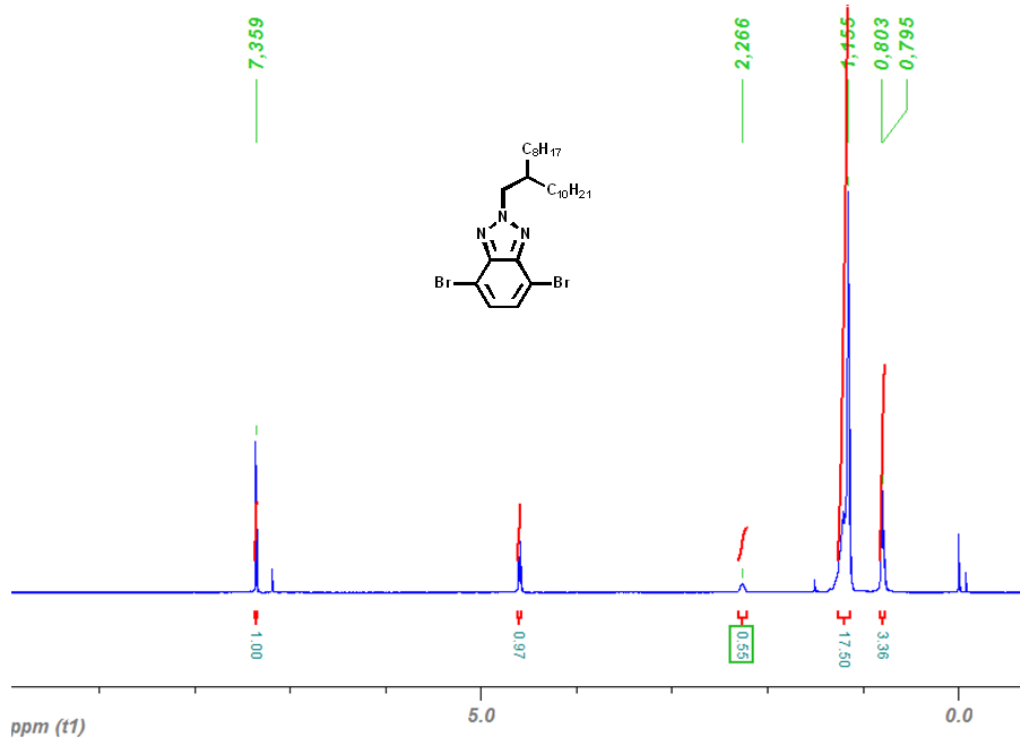


**Figure 58.** <sup>1</sup>H NMR result of 4,7-dibromo-2-(2-octyldodecyl)-2H-benzo[d][1,2,3]triazole (4)

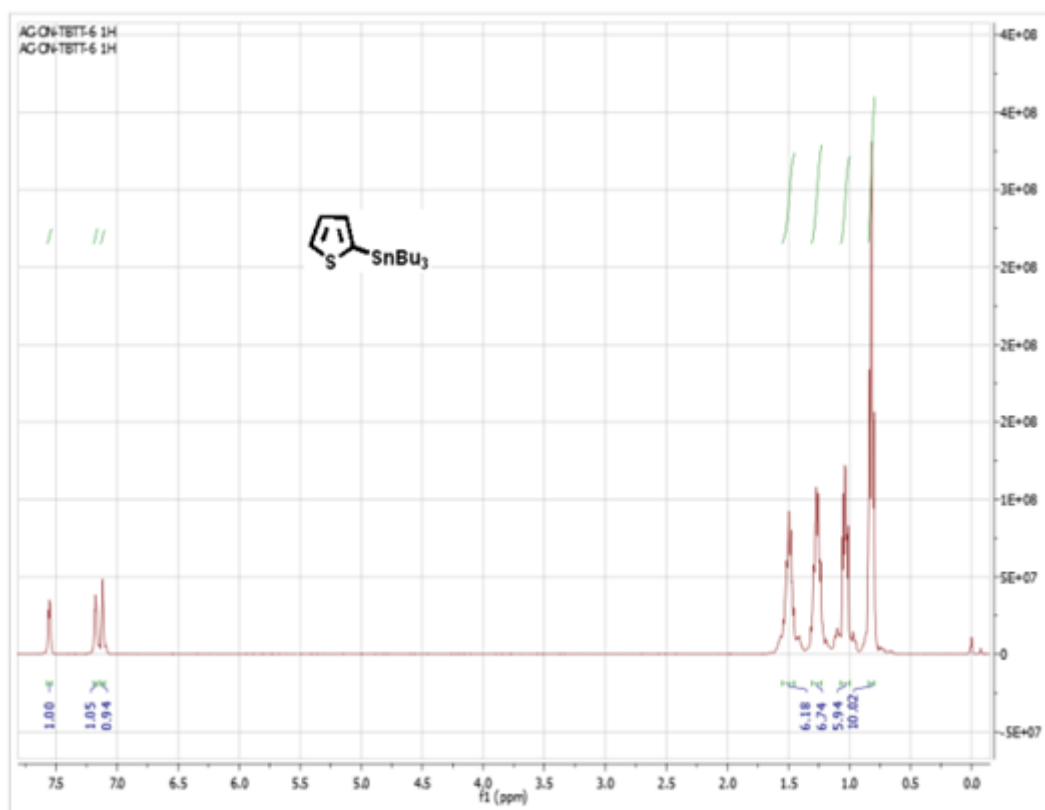


**Figure 59.**  $^1\text{H}$  NMR result of tributyl(thiophen-2-yl)stannane (5)

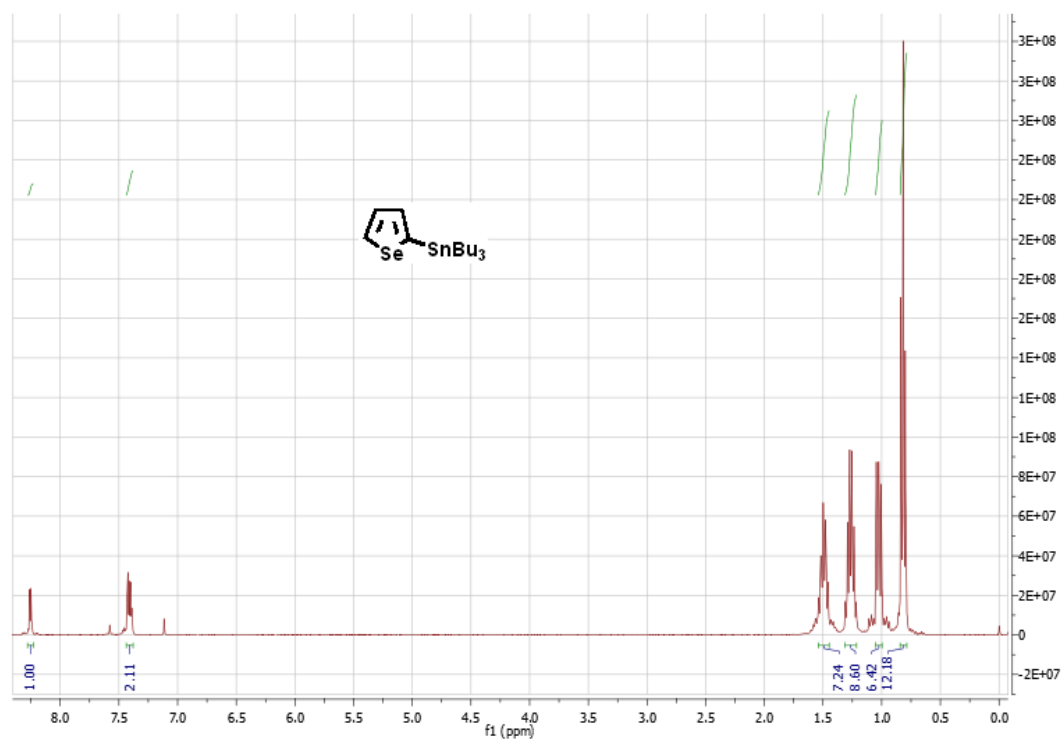


**Figure 60.** <sup>1</sup>H NMR of tributyl(selenophen-2-yl)stannane (6)

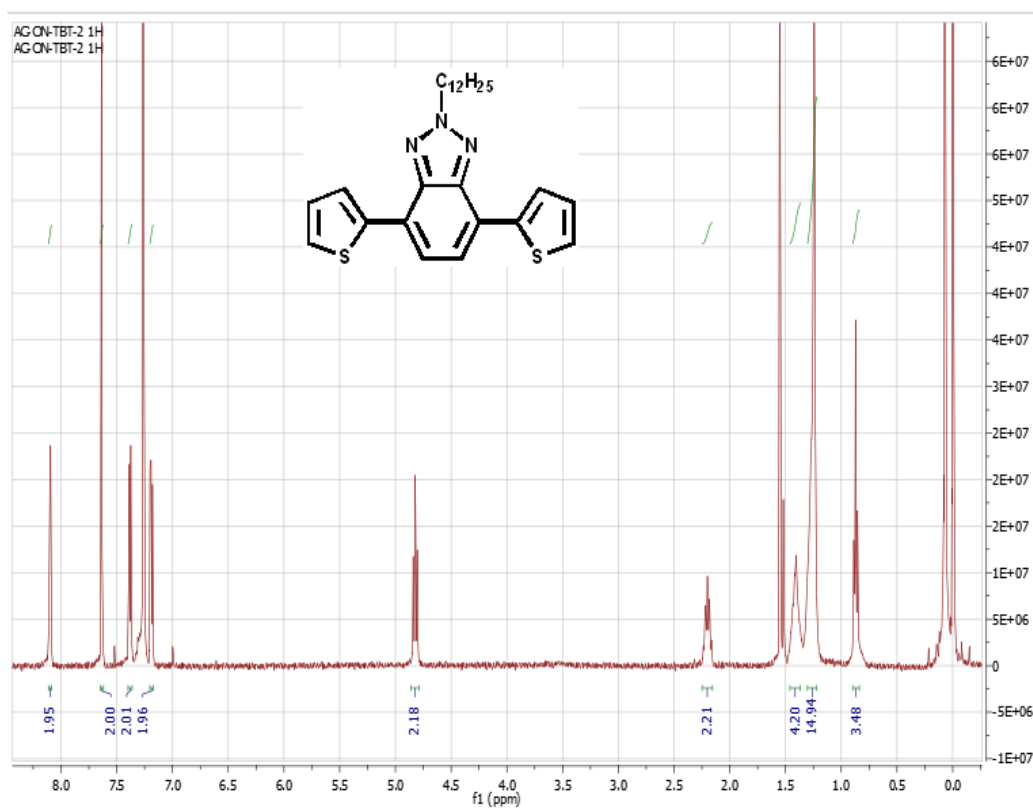


**Figure 61.**  $^1\text{H}$  NMR result of 2-dodecyl-4,7-di(thiophen-2-yl)-2H-benzo[d][1,2,3]triazole (7)

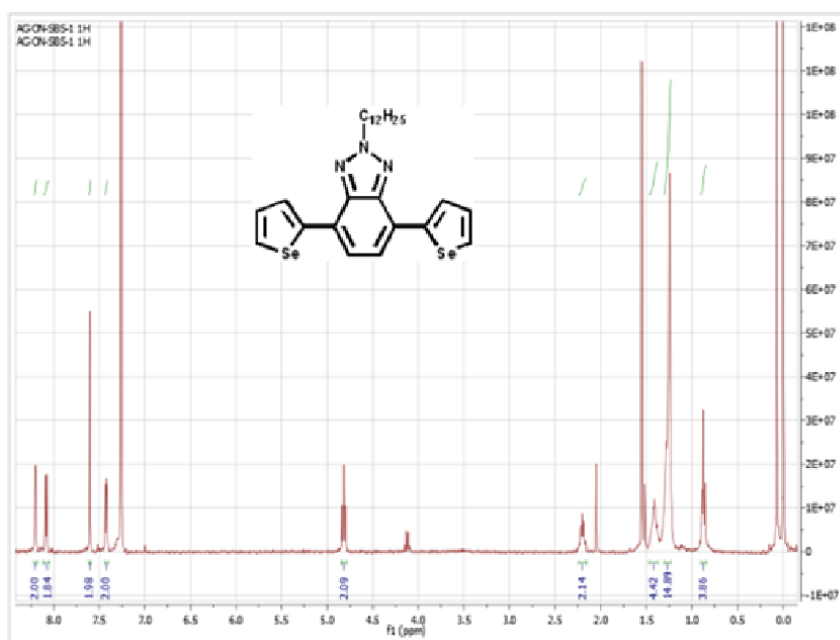


**Figure 62.**  $^1\text{H}$  NMR result of 2-dodecyl-4,7-di(selenophen-2-yl)-2H-benzo[d][1,2,3]triazole (8)

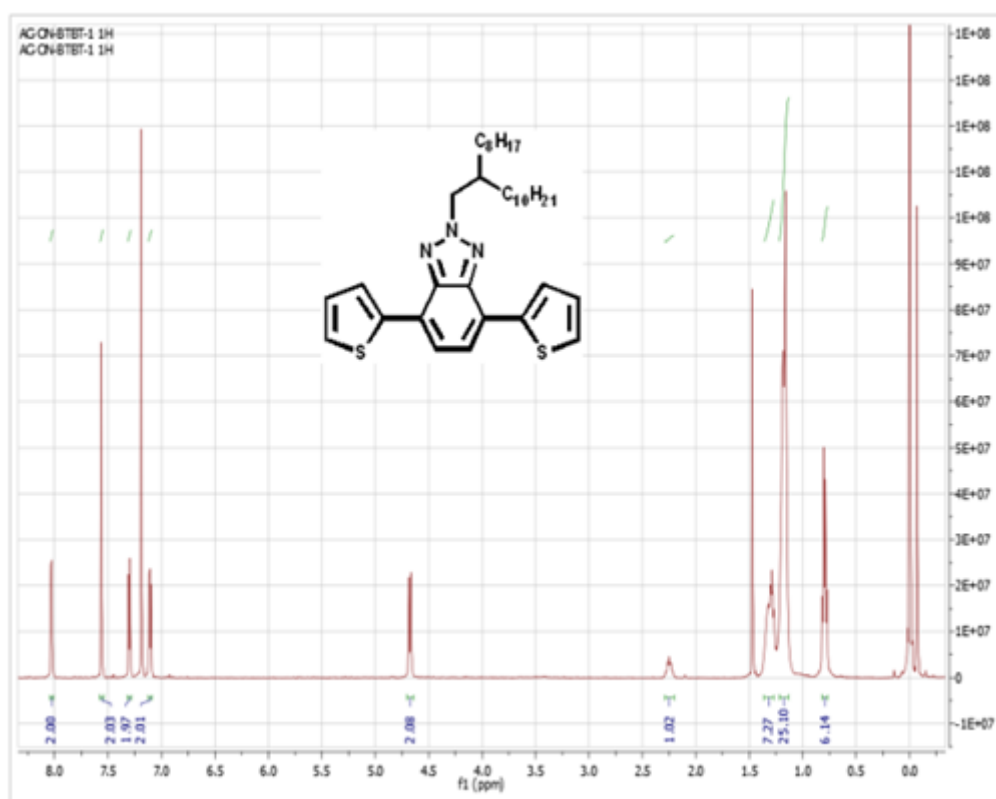


**Figure 63.**  $^1\text{H}$  NMR result of Synthesis of 2-(2-octyldodecyl)-4,7-di(thiophen-2-yl)-2H-benzo[d][1,2,3]triazole (9)

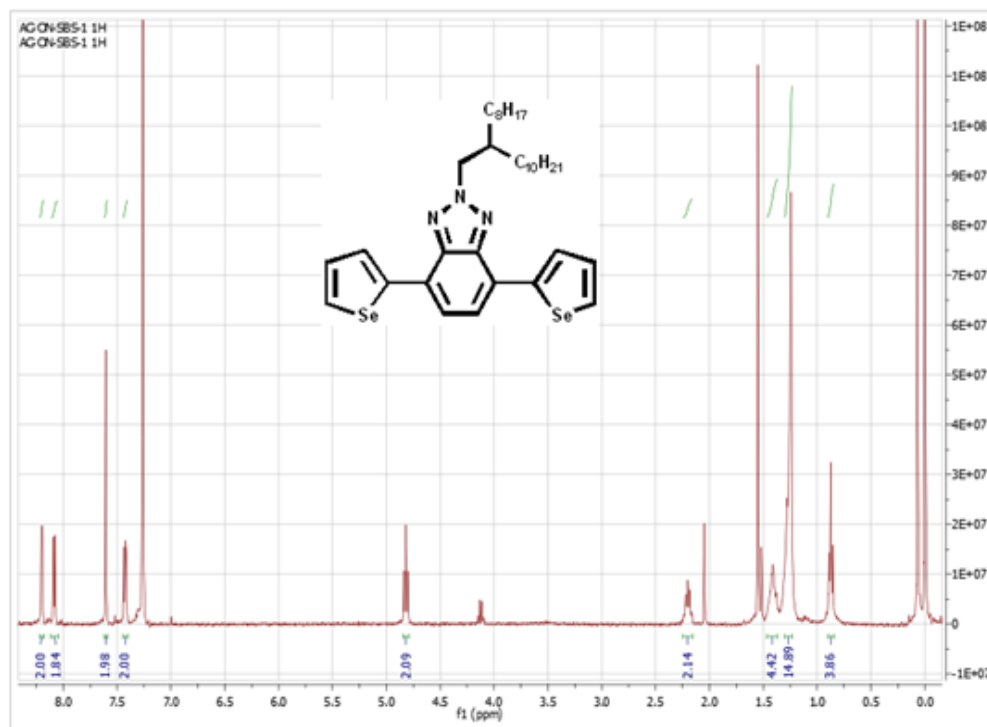


**Figure 64.** <sup>1</sup>H NMR result of the 2-(2-octyldodecyl)-4,7-di(selenophen-2-yl)-2H-benzo[d][1,2,3]triazole (10)

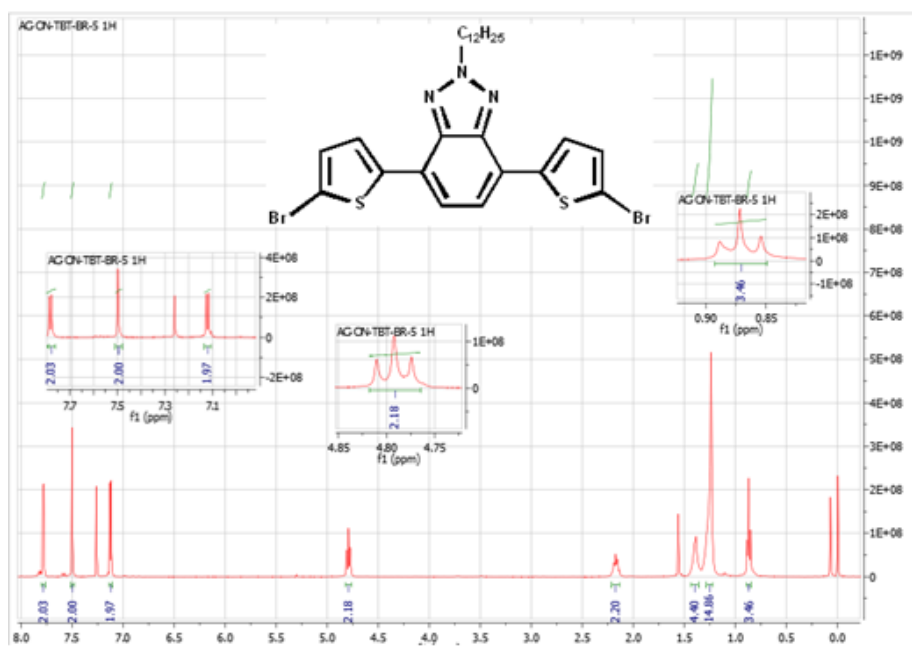


**Figure 65.** <sup>1</sup>H NMR result of 4,7-bis(5-bromothiophen-2-yl)-2-dodecyl-2H-benzo[d][1,2,3]triazole (11)

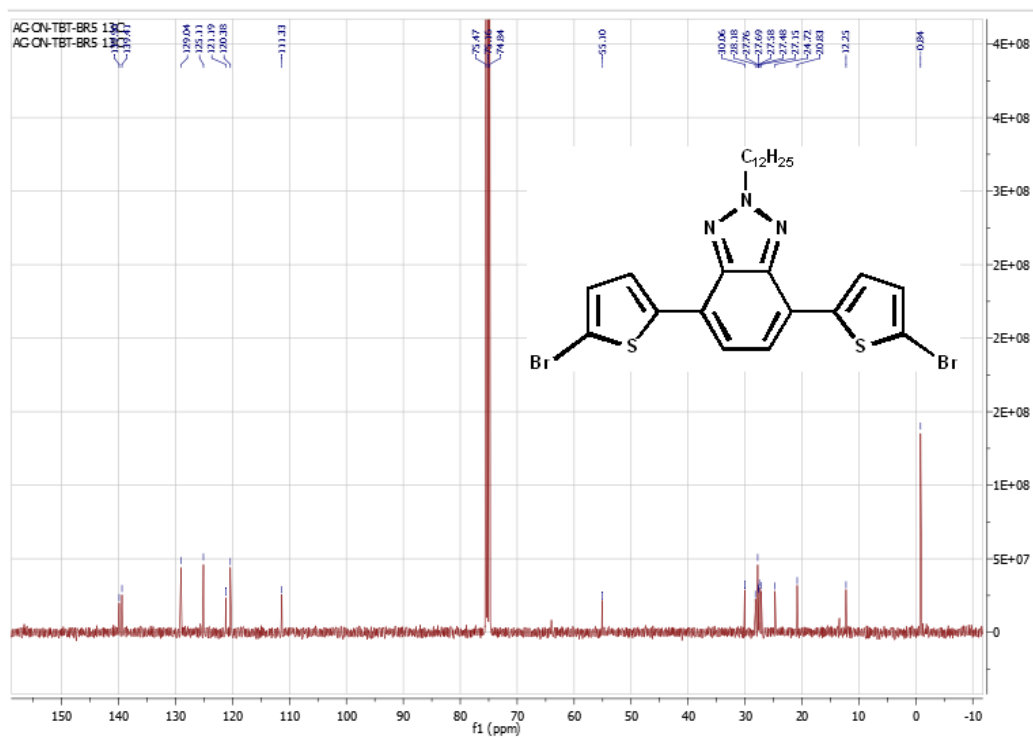


**Figure 66.**  $^{13}\text{C}$  NMR result of 4,7-bis(5-bromothiophen-2-yl)-2-dodecyl-2H-benzo[d][1,2,3]triazole (11)

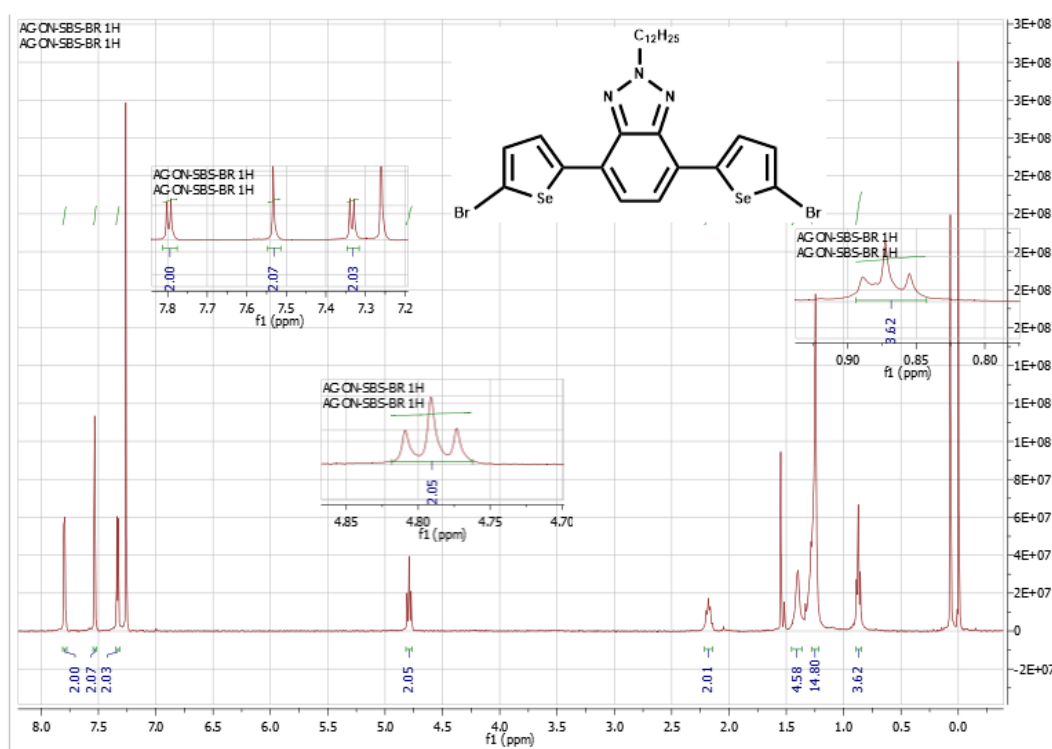


**Figure 67.**  $^1\text{H}$  NMR Result of 4,7-bis(5-bromoselenophen-2-yl)-2-dodecyl-2H-benzo[d][1,2,3]triazole (12)

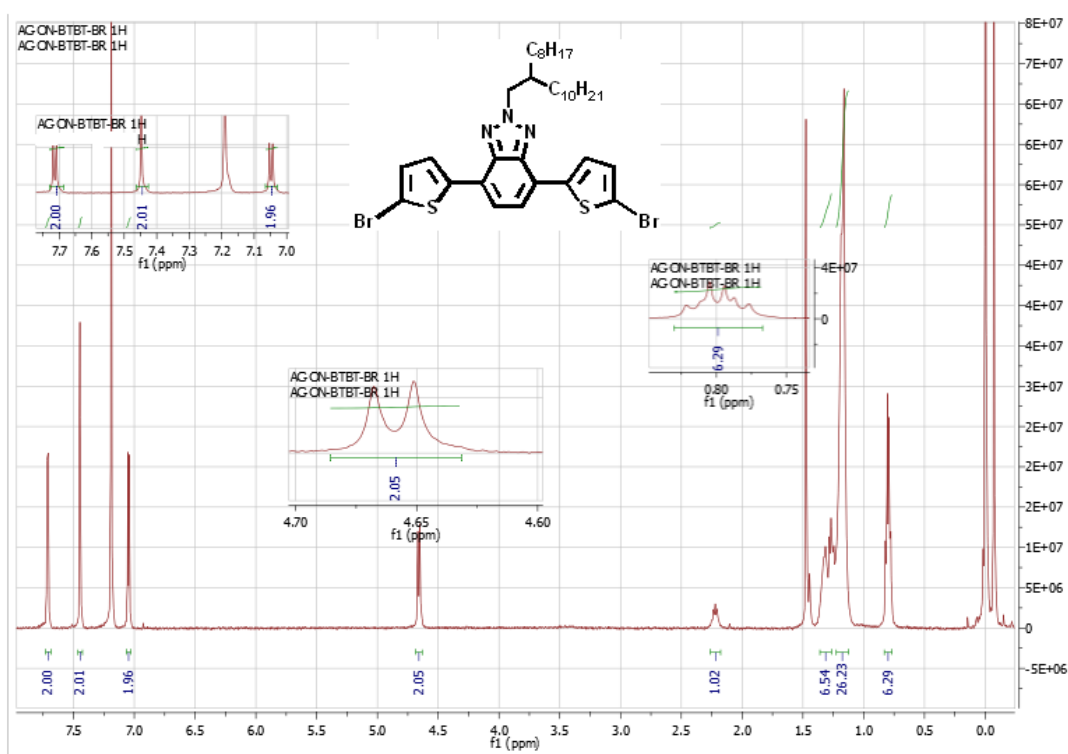


**Figure 68.** <sup>1</sup>H NMR result of 4,7-bis(5-bromothiophen-2-yl)-2-(2-octyldodecyl)-2H-benzo[d][1,2,3]triazole (13)

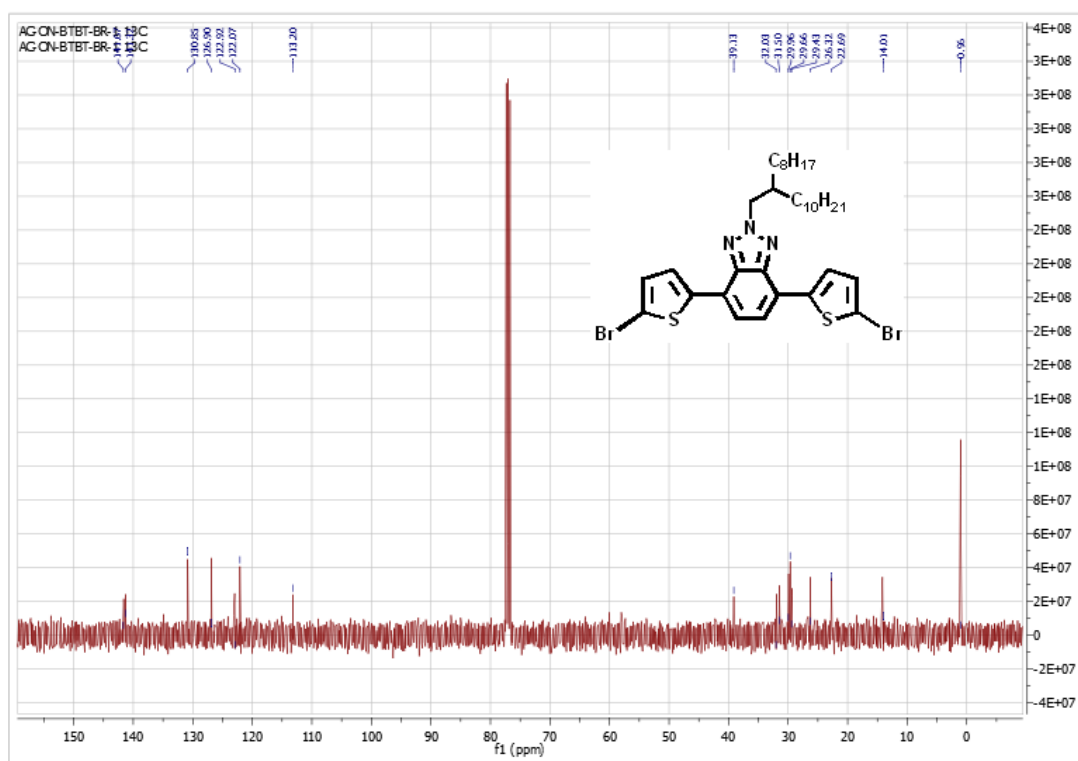


**Figure 69.**  $^{13}\text{C}$  NMR result of 4,7-bis(5-bromothiophen-2-yl)-2-(2-octyldodecyl)-2H-benzo[d][1,2,3]triazole (13)

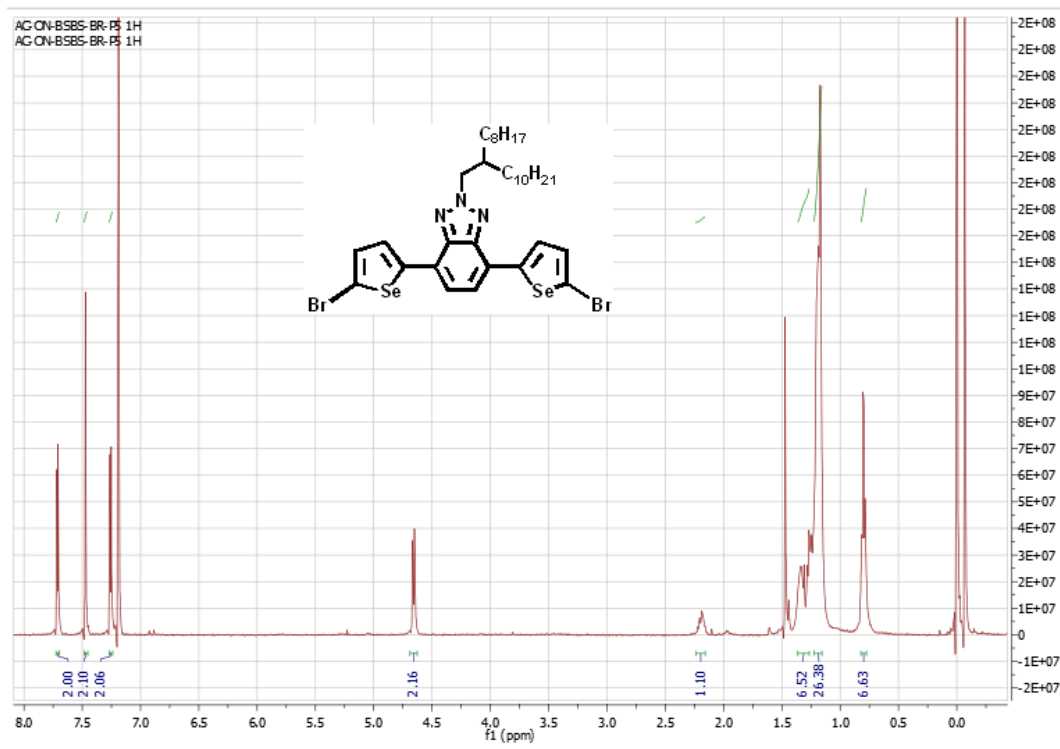


**Figure 70.**  $^1\text{H}$  NMR result of 4,7-bis(5-bromoselenophen-2-yl)-2-(2-octyldodecyl)-2H-benzo[d][1,2,3]triazole (14)

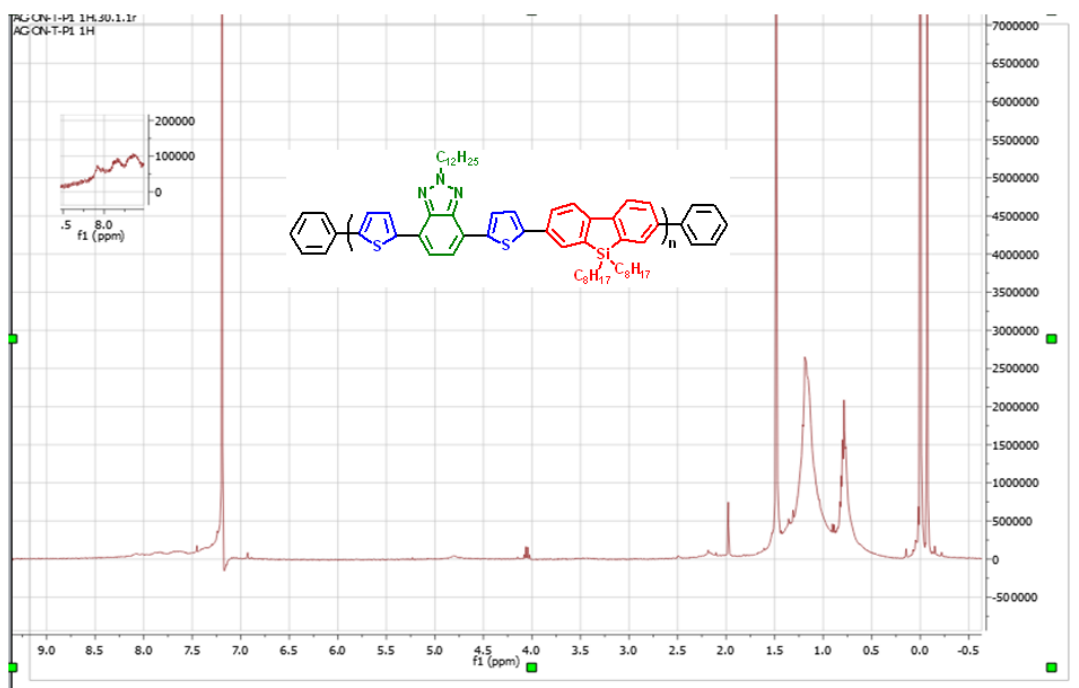


**Figure 71.**  $^1\text{H}$  NMR result of the PTBTsif

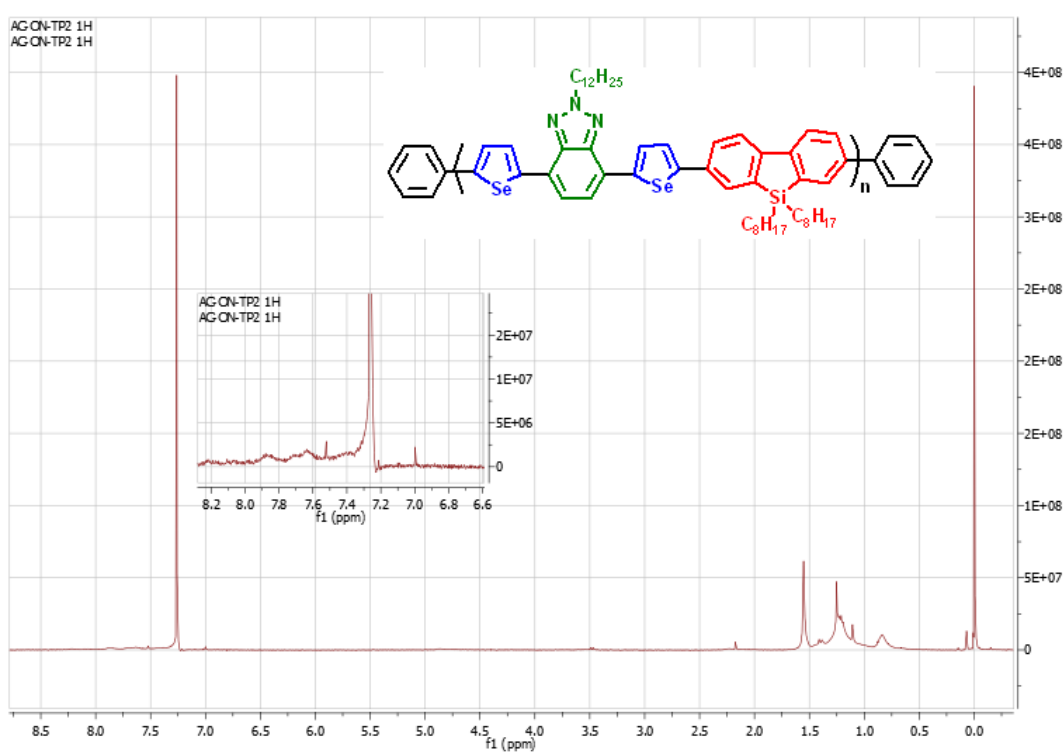


**Figure 72.**  $^1\text{H}$  NMR result of PSBSSif

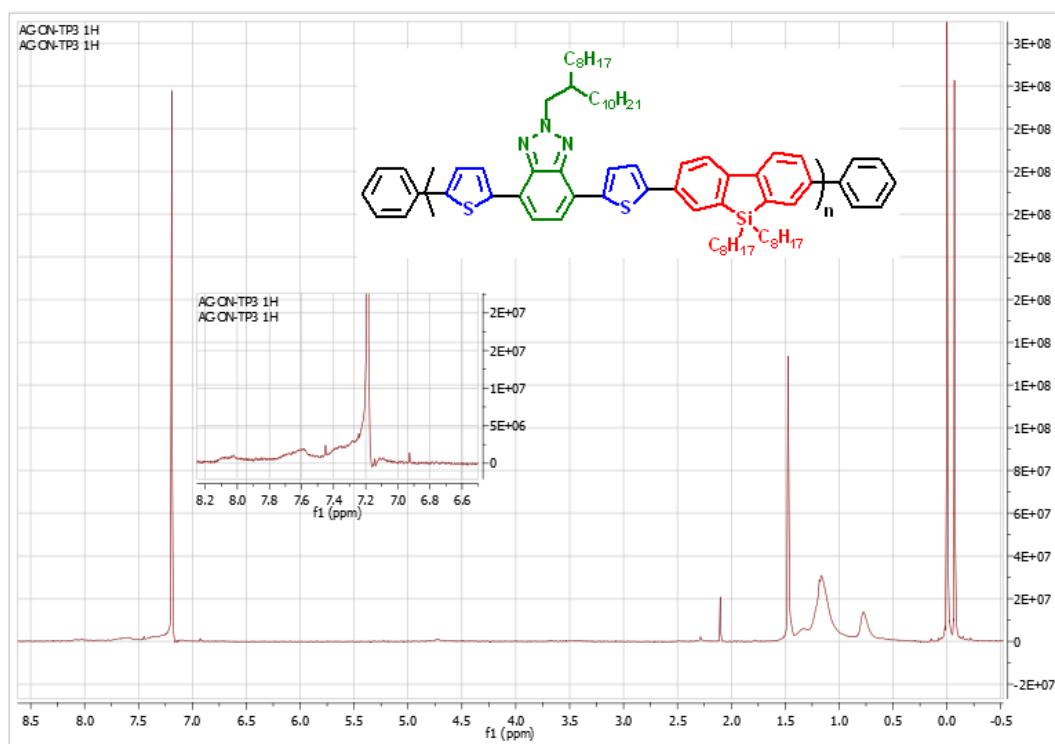


**Figure 73.**  $^1\text{H}$  NMR result of PBTBTSif

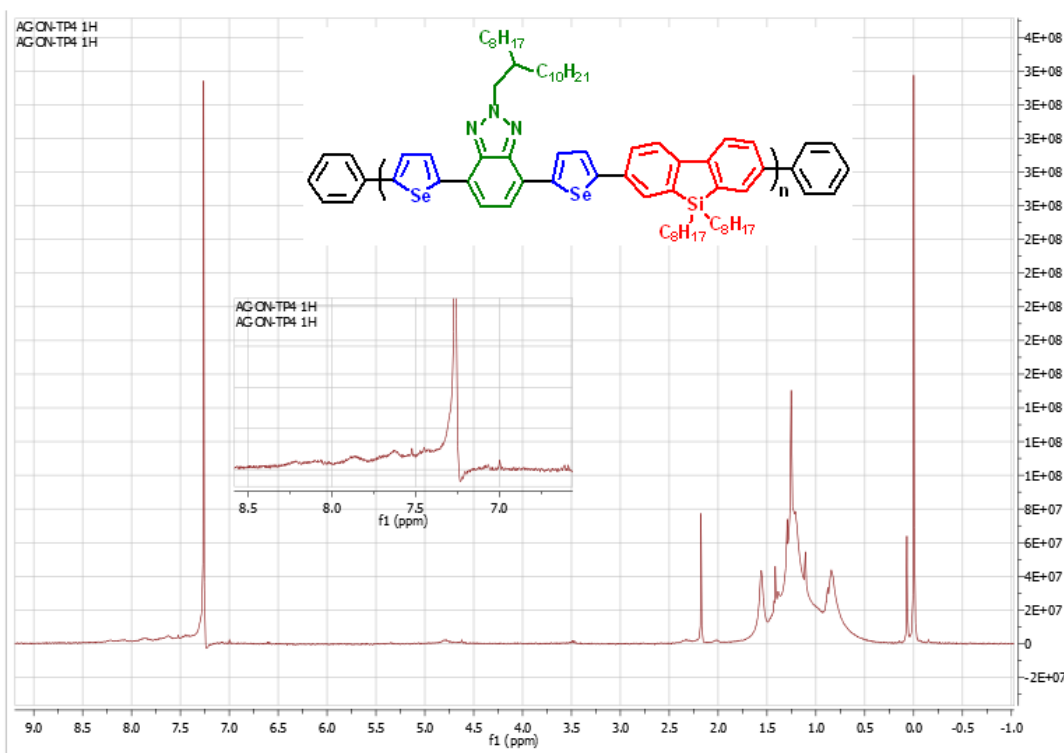


**Figure 74.**  $^1\text{H}$  NMR result of PBSBSSif

## APPENDIX B

### THERMAL ANALYSIS RESULTS

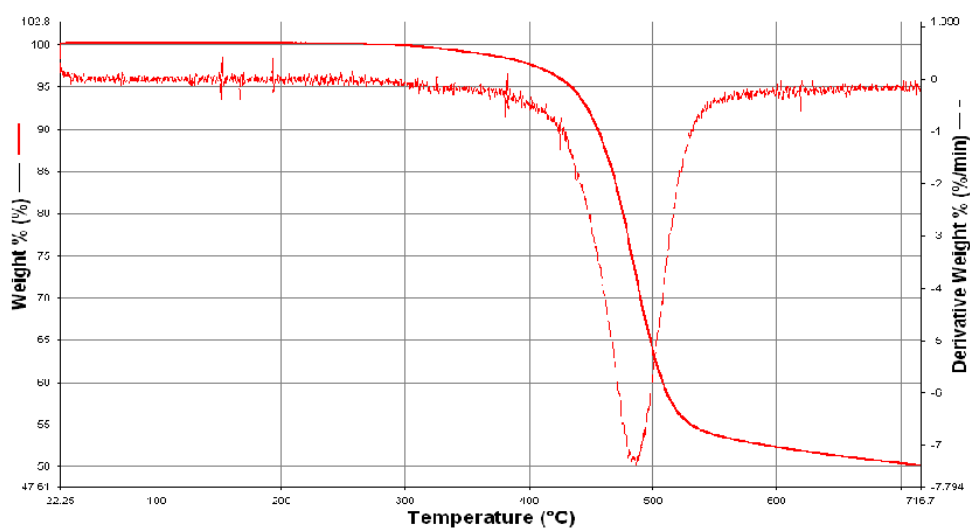


**Figure 75.** TGA result of PTBTSif

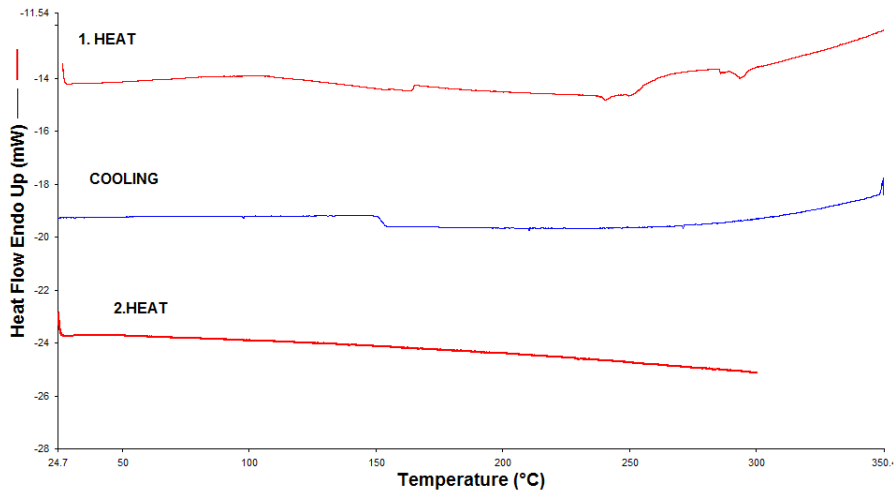


**Figure 76.** DSC result of PTBTSif

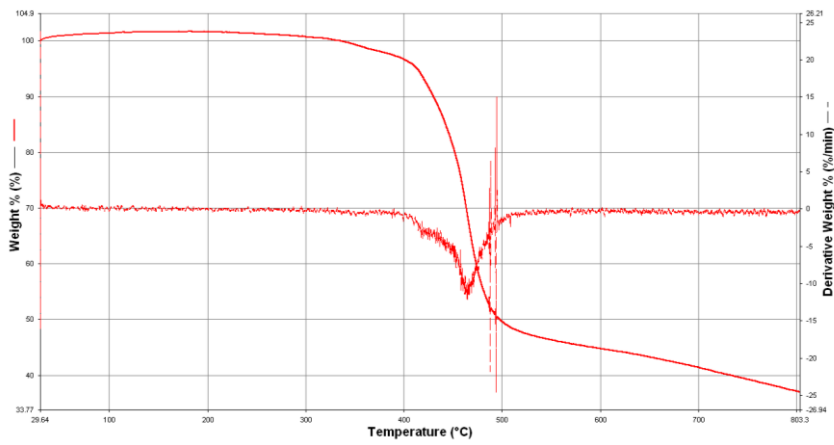


**Figure 77.** TGA result of PSBSSif

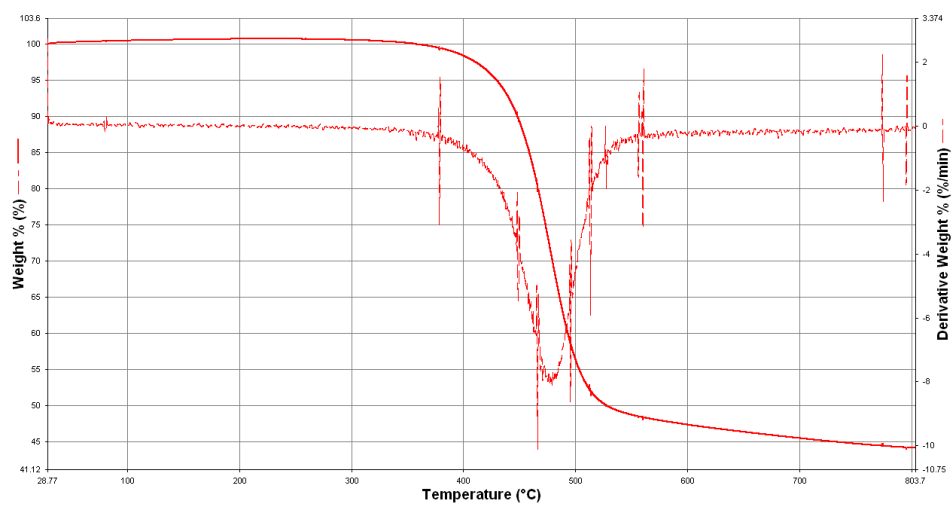


**Figure 78.** TGA result of PBTBTSif

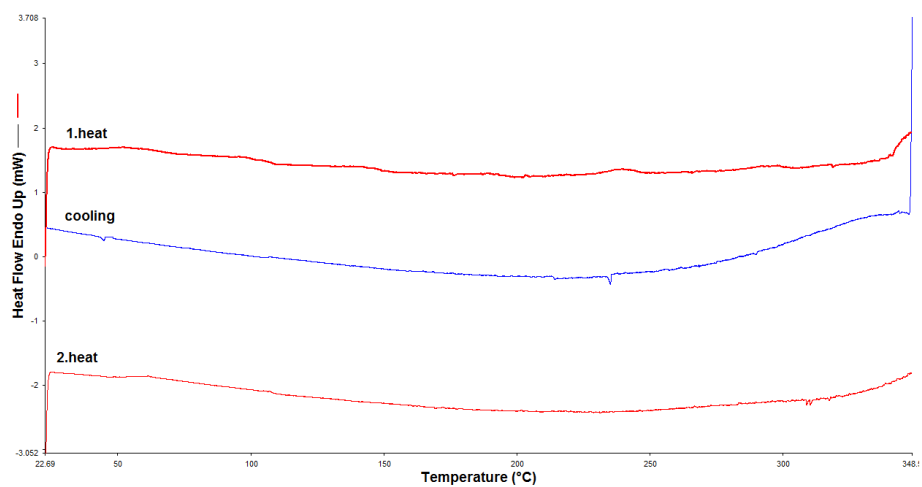


**Figure 79.** DSC result of PBTBTSif